

THESIS FOR THE DEGREE OF DOCTOR OF PHILOSOPHY

Synthesis and Photophysical Characterization of Annihilator-  
Sensitizer Pairs for Triplet-Triplet Annihilation Based Photon  
Upconversion

VICTOR GRAY

Department of Chemistry and Chemical Engineering  
CHALMERS UNIVERSITY OF TECHNOLOGY

Göteborg, Sweden 2017

Synthesis and Photophysical Characterization of Annihilator-  
Sensitizer Pairs for Triplet-Triplet Annihilation Based Photon Upconversion  
VICTOR GRAY  
ISBN 978-91-7597-617-4

© VICTOR GRAY, 2017

Doktorsavhandlingar vid Chalmers tekniska högskola  
Ny serie nr. 4298  
ISSN 0346-718X  
Department of Chemistry and Chemical Engineering  
Division of Applied Chemistry  
Chalmers University of Technology  
SE-412 96 Göteborg  
Sweden  
Telephone: +46 (0)31-772 1000

Cover:

Green light is absorbed by Palladium porphyrin and upconverted and emitted as blue light through triplet-triplet annihilation of 9,10-diphenylanthracene.

Chalmers Reproservice  
Göteborg, Sweden 2017

Synthesis and Photophysical Characterization of Annihilator-Sensitizer Pairs for Triplet-Triplet Annihilation Based Photon Upconversion  
VICTOR GRAY

Department of Chemistry and Chemical Engineering  
Division of Applied Chemistry  
Chalmers University of Technology

## ABSTRACT

Transitioning to a future society, independent of fossil fuels, will definitely require the use of solar radiation for power and fuel production. Due to energy mismatch between device absorption and the broad band irradiation provided by the sun there are severe limitations to how efficient devices for direct conversion of solar radiation can be. One way to better use the solar radiation would be to use transmitted low energy photons and convert them to higher energy photons that can be used in the device. Triplet-triplet annihilation (TTA) based photon upconversion (UC) is one viable way of utilizing these transmitted low energy photons. In TTA-UC two low energy photons are fused into one photon of higher energy. To achieve TTA-UC two components are required. The first type, the sensitizer, absorbs the photon energy and transfers it through triplet energy transfer (TET) to the second type, the annihilator. Photon absorption and energy transfer must occur at least twice for two distinct annihilators to be able to fuse the energy of two photons through triplet-triplet annihilation, forming one annihilator in its first excited singlet state. The singlet excited annihilator can then emit a photon of high energy.

This Thesis covers the design, synthesis and characterization of new annihilators and sensitizers with the overall aim to develop design parameters to rationally design efficient annihilator-sensitizer pairs capable of forming supra-molecular structures with *intra*-molecular TET and TTA. First, semiconductor nanocrystals (NCs) based on CdS are explored as triplet sensitizers for visible to UV upconversion using 2,5-diphenyloxazole (PPO) as the annihilator. With the NC based sensitizers a 5 times improvement of upconversion quantum yield ( $\Phi_{UC}$ ) is realized. Further improvements of  $\Phi_{UC}$  would require better annihilators. Looking closer at the popular blue-emitting annihilator 9,10-diphenylanthracene (DPA) I show that substitution on the phenyl rings does not affect the energy levels, resulting in similar UC properties for all studied 9,10-phenylsubstituted anthracenes. In the conformationally flexible anthracene 9,10-bis(phenylethynyl)anthracene (BPEA), however, a more than 7 times reduction in  $\Phi_{UC}$  is observed. A new loss mechanism based on the shapes of the singlet and triplet energy surfaces is introduced to explain the lower  $\Phi_{UC}$ .

Finally, anthracene annihilators are connected axially to metal porphyrin sensitizers through coordination. Both the desired triplet energy transfer from sensitizer to annihilator and the undesired singlet energy transfer from annihilator to sensitizer are studied in these systems by time resolved emission and absorption techniques. Based on the results presented herein we are now moving closer to developing supra-molecular structures suitable for *intra*-molecular TTA-UC.

Keywords: Anthracene, Photon Upconversion, Triplet-triplet annihilation



*To my parents*



## NOMENCLATURE

**AO** Atomic orbital

**BPEA** 9,10-bis(phenylethynyl)anthracene

**DPA** 9,10-diphenylanthracene

**fs** Femtosecond

**1G** First generation

**2G** Second generation

**3G** Third generation

**GS** Ground state

**HOMO** Highest occupied molecular orbital

**IC** Internal Conversion

**IRF** Instrument response function

**ISC** Inter-system crossing

**LUMO** Lowest unoccupied molecular orbital

**MO** Molecular orbital

**NC** Nanocrystal

**NIR** Near-infrared

**PdOEP** Palladium octaethylporphyrin

**PtOEP** Platinum octaethylporphyrin

**PV** Photovoltaic

**RuOEP(CO)** ruthenium(II) carbonyl octaethylporphyrin

**SQ** Shockley-Queisser

**TAS** Transient absorption spectroscopy

**TCSPC** Time-Correlated Single Photon Counting

**TET** Triplet energy transfer

**TRPL** Time-resolved photoluminescence

**TTA** Triplet-triplet annihilation

**UC** Upconversion (referred to photons)

**UV** Ultraviolet

**VIS** visible

**VR** Vibrational relaxation

**ZnOEP** Zinc octaethylporphyrin

# THESIS

This thesis is based on work reported in the following papers, referred to by Roman numerals in the text:

- Paper I**      **Photophysical characterization of the 9,10-disubstituted anthracene chromophore and its application in triplet-triplet annihilation photon upconversion**, Gray, V., Dzebo, D., Lundin, A., Alborzpour, J., Abrahamsson, M., Albinsson, B. and Moth-Poulsen K., *J. Mater. Chem. C*, 2015, **3**, 11111-11121.
- Paper II**      **Loss channels in triplet-triplet annihilation photon upconversion: importance of annihilator singlet and triplet surface shapes**, Gray, V., Dreos, A., Erhart, P., Albinsson, B., Moth-Poulsen K., and Abrahamsson, M., *Phys. Chem. Chem. Phys.*, 2017, **19**, 10931-10939.
- Paper III**      **Singlet and Triplet Energy Transfer in Porphyrin-Anthracene Complexes: Potential in Triplet-Triplet Annihilation Upconversion**, Gray, V., Börjesson, K., Dzebo, D., Abrahamsson, M., Albinsson, B., and Moth-Poulsen K., *J. Phys. Chem. C*, 2016, **120**, 19018-19026.
- Paper IV**      **CdS/ZnS core-shell nanocrystal photosensitizers for visible to UV upconversion**, Gray, V., Xia, P., Huang, Z., Moses, E., Fast, A., Fishman, D., Abrahamsson, M., Moth-Poulsen K., and Tang, M. L., *Chem. Sci.*, 2017, **8**, 5488-5496.

## CONTRIBUTION REPORT

- Paper I**      Performed the synthesis of new compounds, all photophysical characterization and wrote most of the paper.
- Paper II**      Performed the synthesis of new compounds, all photophysical characterization, analyzed most of the data and wrote the paper together with the other authors.
- Paper III**      Performed the synthesis of new compounds, most of the photophysical characterization, analyzed most of the data and wrote the paper together with the other authors.
- Paper IV**      Conceived the idea with input from the other authors. Performed the nanocrystal synthesis, all steady state photophysical measurements as well as the TCSPC measurements. Analyzed most of the data and wrote the paper together with the other authors. The experimental work was carried out at the University of California Riverside.

DFT calculations were carried out by Dr. Angelica Lundin, Jonathan Alborzpour and

Prof. Paul Erhart. SVD analysis of the binding dynamics was done by Dr. Damir Dzebo. fs-Transient absorption was performed at University of California Irvine, by Alexander Fast, Dr. Dmitry Fishman and Zhiyuan Huang.

The author has published the following papers which are not included in the thesis.

- Paper A** **Triplet–triplet annihilation photon-upconversion: towards solar energy applications**, Gray, V., Dzebo, D., Abrahamsson, M., Albinsson, B. and Moth-Poulsen, K., *Phys. Chem. Chem. Phys.*, 2014, **16**, 10345-10352.
- Paper B** **Diaryl-substituted norbornadienes with red-shifted absorption for molecular solar thermal energy storage**, Gray, V., Lennartson, A., Ratanalert, P., Börjesson K. and Moth-Poulsen, K., *Chem. Commun.*, 2014, **50**, 5330-5332.
- Paper C** **Exploring the Potential of Fulvalene Dimetals as Platforms for Molecular Solar Thermal Energy Storage: Computations, Syntheses, Structures, Kinetics, and Catalysis**, Börjesson, K., Coso, D., Gray, V., Grossman, J. C., Guan, J., Harris, C. B., Hertkorn, N., Hou, Z., Kanai, Y., Lee, D., Lomont, J. P., Majumdar, A., Meier, S. K., Moth-Poulsen, K., Myrabo, R. L., Nguyen, S. C., Segalman, R. A., Srinivasan, V., Tolman, W. B., Vinokurov, N., Vollhardt, K. P. C. and Weidman, T. *W.Chem. Eur. J.*, 2014, **20**, 15587–15604.
- Paper D** **Photon Upconversion with directed emission**, Börjesson K., Rudquist, P., Gray, V., and Moth-Poulsen, K., *Nat. Commun.*, 2016, 12689
- Paper E** **Intramolecular triplet-triplet annihilation upconversion in 9,10-diphenylanthracene oligomers and dendrimers**, Dzebo, D., Börjesson K., Gray, V., Moth-Poulsen, K., and Albinsson, B., *J. Phys. Chem. C.*, 2016, **120**, 23397-23406.
- Paper F** **Tuning the photochemical properties of the fulvalene-tetracarbonyl diruthenium system**, Lennartson, A., Lundin, A., Börjesson, K., Gray, V., and Moth-Poulsen, K., *Dalt. Trans.*, 2016, **45**, 8740-8744.



# CONTENTS

<b>Abstract</b>	<b>i</b>
<b>Nomenclature</b>	<b>v</b>
<b>Thesis</b>	<b>vii</b>
<b>Contents</b>	<b>xi</b>
<b>1 Introduction</b>	<b>1</b>
1.1 Photon Upconversion - A brief overview . . . . .	3
1.1.1 Research Questions and Hypotheses . . . . .	5
<b>2 Light, Matter and their Interactions</b>	<b>7</b>
2.1 Light . . . . .	7
2.2 Matter . . . . .	8
2.2.1 Atoms and Molecules . . . . .	8
2.2.2 A closer look at spin and spin-states . . . . .	9
2.3 Light-Matter Interactions . . . . .	10
2.4 Photoinduced Processes . . . . .	12
2.4.1 Rates and Quantum Yield . . . . .	13
2.4.2 Electron Transfer . . . . .	14
2.4.3 Energy Transfer . . . . .	15
2.4.4 Photon Upconversion Through Triplet-Triplet Annihilation . . . . .	19
2.4.5 Semiconductor Nanocrystals . . . . .	23
2.5 Binding Dynamics . . . . .	25
<b>3 Triplet Sensitizers for Efficient Triplet-Triplet Annihilation</b>	<b>27</b>
3.1 Design Parameters for Triplet Sensitizers . . . . .	27
3.1.1 Molecular Sensitizers . . . . .	27
3.1.2 Semiconductor Nanocrystal Sensitizers . . . . .	28
3.2 Studying Triplet Energy Transfer from Sensitizer to Annihilator . . . . .	29
3.3 CdS/ZnS core-shell NCs for Visible to Ultraviolet Upconversion . . . . .	30
3.3.1 Synthesis and Characterization of Nanocrystals . . . . .	31
3.4 Summary and Evaluation of Hypotheses . . . . .	34
<b>4 Design of Efficient Annihilator Molecules</b>	<b>35</b>
4.1 Design Parameters for the Annihilator . . . . .	35
4.2 Substitution Effects on 9,10-Disubstituted Anthracenes . . . . .	36
4.2.1 Synthesis . . . . .	37
4.2.2 Photophysical characterization . . . . .	37
4.2.3 Triplet-Triplet Annihilation Photon Upconversion . . . . .	40
4.2.4 Loss Channels in Triplet-Triplet Annihilation . . . . .	42
4.3 Evaluation of PPO and other UV annihilators . . . . .	43

4.4	Summary and Evaluation of Hypotheses . . . . .	44
<b>5</b>	<b>Coordination between Porphyrin Sensitizers and Annihilators</b>	<b>47</b>
5.1	Synthesis . . . . .	47
5.2	Annihilator Coordination to ZnOEP . . . . .	49
5.2.1	Triplet Energy Transfer . . . . .	50
5.2.2	Singlet Energy Transfer . . . . .	50
5.2.3	Triplet-Triplet Annihilation Photon Upconversion . . . . .	51
5.3	Annihilator Coordination to RuOEP(CO) . . . . .	52
5.3.1	Triplet Energy Transfer . . . . .	52
5.4	Outlook - Towards all <i>Intra</i> -Molecular Triplet-Triplet Annihilation Supra- molecular Structures . . . . .	54
5.5	Evaluation of Hypothesis . . . . .	54
<b>6</b>	<b>Concluding Remarks and Outlook</b>	<b>55</b>
<b>7</b>	<b>Methods</b>	<b>59</b>
7.1	Absorption and Emission . . . . .	59
7.1.1	Steady State Measurements . . . . .	59
7.1.2	Time-resolved Measurements . . . . .	60
7.2	Synthesis . . . . .	62
7.2.1	Stille and Suzuki Cross-coupling Reactions . . . . .	62
<b>8</b>	<b>Acknowledgements</b>	<b>63</b>

# 1

## Introduction

Without the radiation from The Sun there would be no life on Earth. Plants and algae, powered by solar radiation, produce the oxygen we breathe from carbon dioxide and water in a process called photosynthesis. Even fossil fuels, such as coal and oil, can be considered stored forms of solar energy as they consist of the organic matter once assembled through photosynthesis. To regain this energy humans burn fossil fuels, releasing the carbon dioxide once absorbed by the plants.

Already in 1896 the Swedish Nobel Laureate Svante Arrhenius predicted that the burning of fossil fuels and the subsequent emission of carbon dioxide could lead to a temperature increase of the Earth.<sup>1</sup> Mankind has continued the burning of fossil fuels as it has been a cheap and reliable way to meet our energy demands.<sup>2</sup> Today it is becoming more and more evident that we need a shift to a more direct way of using solar energy. In fact, in 1.5 h The Sun provides Earth with enough energy to meet our energy demands for a whole year.<sup>2,3</sup> If we could directly harvest, convert and store a fraction of this solar energy we could provide clean, secure and sustainable energy world wide.<sup>2,3</sup>

So why isn't solar energy used to a larger extent already? Its is a complicated question that has different answers depending on which solar energy technique that is considered. There are numerous ways of utilizing solar radiation,<sup>2</sup> probably the first thing that comes to mind is the direct conversion of solar radiation to electricity in photovoltaic (PV) devices. PVs have been around for more than half a century, still they only account for less than 1% of the worlds total energy production.<sup>2,4</sup> The main reason for the modest use of PVs is the cost of production.<sup>5</sup> The most common and efficient type of PV cells on the market are those based on crystalline and multi-crystalline silicon (c-Si and mc-Si, respectively). To produce c-Si and mc-Si PVs extremely high-quality and pure silicon is required, explaining the high price. c-Si and mc-Si is often called first generation (1G) PVs as they were the first commercially available PVs. Other types of PVs exists and the second generation (2G) PVs are often cheaper to produce, however with the price of a reduced efficiency.<sup>5</sup> A third generation (3G) of PVs is being developed that hopefully can achieve both cheaper production and higher efficiencies. Examples of 3G PV technologies are organic photovoltaics (OPVs), dye-sensitized solar cells (DSSCs) and multijunction cells. Many of these 3G technologies suffer from a larger band-gap compared to the silicon based PVs. The effect of a larger band-gap is illustrated in Figure 1.1. Only light with energy higher than the band-gap can generate a current, thus a larger band-gap results in a smaller part of the solar spectrum being used, leading to a reduced efficiency.

To use solar radiation to drive photochemical reactions, producing fuels, often called

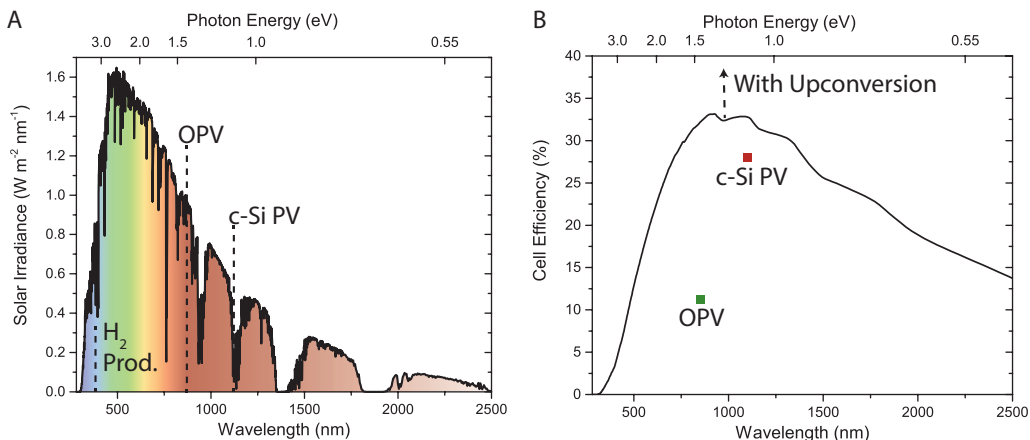


Figure 1.1: A) The solar spectrum, dashed lines mark typical band-gaps for the solar energy techniques; commercial silicon photovoltaic cells (c-Si PV), organic photovoltaic cells (OPV) and hydrogen production from photocatalytic water splitting using TiO<sub>2</sub>. Note that only photons to the left of the dashed lines can be absorbed by the device. B) The theoretical Shockley-Queisser (SQ) limit of a solar energy device as function of band-gap. With photon-upconversion the SQ limit can be surpassed. Representative efficiencies of c-Si PV and OPV are also marked.

solar fuels is another possible way of using The Sun's energy. A typical example of solar fuel production is hydrogen generation from photolysis of water.<sup>6</sup> Similar to 3G PVs, the materials used for solar fuel production often have large band-gaps, also illustrated in Figure 1.1. With large band-gaps more of the solar radiation is wasted. The maximum efficiency of a solar harvesting device depends on the band-gap of the device, as described by Shockley and Queisser in 1961 and illustrated in Figure 1.1B.<sup>7</sup> At large band-gaps few photons are absorbed as most photons are of too low energy. On the other hand if the band-gap is too low, a lot of the absorbed photon energy is lost as heat when the excitation relaxes to the band-gap edge. As can be seen in Figure 1.1B a maximum efficiency of about 34% is obtained for a band-gap of 1.3 eV (corresponding to 950 nm),<sup>7,8</sup> close to the actual efficiency of a commercial crystalline silicon solar cell which has a band-gap of 1.1 eV. To compare, a gasoline engine operates at a fuel efficiency of about 25%.<sup>9,10</sup>

It would be possible to increase the efficiency of solar harvesting devices if either sub band-gap photons could be absorbed or if the excess energy of above band-gap photons could be used to generate multiple charge carriers. A possible means of accessing the wasted solar radiation of sub band-gap photons is through photon upconversion where two low energy photons are fused into one higher energy photon, that can be absorbed by the device. Opposite to upconversion, downconversion generates two excitons for each absorbed high energy photon. Up- and downconversion are complementary to each other. This Thesis focuses on photon upconversion (UC) through a process called triplet-triplet annihilation (TTA). Compared to other types of upconversion, such as two

photon absorption and second harmonic generation, efficient upconversion can be achieved through TTA-UC even with non-coherent low intensity light, making it particularly interesting for solar energy applications.<sup>11-13</sup> TTA-UC can potentially also be useful for other applications besides solar energy, this Thesis however, will focus mainly on the solar energy aspect when considering the applicability of TTA-UC. Related to TTA is the reverse process of singlet fission (SF) which is one possible method of downconversion. Since SF and TTA processes are similar, insightful understanding of one can sometimes be obtained from the other.

In the following Sections I will present a brief overview of the triplet-triplet annihilation photon upconversion research field and how it relates to the research presented in this Thesis, thereafter the research questions and hypothesis addressed in the latter part of this Thesis will be discussed. Chapter 2 gives the necessary theoretical background to follow the work presented in Chapters 3, 4 and 5. Chapters 3-5 are based on the work published in Papers I-IV with some additional results, discussion and outlook. Chapter 6 summarizes the previous Chapters and puts the work into a larger context. For the interested reader experimental techniques and relevant methods are described in Chapter 7.

## 1.1 Photon Upconversion - A brief overview

Fusing two low energy photons into one photon of higher energy through triplet-triplet annihilation (TTA) requires two component. The first type, the sensitizer, absorbs the photon energy and transfers it through triplet energy transfer (TET) to the second type, the annihilator molecule. Photon absorption and energy transfer must occur at least twice to generate two distinct triplet excited annihilators capable of fusing the photon energy. The fusion process is called triplet-triplet annihilation and forms an annihilator in its first excited singlet state. The singlet excited annihilator can then emit a photon of high energy. A detailed description of the TET and TTA-UC process can be found in Section 2.4.3. The first observation of TTA-UC in solution was made by Parker and Hatchard in the 1960s.<sup>14-17</sup> TTA-UC was achieved with a few different anthracene based annihilators and all organic sensitizers.<sup>14-17</sup> These all-organic sensitizers limited the efficiency and it took almost 40 years until Balushev and Castellano, separately, demonstrated TTA-UC sensitized by metal-complexes.<sup>18,19</sup> These initial publications lead to an increased research activity within the field and highly efficient TTA-UC systems have been reported since.<sup>20,21</sup>

There has been several proof-of-principle examples where TTA-UC has been applied to solar energy techniques, such as PV devices,<sup>22-27</sup> hydrogen generation<sup>20,28</sup> and solar thermal energy storage<sup>29</sup>. Furthermore, TTA-UC has been applied to bio-medical applications such as bio-imaging<sup>30-34</sup> and photo-dynamic therapy.<sup>35,36</sup> TTA also plays an important role in understanding organic light emitting diodes (OLEDs).<sup>37,38</sup>

The previous mentioned examples of TTA-UC solar energy devices have all used liquid TTA-UC systems as the efficiencies are higher compared to the solid versions. To compare, the highest efficiency in terms of upconversion quantum yield, in a solution based system is 38%<sup>39</sup> and in a solid system the record is 20%,<sup>28</sup> however values are often

much lower, in the range of a few percent.<sup>27</sup> The lower efficiencies in solid systems stems from the inherent energy transfer processes of TTA-UC which require close proximity of the sensitizer and annihilator, this is easily achieved in liquid systems where molecules can diffuse and move around. In solid systems, annihilators and sensitizers are fixed and cannot diffuse and encounter other molecules than the ones already next to them.

A major part of the TTA-UC research is focused on developing efficient solid state TTA-UC systems and it is motivated by the prospect of a less complex device fabrication compared to liquid systems that would need to be contained and sealed in real-life solar energy applications. The different approaches to achieve solid state systems can be divided into three categories. The simplest approach is to make a film with a mixture of the sensitizer and annihilator, this however, often results in phase separation and large domains with only sensitizer or annihilators and therefore low efficiencies.<sup>40</sup> Another approach is to use a solid matrix, like a rubbery polymer or gel and mix in the sensitizer and annihilator.<sup>28,41-44</sup> The matrix approach can be rather efficient since there is still some molecular diffusion possible and upconversion quantum yields up to 10-20% have been reported.<sup>28,41</sup> The last approach is to pre-arrange the annihilator and/or sensitizer molecules forming supra-molecular structures, either through self-assembly or by incorporating them as monomers into polymeric structures.<sup>18,45-49</sup>

The latter approach, where the annihilator and sensitizer are pre-arranged in close proximity is particularly interesting since it offers a way of overcoming the diffusion limit of the TET and TTA processes. However, there is still plenty to learn about how organizing the annihilator and sensitizer affects the involved processes. For example, often when connecting sensitizer and annihilator molecules, in order to achieve efficient TET, the overall upconversion efficiency is reduced as the upconverted singlet state on the annihilator is readily quenched by the sensitizer.<sup>19,45,50</sup> We studied the effect of axially coordinating the annihilator to the sensitizer<sup>50</sup> and these results are summarized in Chapter 5. We, and others, have also studied the *intra*-molecular triplet migration and TTA in oligomeric, polymeric and dendrimeric annihilator structures and showed that under certain conditions *intra*-molecular TTA is more efficient than *inter*-molecular TTA.<sup>45,46,49</sup>

Common for all proof-of-principle examples and solid-state versions of TTA-UC is that they all use metal-complexes, most often metalloporphyrins, as sensitizers and 9,10-diphenylanthracene (DPA) or similar acenes as the annihilator. These TTA-UC systems can be very efficient in liquid media and are therefore perfect for demonstrating new concepts. For practical use, however, the most common DPA and porphyrin systems are not useful as they upconvert green light to blue. For PV applications near-infrared (NIR) to visible (VIS) upconversion would be more beneficial and for solar fuel production, through photocatalysis, VIS to ultraviolet (UV) is more appropriate. To design new annihilator molecules optimized for applications, however, has turned out to be difficult, and even after half a century there are few annihilators that perform better than DPA.<sup>17,20</sup> A greater understanding of the TTA process and how it relates to molecular structure is still necessary to successfully design new annihilators.

Understanding and designing new triplet sensitizers is a whole research field by itself.<sup>51</sup> A major challenge lies in designing sensitizers with high triplet yields and molar absorptivities in a desired spectral region. Molecular triplet sensitizers capable of absorbing

NIR photons, *i.e.* having narrow band-gaps, are particularly difficult to obtain. The reason being an increased non-radiative decay rate of the excited state as the band-gap decreases. Furthermore, to achieve a narrow band-gap a large conjugated structure is required, often leading to difficult and time consuming synthesis. In 2015 an alternative to molecular sensitizers was demonstrated by three research groups independently,<sup>52-54</sup> in these studies the sensitizers consisted of semiconductor nanocrystals (NCs). Semiconductor NCs are promising since they have size-tunable optical properties, *e.g.* the band-gap can be tuned by the size of the crystal, and facile synthesis.

Chapter 3 covers the sensitizer, in particular the work on NC based sensitizers focusing on the work in Paper IV. Together with one of the pioneering NC-sensitizer groups I designed core-shell NCs capable of sensitizing 2,5-diphenyloxazole (PPO) resulting in a relatively efficient VIS-to-UV upconversion system. Even though the efficiency of this system is far from those reported for green-to-blue upconversion systems it is the most efficient VIS-to-UV upconversion system reported in the literature so far, demonstrating the potential for NC sensitizers. Following the discussion of the sensitizer in Chapter 3 the focus turns to the annihilator in Chapter 4 where I discuss existing design parameters for annihilators and expand upon these based on the work in Papers I and II. Some of the studied annihilators in Paper I contain nitrogen atoms with free electron pairs making it possible to coordinate them to metalloporphyrin sensitizers, possibly achieving more efficient TET in future solid-state systems. The initial work on these annihilator-sensitizer complexes were published in Paper III and a detailed summary, including some unpublished results, ends the scientific discussion in Chapter 5.

### 1.1.1 Research Questions and Hypotheses

As mentioned in the overview above a lot of focus is on developing efficient solid state systems and this is also the overall goal of the TTA-UC research carried out at Chalmers University of Technology. The idea is that efficient solid state TTA-UC can be achieved with supra-molecular structures where both TET and TTA occur *intra*-molecularly. The first research question is then: Is it possible to achieve efficient *intra*-molecularly TET and TTA in supra-molecular structures based on dendrimeric structures of DPA capable of coordinating to the sensitizer? This question is related to two hypotheses:

1. *Intra*-molecular triplet-triplet annihilation is possible in oligomeric and dendrimeric DPA structures.
2. Triplet energy transfer can be enhanced while minimizing the parasitic singlet energy back transfer if the annihilator is coordinated axially to a metalloporphyrin.

The first hypothesis has been proven to some extent by us, and others, previously and will not be covered in this Thesis.<sup>45,46,49</sup> The second hypothesis will be discussed in relation to the results presented in Paper III in Chapter 5. Another research question related to the one above is: How sensitive are the inherent TTA properties of DPA to substitutions? The hypotheses are that:

3. Introducing donor and/or acceptor units to DPA can slightly shift the singlet and triplet energies possibly allowing for a more efficient TTA.

4. The energy balance  $2 \times E_{T_1} \geq E_{S_1}$  must be fulfilled for all accessible annihilator geometries in order to achieve efficient triplet-triplet annihilation.

Considering the sensitizer and the fact that nanocrystals have been used successfully as sensitizers for NIR-to-VIS and green-to-blue TTA-UC, I was surprised NC had not been used for VIS-to-UV TTA-UC, leading to the research question: Can a smaller NC efficiently sensitize PPO and achieve VIS-to-UV TTA-UC? The first hypotheses was based on that CdSe nanocrystals can efficiently sensitize green-to-blue TTA-UC:

5. Being similar to CdSe, CdS nanocrystals can also function as triplet sensitizers.
6. A thin ZnS shell can reduce trap states on the nanocrystal surface and thus enhance triplet energy transfer from the nanocrystal to a surface anchored ligand.

# 2

## Light, Matter and their Interactions

As humans we interact with light daily, be it vision and the perception of colours or the production of vitamin D in our bodies.<sup>55</sup> As such most of us probably take it for granted, without much reflection to the nature of light. Herein light will be referred to, as is often the case, the part of the electro-magnetic spectrum containing ultraviolet (UV), visible (VIS) and near-infrared (NIR) radiation. Understanding the interactions of light with matter is fundamental for the research presented herein. This Chapter is intended to give a brief theoretical background to the nature of light, matter and their interactions.

### 2.1 Light

Electro-magnetic radiation can be seen as waves composed of two oscillating fields, one electric and one magnetic. These two fields are perpendicular to each other and propagate in the same direction as illustrated in Figure 2.1. The distance between two maxima (or minima) is termed the wavelength, denoted  $\lambda$ . Light is an electro-magnetic wave with a wavelength between a few nanometer and a few micrometer. Light with a wavelength shorter than 400 nm is called UV light and if the wavelength is longer than 700 nm it is called NIR, in between these extremes lies the visible region of light that we can see.

Electro-magnetic radiation can also be viewed as being composed of discrete packets

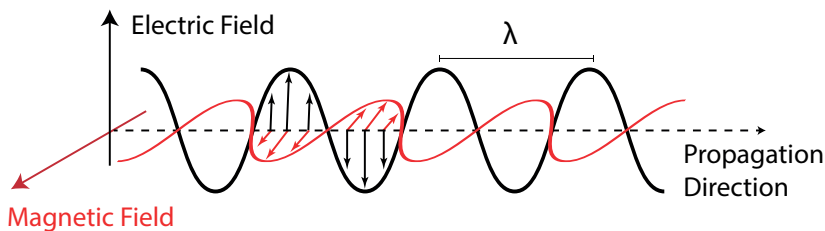


Figure 2.1: An electro-magnetic wave consists of an oscillating magnetic field (red) perpendicular to an oscillating electric field (black), both propagating together in the same direction.

of energy and these particles of light are referred to as photons. The energy of a photon ( $E$ ) is related to the wavelength and frequency ( $\nu$ ) of the electro-magnetic wave through Planck's constant ( $h$ ,  $6.626 \times 10^{-34}$  J s) and the speed of light ( $c$ ,  $2.998 \times 10^8$  m s $^{-1}$ ) as described in Equation 2.1.

$$E = h\nu = \frac{hc}{\lambda} \quad (2.1)$$

As can be understood from Equation 2.1 an UV photon is higher in energy than a visible or NIR photon, just as a blue photon ( $\sim 450$  nm) is higher in energy than a green ( $\sim 550$  nm) or red photon ( $\sim 650$  nm).

## 2.2 Matter

The smallest components of matter that will be considered herein are electrons, protons and neutrons. These three building blocks make up all atoms, which in turn can assemble into molecules comprising different materials. Small particles like electrons, protons, atoms and molecules behave fundamentally different compared to the larger items we interact with daily, as will be highlighted in the following sections.

### 2.2.1 Atoms and Molecules

The core of an atom, called nucleus, consists of positively charged protons and in most cases neutrons that are neutral. The nucleus is surrounded by negatively charged electrons. In a neutral atom the number of protons equals the number of electrons. Electrons can, just as photons, be viewed as either a particle or a wave. The wave nature of electrons means that the electron is distributed throughout space. This wave-particle duality leads to atomic sized objects needing a quantum mechanical description, contrary to macroscopic objects that can be satisfactorily described by classical mechanics. Quantum systems, like atoms and molecules, have discrete energies (energy levels) and they can only exist in states with these energies. This fundamental difference to classical systems can be derived from the Schrödinger equation.<sup>56</sup> Solving the Schrödinger equation for a system gives the energy levels and wave functions related to these states. The wave functions,  $\Psi$  are probability amplitude waves and the square of the wave function  $\Psi^2$  is the probability amplitude, *i.e.* the probability of finding a particle in a region of space. For example, in an atom, the wave functions describe the orbitals in which the electron is located around the nucleus. Some atomic orbitals (AOs) are illustrated in Figure 2.2.

The quantum state of an electron is defined by four quantum numbers together determining: the energy, atomic orbital, orientation and spin of the electron. The principal quantum number,  $n$  has an integer value starting at 1 ( $n = 1, 2, 3, \dots$ ) and is related to the energy of the state.<sup>57,58</sup> The second quantum number, called the azimuthal quantum number ( $l$ ), describes the angular momentum of the atomic orbital. Each state related to an principal quantum number can take on  $n-1$  values of  $l$  starting at 0 ( $l = 0, 1, 2, \dots, n-1$ ). Furthermore, each orbital in a state described by an  $n$  and  $l$  can be oriented in different directions described by the magnetic quantum number,  $m_l$ , where  $m_l = 0, \pm 1, \dots, \pm l$ . The spin magnetic quantum number,  $m_s$ , is the fourth quantum number and describes the direction of the electron spin angular momentum. The spin angular momentum  $s$  of

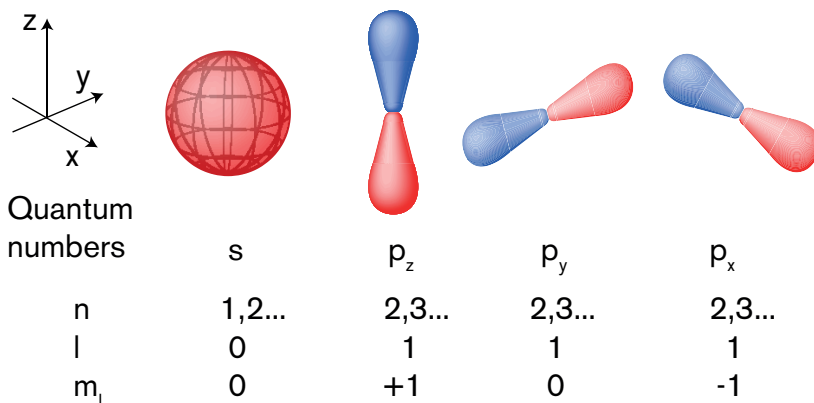


Figure 2.2: The atomic  $s$  and  $p$  orbitals.  $s$  orbitals have  $l=0$  and  $p$  orbitals  $l=1$ . There are three  $p$  orbitals oriented in different directions, defined by  $m_l$ , the  $p_z$ ,  $p_y$  and  $p_x$  orbitals.

a particle is non-negative and for an electron  $s$  is  $1/2$  and can only be oriented in two directions,  $m_s = +1/2$  or  $m_s = -1/2$ , respectively. The two different orientations are often denoted with  $\uparrow$  and  $\downarrow$ , respectively.<sup>57,58</sup> Figure 2.2 illustrates the atomic orbitals with  $n \leq 2$  and the related quantum numbers.

As mentioned previously an atom consists of a nucleus surrounded by electrons in different orbitals. No electrons in an atom can have the same four quantum numbers, furthermore the lowest energy orbitals will be filled first as stated by the Aufbau principle. Each orbital can only contain two electrons, and the Pauli exclusion principle requires these two electrons to have different spin, the spins are said to be paired. Hund's rule however, states that if there are more than one orbital of the same energy, these are filled with single electrons as far as possible, and these electrons will have the same spin, the spins are unpaired.

Molecular orbitals (MOs) are similar to AOs and can be described by linear combinations of AOs. The filling of MO with electrons is governed by the same principles and rules as for atoms. The highest occupied MO is called the HOMO and the lowest unoccupied MO is called the LUMO and these orbitals are especially important when considering the reactivity of molecules or the interaction of light with a molecule.

### 2.2.2 A closer look at spin and spin-states

The spin of an electron is related to its inherent angular momentum and is a fundamental quantity just as its mass and charge.<sup>58,59</sup> It is often, incorrectly, viewed as the angular momentum resulting from the rotation of the negatively charged electron around its axis. As mentioned in the section above, the electron spin can only obtain values of  $m_s = +1/2$  or  $m_s = -1/2$ . The spin is often described as a vector lying in a cone along an axis, arbitrarily chosen as the  $z$ -axis, where  $m_s$  then is the vector component on the  $z$ -axis as illustrated in Figure 2.3A. For two electrons the possible values of the total spin angular

momentum quantum number  $S$  is given by Equation 2.2:<sup>58</sup>

$$S = s_1 + s_2, s_1 + s_2 - 1, \dots, |s_1 - s_2| \quad (2.2)$$

where  $s_i$  is the spin angular momentum quantum number of the individual  $i$ th electron. With  $s_1 = s_2 = 1/2$ ,  $S$  can be either 0 or 1. The number of possible orientations is described by the spin multiplicity  $M$  which is given by Equation 2.3.<sup>58,59</sup>

$$M = 2S + 1 \quad (2.3)$$

The different spin orientations are described by the total spin magnetic quantum number  $M_s = S, S-1, \dots, -S$ .

In the case of  $S=0$   $M=1$  and only one spin orientation of  $M_s=0$  is possible, a molecule with  $S=0$  is said to be in a singlet state. A vectorial picture of the two electron configuration resulting in a singlet state is shown in Figure 2.3B. For  $S=1$   $M=3$  and three different orientations of the total spin can be obtained with  $M_s=+1, 0$  or  $-1$ . A molecule with spin configuration of  $S=1$  is said to be in a triplet state. Figure 2.3C illustrates the vector representation of a triplet configuration.<sup>58,59</sup> In multi-electron systems higher values of  $S$  are possible, for example  $S=2$  and  $M=5$  has five different orientations and is referred to as a quintet state.

According to the Pauli principle electrons in the same orbital must be paired,  $S=0$ . This results in most molecules having singlet ground states, one exception being the oxygen molecule ( $O_2$ ) which has a triplet ground state.

## 2.3 Light-Matter Interactions

Light, being an oscillating electric and magnetic field, can interact with negatively charged electrons in atoms and molecules. If the interaction perturbs the electron wave function in such a way that it resembles another unoccupied wave function an electronic transition can occur, leaving the atom or molecule in an excited state, *i.e.* a photon has been absorbed and an electron promoted to a higher energy orbital. An electron pair which has one electron in the ground state orbital (often referred to as the hole) and one electron in an excited state is also called an exciton. The qualitative description of photon absorption above can be rationalized from the Fermi Golden rule, Equation 2.4,<sup>59</sup>

$$k \propto \rho < \Psi_1 | P | \Psi_2 >^2 \quad (2.4)$$

where  $k$  is the rate of transition between states 1 and 2 described by the wave functions  $\Psi_1$  and  $\Psi_2$ , respectively.  $\rho$  is the density of states capable of mixing  $\Psi_1$  with  $\Psi_2$ .  $P$  describes the perturbation (coupling) brought upon the system inducing the mixing of states  $\Psi_1$  and  $\Psi_2$ . In the case of absorption of a photon, the perturbing force arises from the oscillating electric field associated with the photon. The oscillating electron cloud produced from the interaction with the electric field of a photon induces a dipole moment, called the transition dipole moment. A larger interaction results in a larger transition dipole, resulting in a larger probability of a transition to occur, experimentally this is observed as a stronger absorption in spectroscopic measurements. However, for a

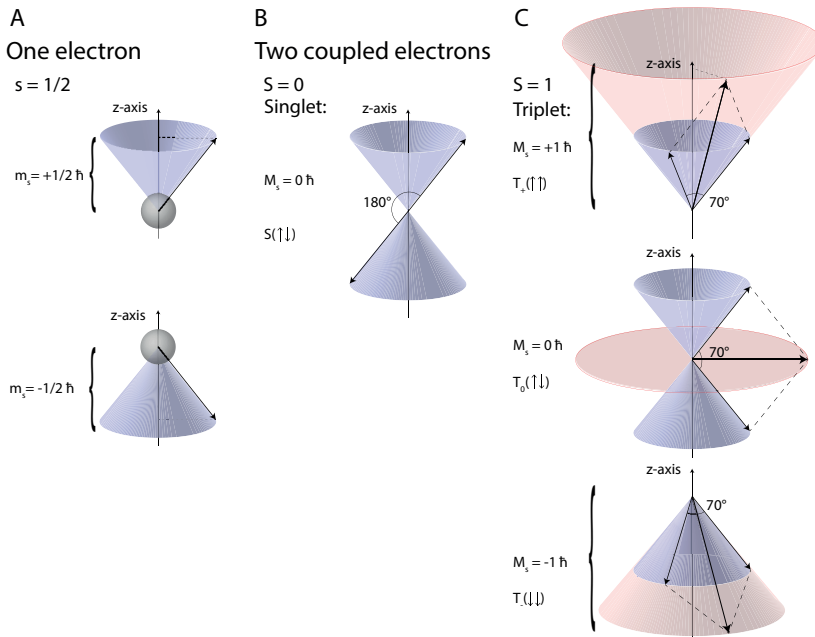


Figure 2.3: Spin of an electron represented by a vector lying in a cone along the z-axis. A) Spin of a single electron can have spin  $m_s = \pm 1/2 \hbar$ . Two coupled electrons can be either in a singlet (B) or triplet (C) configuration. In a singlet the spin vectors are always in  $180^\circ$  angle to one another and the overall spin is canceled,  $M_s = 0$ . In a triplet the spin vectors lie either in the same cone (C, top and bottom) with an relative angle of  $70^\circ$ , resulting in a total spin of  $M_s = \pm 1 \hbar$  or in opposite cones but in phase (C, middle), resulting in a net spin with zero component along the z-axis,  $M_s = 0$

transition to occur the transition dipole moment must also be aligned with the electric field of the electro-magnetic wave.<sup>59</sup>

Furthermore, for light to induce an electronic transition both energy and momentum must be conserved. The former results in the Bohr frequency condition which requires the photon's energy to equal the energy difference ( $\Delta E$ ) between two states in order to induce a transition between these states, Equation 2.5.<sup>59</sup>

$$\Delta E = h\nu \tag{2.5}$$

Often the HOMO and LUMO states of organic molecules are separated by energies corresponding to wavelengths in the visible spectra. The conservation of momentum, leads, among others, to the preservation of spin upon a transition. A transition between two singlet states (or two triplet states) that also conserves energy and has a large overlap is termed an "allowed transition", whereas a transition between a singlet and a triplet state is an example of a "forbidden transition".<sup>59</sup> The fate of excited atoms and molecules will be discussed in detail in the following sections.

## 2.4 Photoinduced Processes

Most molecules have singlet ground state (GS) configurations ( $S_0$ ), thus absorption usually results in a transition from  $S_0$  to the first ( $S_1$ ) or second ( $S_2$ ) singlet excited state as illustrated in the Jablonski diagram in Figure 2.4. Furthermore, each electronic state has a set of vibrational states. Electronic transitions, such as absorption or emission, often occur from the lowest vibrational level in the initial electronic state to a higher lying vibrational level in the final electronic state. A molecule in a higher excited state  $S_{n>1}$  (or  $T_{n>1}$ ) quickly relaxes to its vibrationally relaxed  $S_1$  (or  $T_1$ ) state, as illustrated for  $S_2$  in Figure 2.4. This occurs through internal conversion (IC) and vibrational relaxation (VR), dissipating the excess energy as heat. Consequently, photochemical and photophysical processes predominantly occur from the  $S_1$  or  $T_1$  states, known as Kasha's rule.<sup>59,60</sup>

Relaxation from  $S_1$  to  $S_0$  can occur either nonradiatively or radiatively. Similar to the relaxation from  $S_2$  to  $S_1$ , nonradiative relaxation to  $S_0$  occurs through internal conversion and vibrational relaxation. Radiative relaxation from a singlet state is called fluorescence and results in the emission of a photon. Besides these processes,  $S_1$  can under certain conditions also undergo intersystem crossing (ISC) which induces a spin-flip, transforming the  $S_1$  state to a triplet state ( $T_n$ ).<sup>59,60</sup> ISC is a spin-forbidden process, meaning that to a first approximation it is quantum mechanically forbidden. The change in angular momentum associated with a spin-flip can, however, be compensated for if the spin angular momentum and the orbital angular momentum is mixed through spin-orbit coupling. The magnitude of spin-orbit coupling is proportional to  $Z^4$ , where  $Z$  is the nuclear charge. In other words, a heavier atom induces a larger spin-orbit coupling, which in turn increases the rate of ISC.<sup>59</sup>

A molecule in its  $T_1$  state can also undergo radiative and non-radiative relaxation to  $S_0$ . In both cases, however, a spin-flip is necessary. Thus, non-radiative decay from  $T_1$  occurs through ISC followed by vibrational relaxation. Radiative relaxation from a triplet state is called phosphorescence. According to Kasha's rule both fluorescence and

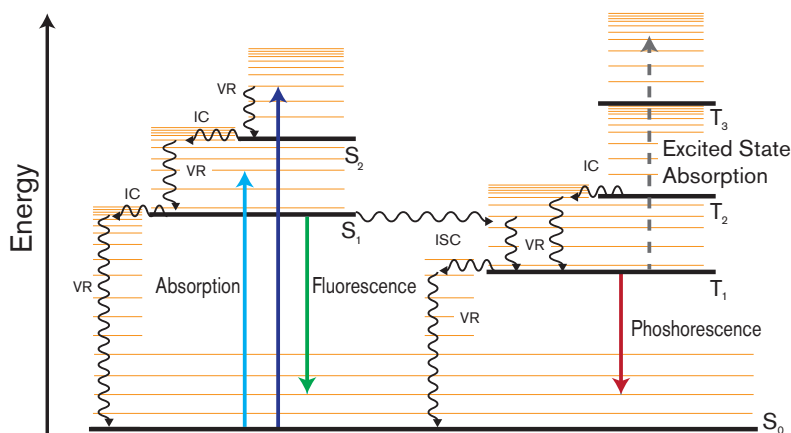


Figure 2.4: Jablonski diagram illustrating the photophysical processes; absorption, fluorescence, phosphorescence, excited state absorption, internal conversion (IC), vibrational relaxation (VR) and intersystem crossing (ISC). Horizontal black lines depict electronic energy levels and orange lines the vibrational energy levels.  $S_n$  and  $T_n$  denote the singlet and triplet states. Radiative and non-radiative transitions are represented by straight and undulated arrows respectively.

phosphorescence occurs from the lowest vibrational levels in  $S_1$  and  $T_1$ , respectively. This leads to the general observation that emission resembles a mirror image of the absorption and occurs at lower energies (longer wavelengths) compared to the absorption, as seen in Figure 2.5. The energy difference between the absorption and emission is called the Stokes-shift.<sup>59,60</sup>

### 2.4.1 Rates and Quantum Yield

As can be seen in Equation 2.4, Fermi's golden rule, the rate of a transition,  $k_i$ , is proportional to the orbital overlap between the initial and final states when considering the coupling or perturbation on the states. The transitions described in the previous sections have different initial and final states, as well as different couplings related to them, therefore it can be expected that different transitions occur with different rates. Vibrational relaxation and internal conversion which occur between states with similar energies and identical spin occur fast, in the order of picoseconds ( $10^{-12}s$ ) or faster. ISC which requires a change in spin is usually much slower, with a large spin-orbit coupling however, it can also approach the picosecond timescale. Fluorescence usually occurs in a few nanoseconds ( $10^{-9}s$ ) whereas phosphorescence is much slower, in the range of microseconds ( $10^{-6}s$ ) to seconds.

The fate of a molecule in an excited state can be predicted if the rates of all possible deactivation processes are known. For example, a molecule in  $S_1$  can undergo radiative (fluorescence) and non-radiative (IC, VR and ISC) relaxation. The probability of this

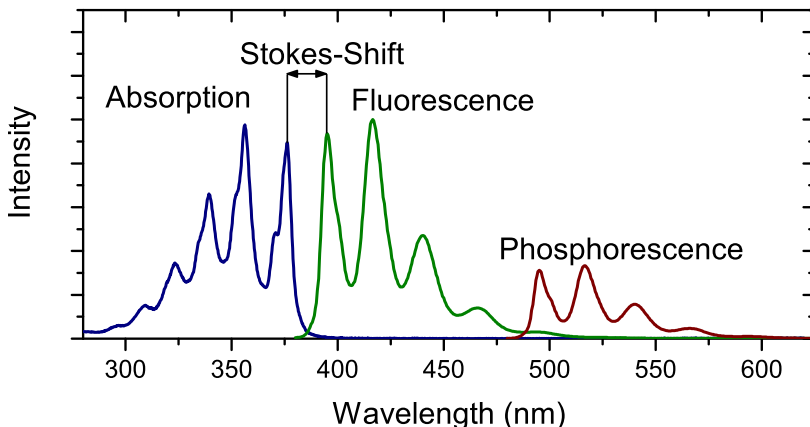


Figure 2.5: The absorption, fluorescence and phosphorescence of a hypothetical molecule. Shown is also the Stokes-shift of the fluorescence.

molecule to undergo fluorescence is described by the quantum yield of fluorescence,  $\Phi_f$ , as described by Equation 2.6a which is a specific case for the more general expression 2.6b:

$$\Phi_f = \frac{k_r}{k_r + k_{nr}} \quad (2.6a)$$

$$\Phi_i = \frac{k_i}{\sum_j k_j} \quad (2.6b)$$

$\Phi_i$  is the quantum yield of the process  $i$ ,  $k_i$  is the rate of process  $i$ , the sum is over all possible deactivation processes with rates  $k_j$ . In the case of fluorescence,  $k_r$  is the rate of radiative relaxation and  $k_{nr}$  is the sum of the rates of all non-radiative processes. The average time a molecule spends in its excited state is characterized by its lifetime. The lifetime of a state,  $\tau$ , is inversely proportional to the rates of deactivation of this state as described by Equation 2.7.

$$\tau = \frac{1}{\sum_j k_j} \quad (2.7)$$

### 2.4.2 Electron Transfer

So far we have only considered transitions within a molecule. A molecule can also interact with other molecules, for example both energy and electron transfer is possible between molecules (or between parts within a large molecule). Electron transfer can occur either between two ground state molecules or between an excited molecule and a ground state species. A molecule is oxidized if an electron is removed, if an electron instead is accepted the molecule is reduced. Thus electron transfer results in the oxidation of the donor molecule (D) and the reduction of the acceptor molecule (A) and is also referred to as charge transfer.

For electron transfer to occur there must be an driving force, *i.e.*  $\Delta G_{EIT}^0 < 0$ . The change in Gibbs free energy for photo induced electron transfer ( $\Delta G_{EIT}^0$ ) can be expressed by Equation 2.8<sup>59</sup>:

$$\Delta G_{EIT}^0 = E_{D^+/D}^0 - E_{A/A^-}^0 - E_{Ex} - N_A \frac{e^2}{4\pi\epsilon_0\epsilon r} \quad (2.8)$$

where  $E_{D^+/D}^0$  and  $E_{A/A^-}^0$  are the electrochemical potentials in free energy units for the donor and acceptor, respectively.  $E_{Ex}$  is the excitation energy and the last term is related to the gain in energy from Coulombic interaction between the formed charges, and  $N_A$  is Avogadro's number,  $e$  is the electron charge,  $\epsilon_0$  is the permittivity of vacuum,  $\epsilon$  is the dielectric constant of the media and  $r$  is the distance between the charges.<sup>59</sup> As can be seen in Equation 2.8 the excitation energy increases the driving force for electron transfer, which explains why the excited state species always oxidizes and reduces more readily than the ground state species.

From transition state theory one can obtain an expression for the rate of electron transfer ( $k_{EIT}$ ), as described in Equation 2.9:<sup>57-59</sup>

$$k_{EIT} = \kappa\nu^\ddagger \exp\left(\frac{-\Delta^\ddagger G}{RT}\right) \quad (2.9)$$

where  $\kappa$  is the transmission coefficient and  $\nu^\ddagger$  is an electronic factor determining the maximum possible value of  $k_{EIT}$ , together they account for the rate at which the transition state converts to the charge transfer product.  $\Delta^\ddagger G$  is the free energy of activation,  $R$  is the ideal gas constant and  $T$  is the absolute temperature.

By considering the parabolic energy surfaces of the initial ( $D^* + A$ ) and final states ( $D^+ + A^-$ ) and using geometric arguments Marcus showed in the 1950s that  $\Delta^\ddagger G$  is related to  $\Delta G_{EIT}^0$  through Equation 2.10:<sup>57,58,61-65</sup>

$$\Delta^\ddagger G = \frac{(\Delta G_{EIT}^0 + \lambda)^2}{4\lambda} \quad (2.10)$$

where  $\lambda$  is termed the reorganization energy and is the energy required to transform the initial state to have the same nuclear coordinates as the final product without electron transfer, as illustrated in Figure 2.6. The theory put forward by Marcus, often referred to as Marcus Theory, predicts an increased rate of electron transfer as  $-\Delta G_{EIT}^0$  increases from 0 to  $\lambda$ . A further increase in  $-\Delta G_{EIT}^0$ , however, leads to a decreased rate of electron transfer, as illustrated in Figure 2.6. Electron transfer reactions with  $-\Delta G_{EIT}^0 > \lambda$  are said to be in the (Marcus) inverted region.<sup>57,58,66</sup>

### 2.4.3 Energy Transfer

Contrary to electron transfer, energy transfer only occurs from an excited molecule to a ground state molecule. The energy can be transferred from either the excited singlet or triplet state and is referred to as singlet and triplet energy transfer, respectively. In the following sections the different types of energy transfer relevant to this Thesis are described. Singlet energy transfer (SET) can occur in two physically distinct ways, through Förster Resonance Energy Transfer or Dexter Energy Transfer. Triplet energy transfer (TET) on the other hand only occurs through the Dexter mechanism.<sup>60</sup>

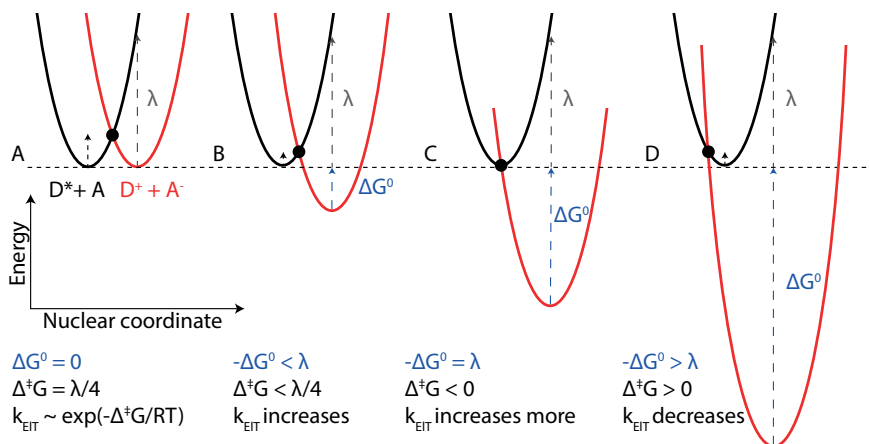


Figure 2.6: Potential energy illustration of photo induced electron transfer and Marcus Theory parameters. Black potential energy surface corresponds to the initial donor ( $D^* + A$ ) excited state and the red surface is the final charge transfer state ( $D^+ + A^-$ ). The reorganization energy,  $\lambda$ , is illustrated by the grey arrow,  $\Delta G_{\text{EIT}}^0$  by the blue arrow and  $\Delta^\ddagger G$  by the black arrow and dot.

### Förster Resonance Energy Transfer

Excited singlet molecules can transfer the excited state energy to another molecule in its ground state if there exists a spectral overlap between the donating molecule's emission spectra and the accepting molecule's absorption spectra. This type of singlet energy transfer is called Förster resonance energy transfer (FRET). It is important to point out that FRET does not involve the emission and subsequent absorption of a photon, instead it relies on dipole-dipole interactions between the transition dipole moments in the two chromophores.<sup>60</sup> Since  $S_0 \rightarrow T_1$  transitions are spin-forbidden they have extremely small transition dipole moments, leading to negligible FRET from triplet excited molecules. FRET can be rather efficient over large distances as it relies on through space interactions, often over a few nm.<sup>60</sup>

The efficiency of FRET depends on the spectral overlap, distance and relative orientation between the donor and acceptor. Two important equations relating these properties to the FRET efficiency are Equations 2.11 and 2.13.  $R_0$  is the distance between a donor-acceptor pair that corresponds to 50% efficiency in energy transfer.

$$R_0 = 0.211(\kappa^2 n^{-4} \Phi_D \int_0^\infty F_D(\lambda) \epsilon_A(\lambda) \lambda^4 d\lambda)^{\frac{1}{6}} \quad (2.11)$$

where  $\kappa^2$  is an orientation factor related to the relative orientations of the transition dipoles in the donor and acceptor,  $n$  is the refractive index,  $\Phi_D$  is the fluorescence quantum yield of the donor,  $F_D$  is the normalized fluorescence of the donor,  $\epsilon_A$  is the molar absorptivity of the acceptor and  $\lambda$  is the wavelength. The integral in Equation 2.11 is called the overlap integral and is illustrated in Figure 2.7B. The orientation factor  $\kappa^2$

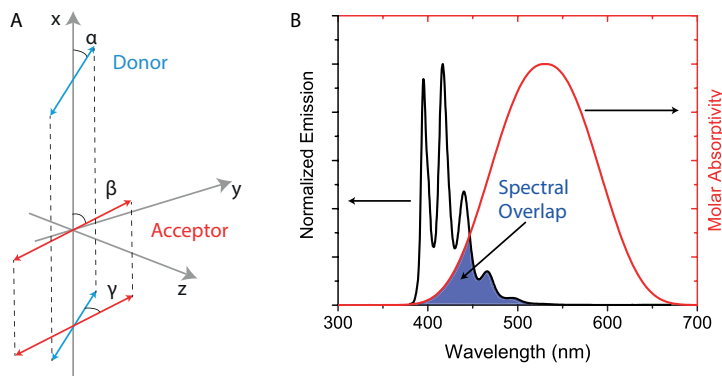


Figure 2.7: Illustration of angles between donor (blue) and acceptor (red) transition dipole moments used for calculating the orientation factor,  $\kappa^2$ , for a donor-acceptor FRET pair.

lies between 0 and 4, where  $2/3$  is the value for two freely rotating chromophores. If the chromophores are fixed  $\kappa^2$  can be calculated from Equation 2.12, where the angles  $\alpha$ ,  $\beta$  and  $\gamma$  are defined as in Figure 2.7A.<sup>60</sup>

$$\kappa^2 = [\cos(\gamma) - 3\cos(\alpha)\cos(\beta)]^2 \quad (2.12)$$

If the transition dipole moments are perpendicular to each other, for example if  $\alpha=0$  and  $\beta=\gamma=90^\circ$ , energy transfer is not possible since  $\kappa^2=0$ .

If  $R_0$  and the actual distance between donor and acceptor,  $r$ , is known, the FRET efficiency ( $\eta_{FRET}$ ) can be determined according to equation 2.13.

$$\eta_{FRET} = \frac{R_0^6}{R_0^6 + r^6} \quad (2.13)$$

$\eta_{FRET}$  can also be determined from the amount of quenched donor emission as in Equation 2.14

$$\eta_{FRET} = 1 - \frac{F_{DA}}{F_D} \quad (2.14)$$

where  $F_{DA}$  and  $F_D$  is the integrated donor fluorescence intensity with and without acceptor present respectively. The fluorescence intensities in Equation 2.14 can also be exchanged for the fluorescence lifetimes.

### Dexter Energy Transfer

Dexter energy transfer, or electron exchange energy transfer, can be viewed as the simultaneous transfer of two electrons as described in Figure 2.8. For energy transfer to occur through a Dexter mechanism there must be orbital overlap between the donor and acceptor. Since the electron density in an orbital decreases exponentially with distance from the nucleus, the orbital overlap, and thus rate of energy transfer, will decrease

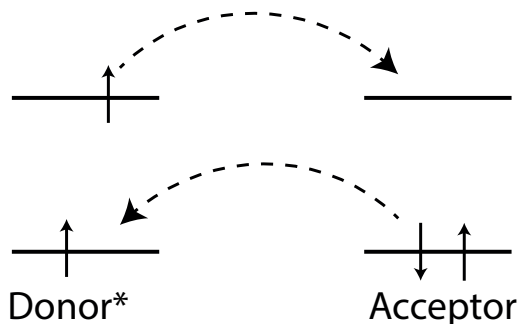


Figure 2.8: Schematic illustration of Dexter energy transfer from a triplet excited donor to an acceptor. Energy transfer is also possible from a singlet excited donor.

exponentially. Equation 2.15 describes the distance dependence of the energy transfer rate  $k_{ET}$ :<sup>59,67–69</sup>

$$k_{ET} \propto J \exp(-\beta R_{DA}) \quad (2.15)$$

where  $R_{DA}$  is the distance between the donor and acceptor.  $J$  is the spectral-overlap between the donor and acceptor and  $\beta$  describes the sensitivity to distance separation.<sup>59,67–69</sup>

In principle, this means that the donor and acceptor must be very close or come into contact in order to transfer the energy. In solution this occurs through collisions between the two diffusing molecules. Since the rate of energy transfer between two molecules in contact usually is fast the transfer between freely diffusing molecules is limited by the rate of bimolecular collisions resulting in an encounter complex.<sup>59,70,71</sup> The efficiency of energy transfer through diffusion depends on the acceptor concentration  $[A]$  and the bimolecular quenching rate constant  $k_{TET}$  and can be obtained from the Stern-Volmer relationship in Equation 2.16:

$$\frac{F_D}{F_{DA}} = \frac{\tau_D}{\tau_{DA}} = 1 + k_{TET}\tau_D[A] \quad (2.16)$$

where  $F$  and  $\tau$  are the emission intensity and lifetime of the donor, respectively. The subscript  $DA$  and  $D$  is for the case with and without acceptor, respectively.  $k_{TET}$  can be estimated from  $k_{ET}$  and vice versa, if the association ( $k_d$ ) and dissociation ( $k-d$ ) rates of the encounter complex is known, through Equation 2.17.<sup>59,70,71</sup>

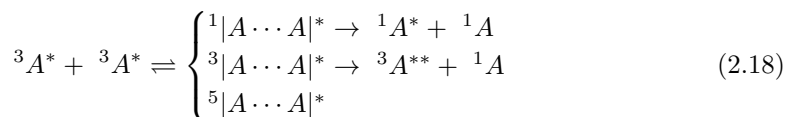
$$k_{TET} = \frac{k_d k_{ET}}{k_{-d} + k_{ET}} \quad (2.17)$$

### Triplet-Triplet Annihilation

The energy transfer processes discussed so far have involved one excited molecule, the donor, that transfers its energy to a ground state molecule, the acceptor. Triplet-triplet annihilation (TTA) is a special case of energy transfer where two triplet excited molecules interact.<sup>59</sup> As described in section 2.2.2 a triplet molecule can exist in three distinct forms, combining two molecules in their triplet states then leads to  $3 \times 3$  different combinations.

These combinations result in either a singlet, triplet or quintet encounter complex. For example if a molecule in a  $T_+(\uparrow\uparrow)$  state combines with another molecule in  $T_-(\downarrow\downarrow)$  the overall spin cancels out ( $\uparrow\uparrow\downarrow\downarrow$ ) and the result is a singlet complex. Considering the number of spin states in each spin configuration, 1 for singlet, 3 for triplet and 5 for quintet, the probability of forming a singlet, triplet or quintet configuration is 1/9, 3/9 and 5/9, respectively.<sup>59,72,73</sup>

The encounter complex can dissociate either back into its original two triplet molecules, or the energy of the two triplets ( $2 \times E_{T_1}$ ) can be fused and end up on one of the molecules, leaving the other in its ground state. For fusion of the energy to occur there must exist an energetically accessible excited state with the same spin-multiplicity as the overall encounter complex.<sup>59,72-74</sup> The different possibilities for two triplet excited molecules ( ${}^3A^*$ ) to interact are described in Equation 2.18. The reactions proceeding to the right in Equation 2.18 can only occur if the energy relation in Equation 2.19 is fulfilled.



$$2 \times E_{T_1} \geq E_x \quad (2.19)$$

In Equation 2.19  $E_x$  is the energy of the formed excited state. For a singlet encounter complex the formed state would be the first excited singlet state ( $S_1$  or  ${}^1A^*$ ) and for the triplet the second excited triplet state ( $T_2$  or  ${}^3A^{**}$ ). In most cases the first excited quintet state is energetically inaccessible and the encounter complex disassociates into the original triplet molecules.<sup>59,72-75</sup> The fusion of two excited triplets into one excited singlet is the basis for photon upconversion through TTA and is described in more detail in the next section.

#### 2.4.4 Photon Upconversion Through Triplet-Triplet Annihilation

To achieve upconversion through TTA two low energy photons must produce two excited triplets which through TTA can form a singlet excited state that relaxes to the ground state by fluorescence, emitting a photon of higher frequency. To achieve this, a combination of two molecules is used, a triplet sensitizer (*Sen*) and an annihilator (*A*). The triplet sensitizer absorbs a photon (Equation 2.20a) and forms its first excited triplet state through ISC, Equation 2.20b. Through triplet energy transfer (TET) (section 2.4.3) the annihilator is excited to its first excited triplet state, Equation 2.20c. Two triplet excited annihilators can subsequently undergo TTA to form one singlet excited annihilator,

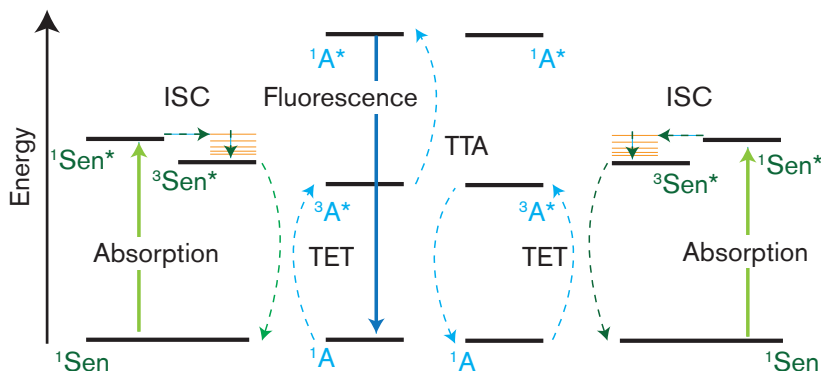
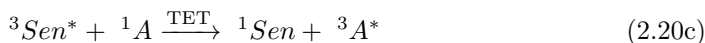
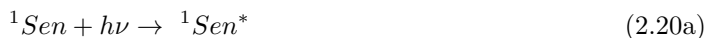


Figure 2.9: Jablonski diagram describing the processes involved in sensitized triplet-triplet annihilation photon upconversion. First a sensitizer absorbs a low energy photon and rapidly populates its first triplet excited state after intersystem crossing (ISC). The triplet energy is then transferred to an annihilator molecule through triplet energy transfer (TET) generating one triplet excited annihilator molecule. When two triplet excited annihilator molecules come together they can undergo triplet-triplet annihilation to generate one singlet excited annihilator, which can decay to its ground state through fluorescence.

Equation 2.20d, emitting a photon upon relaxation, Equation 2.20e.



The processes described by Equations 2.20a-2.20e are shown in a Jablonski diagram in Figure 2.9. Except for the energy requirement in Equation 2.19, Figure 2.9 also illustrates some other energetic considerations. For example, the sensitizer's singlet-triplet splitting is ideally small to minimize energy loss. Furthermore the difference between the sensitizer and annihilator triplet energies should also be small, but exothermic in order to achieve efficient energy transfer. These and other design considerations for sensitizer-annihilator pairs will be discussed further in Chapter 4 in relation to the upconversion efficiency.

### Photon Upconversion Efficiency

It is not straight forward to evaluate the efficiency of TTA-UC systems. The most common quantity to report regarding the efficiency is the upconversion quantum yield  $\Phi_{UC}$ .<sup>27</sup> The upconversion quantum yield is the number of emitted high-energy photons compared to the number of absorbed low energy photons. As TTA-UC requires two low energy photons

to produce one high energy photon the maximum quantum yield for an upconversion system is 50% and all reported values in this Thesis are on a basis of 50% maximum.

$\Phi_{UC}$  is challenging to determine and comparing reported values requires the knowledge of the exact experimental conditions, such as sensitizer and annihilator concentrations, light intensity and oxygen concentration.<sup>27</sup> The upconversion quantum yield is the product of the quantum yields for each step required to produce upconverted photons, Equation 2.21:

$$\Phi_{UC} = f\Phi_{ISC} \times \Phi_{TET} \times \Phi_{TTA} \times \Phi_f \quad (2.21)$$

where  $f$  is a spin-factor accounting for the probability of forming a singlet state upon TTA,  $\Phi_{ISC}$  is the quantum yield of intersystem crossing of the triplet sensitizer,  $\Phi_{TET}$  is the triplet-energy transfer efficiency from sensitizer to annihilator,  $\Phi_{TTA}$  is the triplet-triplet annihilation quantum yield and  $\Phi_f$  is the fluorescence quantum yield of the annihilator. It is, however, not always practical to determine each of these quantum yields individually for an upconverting system. Instead it is common to apply the method of relative actinometry which is frequently used for normal fluorescence quantum yield determination and described in the Methods section 7.1.1 and Equation 7.3.

In solutions with low oxygen concentration (*e.g.* degassed), with appropriate sensitizer and annihilator concentrations  $\Phi_{ISC}$ ,  $\Phi_{TET}$ ,  $\Phi_{TTA}$  and  $\Phi_f$  can approach unity, and the limiting factor is then the spin-factor  $f$  or any other unaccounted loss factor. Initially it was believed that  $f$  would be 1/9 as the spin-statistical probability of forming a singlet upon TTA, thus limiting  $\Phi_{UC}$  to 5.5% (50% of 1/9).<sup>72,73</sup> Efficiencies far exceeding 5.5% has been reported since, thus disproving this limit.<sup>20,39,72,76</sup> It has been argued that since the quintet state seldom partakes in TTA,  $f$  will be 2/5 in the case when  $T_2$  is accessible, and approach unity if also the  $T_2$  state is inaccessible.<sup>39,72,73,76</sup>

### Intensity Dependence

The reactions described in Equations 2.20a-2.20e and Figure 2.9 can be described by a set of coupled rate equations, Equations 2.22a-2.22e. Since the rate of ISC in a good sensitizer is fast, in comparison to other competing processes, it has been assumed in Equations 2.22a and 2.22b that the triplet state formation is described by the rate of absorption, multiplied by the ISC quantum yield,  $\Phi_{ISC}$ .

$$\frac{d[{}^1S]}{dt} = -k_{EX}[{}^1S]\Phi_{ISC} + k_{TET}[{}^3S^*][{}^1A] + k_{PS}[{}^3S^*] \quad (2.22a)$$

$$\frac{d[{}^3S^*]}{dt} = k_{EX}[{}^1S]\Phi_{ISC} - k_{TET}[{}^3S^*][{}^1A] - k_{PS}[{}^3S^*] \quad (2.22b)$$

$$\frac{d[{}^3A^*]}{dt} = k_{TET}[{}^3S^*][{}^1A] - 2k_{TTA}[{}^3A^*]^2 - k_{PA}[{}^3A^*] \quad (2.22c)$$

$$\frac{d[{}^1A^*]}{dt} = k_{TTA}[{}^3A^*]^2 - k_F[{}^1A^*] \quad (2.22d)$$

$$\frac{d[{}^1A]}{dt} = -k_{TET}[{}^3S^*][{}^1A] + k_{TTA}[{}^3A^*]^2 + k_F[{}^1A^*] \quad (2.22e)$$

where  $[^3S^*]$  and  $[^3A^*]$  are the sensitizer and annihilator triplet concentrations respectively. Correspondingly  $[^1A^*]$  and  $[^1A]$  are the concentrations of annihilator in the excited singlet and ground state respectively. The  $k_i$ 's are the rate constants of the different processes; triplet energy transfer (TET), sensitizer phosphorescence (PS), annihilator triplet decay (PA), triplet-triplet annihilation (TTA), annihilator fluorescence and excitation (EX).  $k_{EX}$  is calculated from the absorption cross section of the sensitizer,  $\alpha$ , in  $\text{cm}^2$  and the photon flux,  $I_{EX}$ , in  $\text{photons} \cdot \text{s}^{-1} \cdot \text{cm}^{-2}$ ) according to Equation 2.23. In Equations 2.22a-2.22e above the spin-factor has not been considered.

$$k_{EX} = \alpha I_{EX} \quad (2.23)$$

From Equation 2.22c it is evident that the annihilator triplet can decay through two distinct pathways. Either through first-order intrinsic deactivation ( $k_{PS}[^3S^*]$ ) or through TTA ( $2k_{TTA}[^3A^*]^2$ ). Which of the pathways is dominating affects the efficiency of the system. At low excitation intensities, where  $[^3A^*]$  is low, the TTA pathway is small and can be neglected ( $2k_{TTA}[^3A^*]^2 \ll k_{PS}[^3A^*]$ ). With steady-state conditions and assuming efficient TET from sensitizer to annihilator it can be shown that the intensity of upconverted emission, which is proportional to  $[^1A^*]$ , is quadratically dependent on the excitation intensity  $I_{EX}$ :<sup>77</sup>

$$[^1A^*] = \frac{k_{TTA}}{k_{FA}k_{PA}^2} (I_{EX}\alpha[^1S])^2 \quad (2.24)$$

On the other hand, at high excitation intensities  $[^3A^*]$  is high, the TTA pathway is large and the intrinsic decay can be neglected ( $2k_{TTA}[^3A^*]^2 \gg k_{PS}[^3A^*]$ ). Using the same assumptions as above it can be shown that the upconverted emission intensity depends linearly on the excitation intensity:<sup>77</sup>

$$[^1A^*] = \frac{1}{2k_{FA}} I_{EX}\alpha[^1S] \quad (2.25)$$

It is therefore important to note that  $\Phi_{UC}$  will increase with the excitation intensity until the linear regime in Equation 2.25 is reached. Figure 2.10 shows the intensity dependence of  $\Phi_{UC}$  and upconversion emission, calculated for a diffusion limited system, without considering spin-statistics, *i.e.* based on Equations 2.22a-2.22e.

The intensity where the dependence shifts from quadratic to linear is also an important parameter for UC systems and is referred to as the threshold intensity  $I_{th}$ . It is obtained by equating Equations 2.24 and 2.25.

$$I_{th} = \frac{k_{PA}^2}{2k_{TTA}\alpha[^1S]} \quad (2.26)$$

A low  $I_{th}$  is desired in order to achieve efficient upconversion even with relatively low excitation intensities, *e.g.* sunlight. For an efficient and practical system  $I_{th}$  should be lower than the intensity of the Sun. It should be noted that Equations 2.24-2.26 are only valid when the assumption of efficient TET is met, which is easily achieved in solution. In solid matrices, however, TET might not be efficient and pure linear and quadratic regions might not be reached.<sup>49</sup>

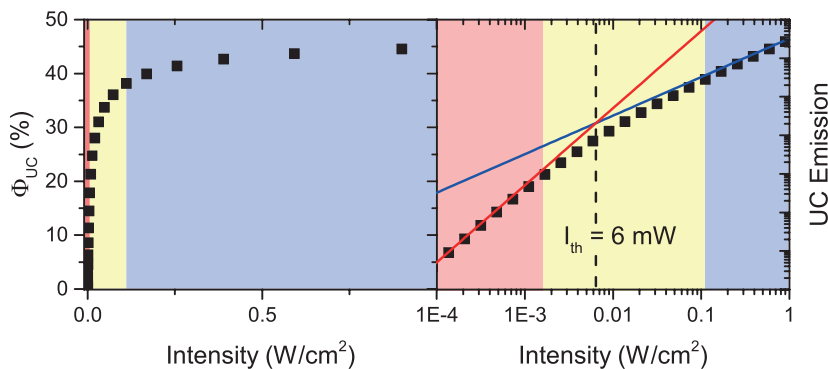


Figure 2.10: Calculated theoretical upconversion quantum yield ( $\Phi_{UC}$ ) (left) and upconversion emission intensity (right) as a function of excitation intensity. Red and blue lines correspond to Equations 2.24 and 2.25. The linear region is highlighted with blue, the quadratic region with red and the intermediate region with yellow.

### 2.4.5 Semiconductor Nanocrystals

Atoms or molecules arranged in an ordered structure form crystals. If the size of the crystal domain in at least one dimension is on the order of nanometers, they are called nanocrystals. The properties of nanocrystals depend on the size, shape and material, herein only semiconductor nanocrystals (NCs) will be considered. Being in the same size range as molecules it is not surprising that NCs exhibit atom and molecule like properties, such as distinct energy levels. Furthermore, many of the above described processes have also been observed and studied in systems containing NCs. For example triplet<sup>52,54,78,79</sup> and singlet<sup>80-84</sup> energy transfer as well as electron transfer<sup>84,85</sup> between organic molecules and NCs have all been observed and studied to varying extents.

Changing the size and shape of a nanocrystal will change its energy level distribution and hence also its optical and electronic properties.<sup>86</sup> The size tunable optical properties of spherical nanocrystals can be described by the Brus Equation, Equation 2.27.<sup>87-89</sup> Taking into account the bulk band-gap energy of the material,  $E_{bg}$ , the radius of the crystal,  $r$ , the effective mass of the electron and hole,  $m_e^*$  and  $m_h^*$ , respectively, the optical bandgap  $\Delta E$  of a spherical nanocrystal can be calculated.<sup>87-89</sup>

$$\Delta E = E_{bg} + \frac{h^2}{8r^2} \left( \frac{1}{m_e^*} + \frac{1}{m_h^*} \right) \quad (2.27)$$

In NCs the energy level separation is much smaller compared to molecules.<sup>90,91</sup> Therefore the filled and unfilled states are often effectively considered as continuous bands, separated in energy by the band-gap  $\Delta E_{bg}$ , corresponding to the HOMO-LUMO difference. Figure 2.11A schematically illustrates the difference between energy levels in molecules, NCs and bulk semiconductors. Furthermore, the spin-orbit coupling is relatively large in NCs leading to a small singlet-triplet splitting in NCs, on the order of  $k_b T$ .<sup>91,92</sup>

An atom in a crystal will have substantial orbital overlap and electron sharing with its neighbouring atoms. Since the surface of a crystal is a disruption to the ordered structure,

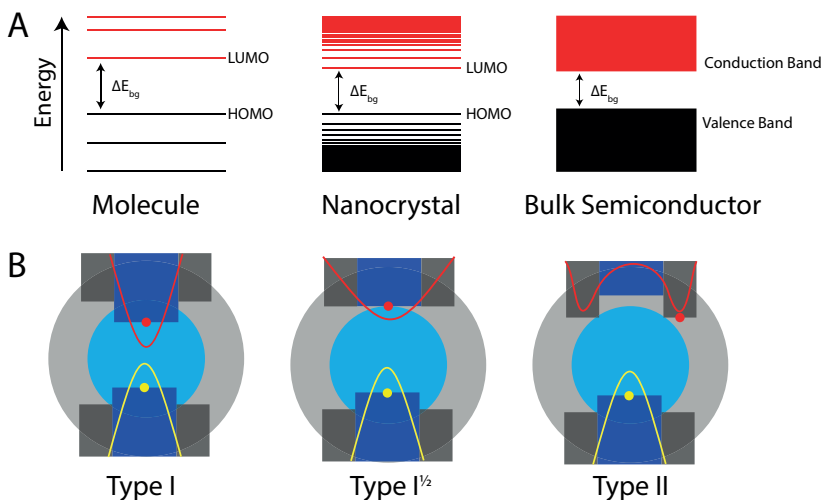


Figure 2.11: A) Schematic illustration of the energy level distribution in a molecule, semiconductor nanocrystal (NCs) and semiconductor bulk material. Occupied states are coloured black and unoccupied states red. B) Wave function localization of the exciton hole (yellow) and electron (red) in three types of core-shell NCs. For simplicity the NC energy levels are illustrated as continuous bands. In Type I core-shell NCs the band-gap of the core (blue) lies within the band-gap of the shell (grey) and both the electron and hole wave functions are localized to the core material. With a hole (or electron) localized to the core and the electron (or hole) distributed over the whole NC the core-shell NC is of Type I<sup>1/2</sup>. A Type II core-shell NC has one of the exciton wave functions localized to the core and the other localized in the shell, here illustrated for a hole localized in the core. Such an localization occurs if the band-gaps are aligned in a staggered manner.

atoms at the surface will have electrons and orbitals not shared with any neighbouring atoms. These non interacting orbitals are also referred to as "dangling bonds". As the surface to volume ratio is high in NCs, "dangling bonds" and surface interactions can greatly influence NC properties.<sup>86,90</sup> Often carboxylic acids, amines or thiols, are added as passivating ligands to the "dangling bonds". Any unpassivated sites can lead to a low energy state within the NC band-gap resulting in a trap state affecting the optical properties. To achieve highly emissive NCs surface traps should be minimized.<sup>86,90</sup>

### Core-Shell Nanocrystals

It is possible to reduce the amount of surface traps by growing a shell on the NC core. In a core-only NC the exciton wave functions of both hole and electron are delocalized over the whole NC, Figure 2.11B. In a core-shell NC, however, the relative energetic properties of the materials used as core and shell affects the localization of the exciton wave functions. As described in Figure 2.11B the localization of the wave functions can be divided into three categories; Type I, Type I<sup>1/2</sup> and Type II.<sup>86,93</sup>

A core material with a band-gap lying completely within the band-gap of the shell

results in both the excited electron and hole wave functions being localized in the core, known as a Type I core-shell NC.<sup>86,93</sup> In a Type II core-shell NC the band-gaps are aligned in an alternate manner resulting in the hole and electron wave functions being localized in different parts of the NC. The intermediate Type I<sup>1/2</sup> NCs have either the electron or hole wave function localized and the other wave function delocalized over the whole NC.<sup>86,93</sup>

## 2.5 Binding Dynamics

So far we have considered single molecules, and the interaction between excited molecules with either ground state molecules or other molecules in the excited state. This section covers interactions between two ground state molecules through the formation of dative bonds. The binding of two molecules through dative bonds can be described by the equilibrium equation:



where  $k_d$  is the rate constant of association and  $k_{-d}$  the rate constant of dissociation. An equilibrium constant ( $K_{bind}$ ) can be defined as in Equation 2.29

$$K_{bind} = \frac{k_d}{k_{-d}} = \frac{[AB]}{[A][B]} = \frac{[AB]}{([A]_0 - [AB])([B]_0 - [AB])} \quad (2.29)$$

where  $[AB]$ ,  $[A]$  and  $[B]$  are the concentrations of the complex AB, molecule A and molecule B, respectively.  $[A]$  and  $[B]$  are related to the total concentrations of A and B,  $[A]_0$  and  $[B]_0$  respectively, through the amount of formed complex. The analytical solution of Equation 2.29 with regards to  $[AB]$  is:

$$[AB] = \frac{K_{bind}[A]_0 + K_{bind}[B]_0 + 1 - \sqrt{(K_{bind}[A]_0 + K_{bind}[B]_0 + 1)^2 - 4K_{bind}^2[A]_0[B]_0}}{2K_{bind}} \quad (2.30)$$

Equation 2.30 can be modelled to experimental data to obtain  $K_{bind}$  which is related to the binding strength.<sup>94</sup> Evaluating the binding strength is important for dynamic complexes as it gives an estimate of the complex lifetime, furthermore the complex concentration can be determined from the initial concentrations of the coordinating species.



# Triplet Sensitizers for Efficient Triplet-Triplet Annihilation

To achieve photon upconversion through triplet-triplet annihilation (TTA) two types of molecules are needed, a sensitizer and an annihilator. This chapter focuses on design parameters for triplet sensitizers and discusses the two different types described in the literature; molecule and nanocrystal based sensitizers. Furthermore, based on the work in Paper IV, an example of nanocrystal based sensitizers is given to demonstrate the tunability of these systems. Examples of molecular sensitizers are also discussed in Chapter 5, in combination with annihilators capable of coordinating to the sensitizer. The annihilator is discussed further in Chapter 4.

## 3.1 Design Parameters for Triplet Sensitizers

From the bimolecular processes necessary to achieve TTA-UC, described in Figure 2.4 and Equations 2.20a-2.20e, one can derive a number of fundamental design criteria regarding the sensitizer and annihilator pair.<sup>95,96</sup> The sensitizer should absorb a photon and efficiently transfer triplet excitation energy to the annihilator, therefore a sensitizer should have:

1. high absorption coefficient,
2. close to quantitative triplet yield,
3. long lived triplet state ( $>10\mu\text{s}$ ),
4. small singlet-triplet splitting (to minimize energy losses),
5. small spectral overlap with annihilator emission (to avoid reabsorption of upconverted emission).

### 3.1.1 Molecular Sensitizers

In molecules high molar absorptivities are achieved by large conjugated systems. Efficient intersystem crossing (ISC) is harder to predict based solely on molecular structure.<sup>51</sup> There are, however, some structural features that often are accompanied by efficient

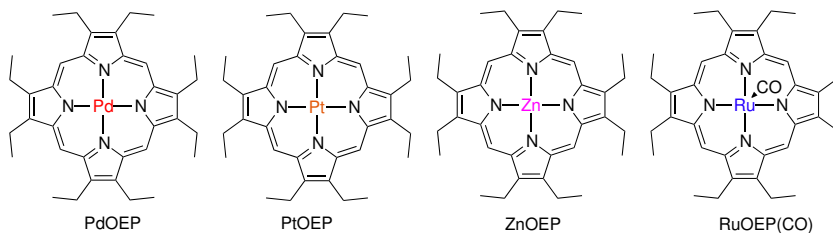


Figure 3.1: Structures of the molecular triplet sensitizers Palladium, Platinum, Zinc and Ruthenium-Carbonyl octaethylporphyrin (PdOEP, PtOEP, ZnOEP, and RuOEP(CO) respectively).

ISC. For example, molecules with low lying  $n, \pi^*$  states, such as benzophenone, often show efficient ISC.<sup>51,59</sup> Further more, molecules with a heavy atom, for example metal complexes, are also efficient in forming triplet states.<sup>51,59</sup>

For sensitized triplet-triplet annihilation, metal complexes are the most common types of sensitizer as they usually have comparatively large absorptions in the visible and also approaching the NIR-region.<sup>13,27,51,97</sup> Of the metal complexes used those based on porphyrin structures are particularly popular since they not only have high molar absorptivities and efficient ISC, but also display a spectral window with low absorption where the upconverted emission is not reabsorbed.<sup>13,27</sup> This has lead to many efficient examples of upconversion in the visible region.<sup>13,18,20,41,98-100</sup> The structures of the four metal porphyrins used for the studies herein are shown in Figure ??.

A challenge with molecular based sensitizers is to develop efficient sensitizers absorbing in the NIR. To red-shift the absorption, large conjugated systems are necessary, often resulting in long and complicated synthetic schemes.<sup>97,101</sup> When the absorption red-shifts, the energy difference between the ground state and triplet excited state decreases, as such the relaxation back to the ground state becomes faster<sup>59</sup> possibly out-competing the diffusion limited triplet energy transfer to the annihilator. Despite these challenges, there are some examples in the literature of NIR sensitizers used for TTA-UC.<sup>97,102-105</sup>

Furthermore, efficient high energy sensitizers for visible to UV upconversion are also scarce.<sup>106-108</sup> This can partly be explained by the lack of good UV annihilator partners. For example UV emitters often have relatively high  $E_{T_1}$  compared to  $E_{S_1}$  and since the sensitizer  $S_1$  and  $T_1$  levels both must lie between the annihilator  $S_1$  and  $T_1$  a sensitizer with small singlet-triplet splitting is necessary. Sensitizers displaying thermally activated delayed fluorescence (TADF) are suitable candidates having narrow  $S_1$  and  $T_1$  gaps. Such sensitizers have been successfully used by Yanai *et al.* for visible to UV upconversion.<sup>108</sup>

### 3.1.2 Semiconductor Nanocrystal Sensitizers

Compared to molecular sensitizers those based on semiconductor nanocrystals (NCs) have higher molar absorptivities and size tunable optical properties that are easily addressed through facile synthetic procedures.<sup>86,90</sup> It was recently shown that semiconductor NCs can donate to<sup>52,54</sup> and accept<sup>78,79</sup> triplet excitons from organic molecules, opening the field of NC based triplet sensitizers. It was early discovered that due to the relatively short excited

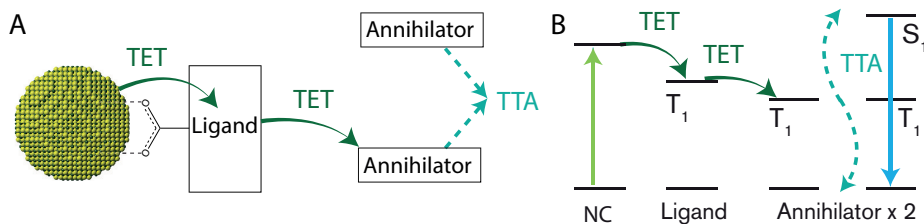


Figure 3.2: A) Schematic illustration of the nanocrystal (NC) sensitized triplet-triplet annihilation photon upconversion. Triplet energy transfer from the NC to a surface bound ligand with a long lived triplet state, followed by triplet energy transfer (TET) to the annihilator. Photon upconversion is achieved after triplet-triplet annihilation between two triplet excited annihilators. B) Energy diagram representation of the processes in A.

lifetime of NC excited states a transmitter ligand with a long triplet lifetime coordinated to the NC surface, capable of accepting the triplet energy and thus extending the lifetime, is necessary to achieve efficient sensitization and subsequent TTA-UC.<sup>52,54,109–111</sup> This concept is illustrated in Figure 3.2

Attaching the transmitter ligand to the NC requires an anchoring group. Carboxylic acid groups are often the anchoring group of choice since it allows for binding to the nanoparticle without quenching of the NC emission,<sup>52,54,112</sup> although other groups are possible.<sup>112–114</sup> Furthermore, the transmitter ligand should have a suitable triplet energy to function as an acceptor and often acene derivatives are used.

There is still plenty to learn regarding the triplet energy transfer process between NCs and surface anchored organic molecules in order to develop efficient NC sensitizers. One possible drawback with NC based sensitizers is the lack of an optical window that is transparent for annihilator emission, resulting in reabsorption of the upconverted light. Depending on the concentration and optical densities in an actual application it might not be a problem. Reabsorption can, however, not be neglected *a priori* and should be considered when designing annihilator-sensitizer pairs and devices.

Due to the large molar absorptivities and facile synthesis of NC NIR absorbers efficient NIR-to-VIS upconversion has already been demonstrated.<sup>52,53,115,116</sup> As NC also have small  $S_1$ - $T_1$  splitting they could potentially be used as sensitizers for VIS-to-UV upconversion. This is studied in Paper IV where CdS and CdS/ZnS core-shell NCs are used as sensitizers and 2,5-diphenyloxazole (PPO) as the annihilator to upconvert 405 nm blue light to 355 nm UV light.

## 3.2 Studying Triplet Energy Transfer from Sensitizer to Annihilator

The rate of triplet energy transfer (TET) in solution is described by the bimolecular quenching rate constant  $k_{TET}$  (see section 2.4.3), often obtained from the Stern-Volmer relation, Equation 2.16. Many molecular sensitizers are phosphorescent and have well defined triplet lifetimes (*i.e.* following a single exponential decay) making it easy to

follow the quenching, and thus the triplet energy transfer. Therefore the TET is well understood in molecular systems. Even when a molecular sensitizer is not phosphorescent the quenching of the triplet lifetime can often be followed through transient absorption measurements and a Stern-Volmer plot can be constructed.

For NCs it becomes more difficult. First the triplet energy transfer occurs in two steps; TET from the NC to the bound ligand, followed by TET from the ligand to the free annihilator, secondly the lifetime of a NC is rather illdefined with multiple decay constants. The first difficulty can be somewhat simplified since the free annihilator is in large excess and the TET from ligand to annihilator is often assumed to be quantitative, the limiting step thus being TET from NC to ligand. Therefore the rate constant of interest in NC based sensitizer system is the rate of triplet energy transfer from NC to ligand,  $k_{ET}$ , rather than the bimolecular TET rate constant  $k_{TET}$ . The same is also true for molecular systems where the TET does not occur through a bimolecular step, for example when the annihilator is coordinated to the sensitizer as described in Chapter 5.

The rate of energy transfer can be studied either directly through transient absorption or indirectly by time-resolved photoluminescence (TRPL) measurements. TRPL is a much easier technique, however, since the NC can be quenched by other mechanisms than TET when attaching a ligand there is not always a correlation between the quenching and the TET. Transient absorption is a more direct way of studying the TET if the formation of the triplet excited ligand can be monitored directly.<sup>54</sup> In the case of CdSe and the common anthracene based ligands this is possible, but complicated as the weak absorption of the anthracene is easily drowned in the strong CdSe transient absorption signal having multi exponential decays.<sup>54,114</sup> The challenges in studying TET in NC-ligand systems are the basis for some uncertainties, for example it is still debatable which states in the NC are responsible for TET or if all excitons are available for TET to the ligand. Also, TET in these inorganic-organic hybrid materials has been observed to occur by both a direct Dexter mechanism and a delayed charge transfer mediated mechanism depending on the systems.<sup>54,117</sup> The results in Paper IV and references<sup>113,115</sup> indicate that the surface trap states are not involved in the TET, and actually impede TET.

### 3.3 CdS/ZnS core-shell NCs for Visible to Ultraviolet Upconversion

Lead sulfide (PbS), lead selenide (PbSe) and cadmium selenide (CdSe) NCs have all been employed as triplet sensitizers for NIR or visible upconversion, respectively.<sup>52-54,112-116</sup> Cadmium sulfide (CdS) NCs which are related to the other chalcogenide NCs, mentioned above, usually have an absorption maximum at the high energy end of the visible spectrum, between 400-500 nm, depending on the size of the crystal (corresponding to 3.1-2.5 eV). This makes CdS NCs good candidates as sensitizers for VIS-to-UV upconversion, for example annihilators previously used for VIS-to-UV upconversion in all molecular systems often have  $T_1$  energies in the range 2.3-3.0 eV.<sup>106,108,118</sup> To evaluate CdS based NCs for VIS-to-UV upconversion we use PPO as the annihilator, 1-naphthoic acid (1NCA) or PPO as the transmitter ligand, and CdS NCs or CdS/ZnS core-shell NCs as sensitizers. The studied systems are illustrated in Figure 3.3.

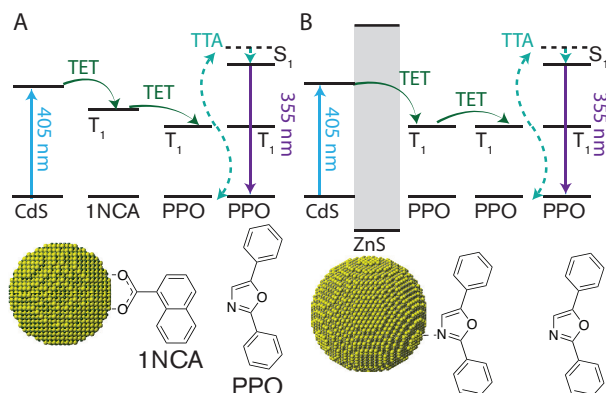


Figure 3.3: Schematic illustration of the studied VIS-to-UV triplet-triplet annihilation (TTA) photon upconversion systems. A) Triplet energy transfer from CdS nanocrystals (NCs) to a bound 1-naphthoic acid (1NCA) molecule, followed by triplet energy transfer (TET) to the annihilator 2,5-diphenyloxazole (PPO). PPO undergoes TTA with another triplet excited PPO upconverting visible light to UV photons. B) Like in A but for CdS/ZnS core-shell NCs with PPO as both the bound transmitter ligand and free annihilator. Adapted from Ref. 127 with permission from The Royal Society of Chemistry.

### 3.3.1 Synthesis and Characterization of Nanocrystals

Synthesis of CdS, CdSe, PbS or PbSe NCs is often done by a hot injection method. In short, for CdS NCs, CdO is dissolved in degassed oleic acid at high temperature, whereupon elemental sulfur is injected followed by rapid cooling to room temperature. CdS NCs with 3.6 nm and 4.3 nm diameter are obtained in this way. A ZnS shell is subsequently grown by stirring the CdS cores with zinc-diethyldithiocarbamate in oleylamine and 1-octadecene at 185°C. The CdS cores are covered by 1-5 monolayers (ML) of ZnS. The absorption and emission spectra of the synthesized NCs are shown in Figure 3.4 where **XML** denotes **X** number of monolayers (ML). For comparison the absorption and emission of the annihilator 2,5-diphenyloxazole (PPO) is also shown.

As can be seen in Figure 3.4 and Table 3.1 the absorption and emission is initially redshifted upon growth of the first ZnS monolayer, followed by a blueshift with further growth, indicative of alloy formation at longer growth times.<sup>119,120</sup> The trend in the radiative rate constants,  $k_r$ , seen in Table 3.1, suggest a Type I localization of the exciton wave functions in the core-shell NC. Since the electron and hole wave functions are both confined to the core in a Type I core-shell NC the radiative rate is expected to increase compared to the core only NC but then to be independent on shell thickness.<sup>86,93</sup> The ZnS shell also passivates surface trap states, contributing to the observed increase in photoluminescence quantum yield,  $\Phi_{PL}$ , with shell growth. The passivation of trap states is essential to achieve efficient TET from the NC to the surface bound ligand, *vide infra*.

Upconverted emission is clearly observed in samples with CdS/ZnS core-shell NCs as sensitizer and PPO as the annihilator, even without 1NCA as the transmitter ligand, as shown in Figure 3.5A. Most likely PPO is capable of binding to the NC by the free

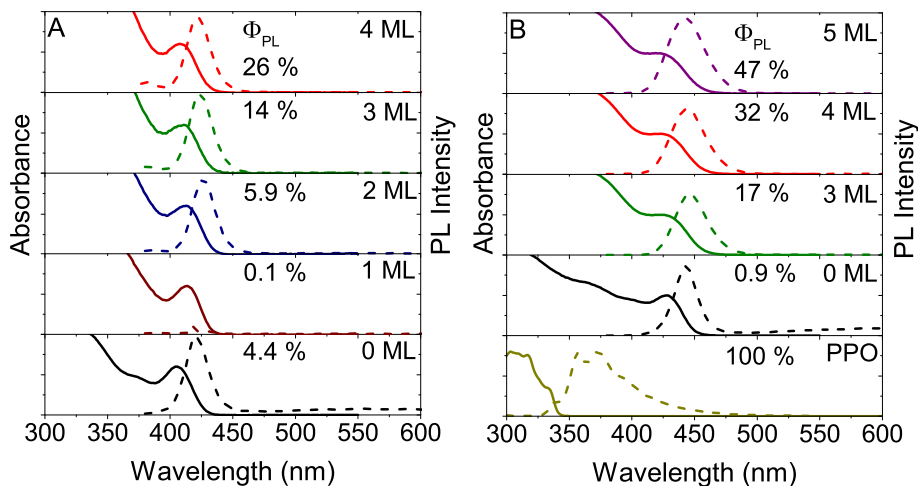


Figure 3.4: Absorption (solid) and emission (dashed) spectra of A) 3.6 nm diameter CdS core nanocrystals with 0-4 monolayers of ZnS (**0ML-4ML**) and B) 4.3 nm diameter CdS core nanocrystals with 0 and 3-5 monolayers of ZnS (**0ML, 3ML-5ML**) and the annihilator 2,5-diphenyloxazole PPO. Displayed are also the photoluminescence quantum yields ( $\Phi_{PL}$ ). Adapted from Ref. 127 with permission from The Royal Society of Chemistry.

electrons on the PPO nitrogen, thus PPO functions as both the annihilator and transmitter ligand. The upconversion quantum yield increases with increasing shell thickness up to 2.6% for **4ML**. Further shell growth results in a decrease in  $\Phi_{UC}$ . The increase in  $\Phi_{UC}$  correlates well with the quenching of the NC average lifetime,  $\Phi_Q$ , suggesting efficient TET, up towards 90%. The increase in  $\Phi_{UC}$  with shell thickness results from the increased passivation of the trap states originally present on the CdS core. The following decrease is then explained by an increased tunnelling barrier with increasing shell thickness.<sup>85,121</sup>

The passivation of surface trap states and efficient TET in the case for **4ML** CdS/ZnS core-shell NCs is also confirmed by fs-transient absorption, Figure 3.6. The lack of an absorption feature to the red side of the NC ground state absorption at 410 nm is indicative of successful removal of surface trap states, such an absorption feature corresponds to a trapped carrier induced Stark effect.<sup>122-126</sup> In fact, in samples with CdS core only NCs this feature is observed.<sup>127</sup> The  $T_1-T_n$  splitting in PPO is, relatively speaking, smaller compared to the  $T_1-T_n$  in the above mentioned anthracene based ligands, this results in the weak absorption of PPO not being obscured by the strong NCs absorption, rather it can be observed in the region 450-650 nm in Figure 3.6. The rise of the PPO absorption corresponds to the rate of TET and is in the case of **4ML** CdS/ZnS and PPO 67 ps, an order of magnitude faster than previously observed with 9-anthracenecarboxylic acid (9ACA) ligands on CdSe NCs.<sup>54</sup> In the case of 9ACA the carboxylic binding group is extended out from the anthracene core, whereas in PPO the hypothesized nitrogen binding site is in the chromophore structure, this difference can perhaps explain the faster TET, as it is well known that TET is distance dependent.<sup>111</sup> The type of binding group, however, also affects the rate and efficiency of TET.<sup>112</sup>

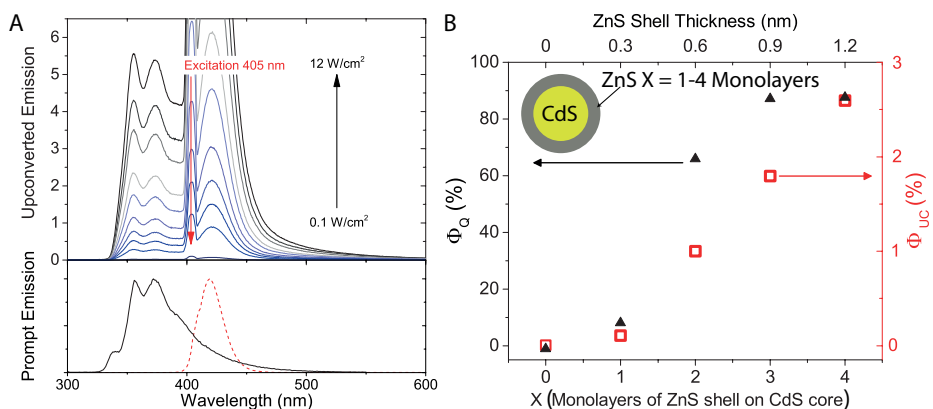


Figure 3.5: A) Top: Upconverted emission from 2,5-diphenyloxazole (PPO) in hexane, sensitized by 3.6 nm CdS core nanocrystals with 4 monolayers (**4ML**) of ZnS shell, excited at 405 nm. Excitation power density is varied from 0.1 W/cm<sup>2</sup> to 12 W/cm<sup>2</sup>. For clarity only spectra with excitation densities >1.3 W/cm<sup>2</sup> are displayed. Bottom: Prompt emission of PPO (solid) and **4ML** (dashed) for comparison. B) Photoluminescence quenching efficiency ( $\Phi_Q$ , black triangles) of 3.6 nm nanocrystals by 5.7 mM 2,5-diphenyloxazole (PPO) in hexane as a function of ZnS shell thickness. The upconversion quantum yield ( $\Phi'_{UC}$ , red squares) for the same samples is shown, upon 405 nm excitation at 7.1 W cm<sup>-2</sup>. Adapted from Ref. 127 with permission from The Royal Society of Chemistry.

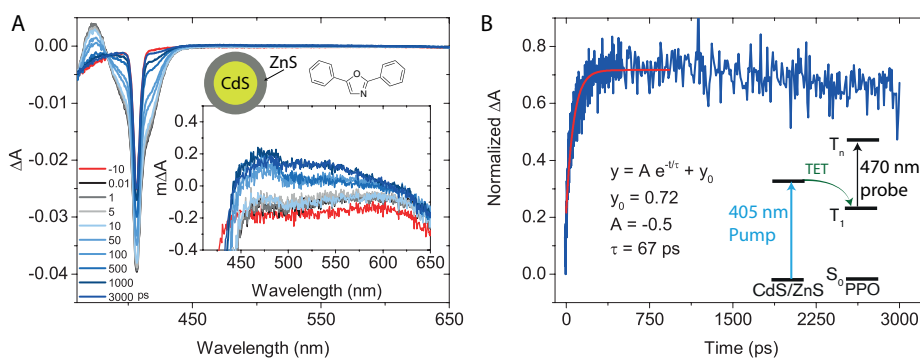


Figure 3.6: A) Transient absorption of CdS/ZnS core-shell nanocrystals **4ML** with 2,5-diphenyloxazole (PPO). Inset shows the region 450-650 nm. B) The rise of the signal at 470 nm in A (blue), corresponding to the PPO  $T_1$ - $T_n$  absorption and monoexponential fit (red). Also shown in B are the fitting parameters and an energy diagram of the  $T_1$ - $T_n$  transition of PPO after sensitization by CdS/ZnS. Adapted from Ref. 127 with permission from The Royal Society of Chemistry.

Table 3.1: The absorption maxima,  $\text{Abs}_{\text{max}}$ ; emission maxima,  $\text{Em}_{\text{max}}$ ; photoluminescence quantum yield,  $\Phi_{PL}$ ; and amplitude weighted average photoluminescence lifetimes of the 3.6 nm diameter CdS nanocrystals (NC) with ZnS shells of different monolayer (ML) thicknesses.  $k_r$  is the radiative rate of the NC and  $k_{nr}$  is the non-radiative rate.  $\langle \tau \rangle_0$  and  $\langle \tau \rangle_{\text{PPO}}$  indicate the NC lifetimes without and with the PPO annihilator.<sup>a</sup>

NC	$\text{Abs}_{\text{max}}$ (nm)	$\text{Em}_{\text{max}}$ (nm)	$\Phi_{PL}$ (%)	$k_r^b$ (s <sup>-1</sup> )	$k_{nr}^b$ (s <sup>-1</sup> )	$\langle \tau \rangle_0$ (ns)	$\langle \tau \rangle_{\text{PPO}}$ (ns)
<b>0ML</b>	405	421	4.4	$5.3 \times 10^5$	$0.1 \times 10^8$	16.9	17.1
<b>1ML</b>	414	418	0.1	$4.2 \times 10^5$	$7.0 \times 10^8$	0.25	0.23
<b>2ML</b>	413	427	5.9	$1.1 \times 10^7$	$1.8 \times 10^8$	1.35	0.46
<b>3ML</b>	411	425	14	$1.6 \times 10^7$	$1.0 \times 10^8$	4.11	0.53
<b>4ML</b>	407	422	26	$2.8 \times 10^7$	$0.8 \times 10^8$	5.80	0.72

<sup>a</sup>All measurements were done in hexane. <sup>b</sup> $k_r$  and  $k_{nr}$  are calculated from the intensity weighted average lifetimes  $\bar{\tau}$ . Adapted from Ref. 127 with permission from The Royal Society of Chemistry

Even though CdS/ZnS core-shell NC are efficient sensitizers, the overall upconversion quantum yield is still low, only 2.6% out of a maximum 50%. The main reason for the low efficiency is believed to be due to inherent properties of the annihilator which are discussed further in Chapter 4 section 4.3.

### 3.4 Summary and Evaluation of Hypotheses

The sensitizer must efficiently absorb photons, populate its triplet state and transfer the triplet energy to the annihilator. Both molecular and nanocrystal based sensitizers are capable of sensitizing triplet states of annihilators. For example, 2,5-diphenyloxazole (PPO) has been applied as an annihilator for visible to UV upconversion with both molecular<sup>106,107</sup> and, as described above, NC sensitizers.<sup>127</sup> In the all-molecular examples the upconversion quantum yield is very low,  $\sim 0.6\%$ . The example of NC sensitization from Paper IV showed a five fold improvement over the all molecular system. Since the main difference between these systems are the type of sensitizer used, the enhancement seen for NC based sensitization is due to superior properties of the CdS/ZnS core-shell NCs, *e.g.* increased TET from the NC sensitizer to PPO. The larger extinction coefficient of CdS/ZnS core-shell NCs compared to the molecular sensitizers also contribute to the improved efficiency.

Contrary to CdSe NCs where TET and upconversion is achieved for core only NCs,<sup>52,54,109</sup> TET is inefficient for CdS NCs without a ZnS shell, due to the quenching by trap states present in CdS core only NCs. As hypothesized, the ZnS efficiently removes trap states enabling efficient TET to PPO. Thus, by efficiently sensitizing PPO with CdS/ZnS core-shell NCs and achieving upconversion of visible 405 nm blue to 355 nm ultra violet light it is clearly demonstrated that also CdS based NCs are suitable triplet sensitizers, verifying the hypothesis.

# Design of Efficient Annihilator Molecules

In Chapter 3 the triplet sensitizer is discussed. This chapter focuses on design parameters for developing new efficient annihilator-sensitizer pairs. In particular the design of new annihilators with desired chemical and photophysical properties is covered. Initially a summary of the existing design parameters is given, which is followed up by a summary and discussion of the results presented in Paper I, Paper II and Paper IV in relation to the existing design criteria.

## 4.1 Design Parameters for the Annihilator

After absorption of a photon by a sensitizer the annihilator must be able to; accept the triplet energy from the sensitizer, fuse two triplet states into one excited singlet, and efficiently emit a photon. One can therefore conclude that efficient annihilators should have:<sup>95,96</sup>

1. a slightly lower triplet energy than that of the sensitizer, ensuring efficient triplet energy transfer,
2. a first excited triplet state energy ( $E_{T_1}$ ) greater than half of the energy of its first excited singlet state ( $E_{S_1}$ ), *i.e.*  $2 \times E_{T_1} \geq E_{S_1}$ , as described in Equation 2.19.
3. Optimally  $2 \times E_{T_1}$  is also less than the energy of the first quintet ( $E_{Q_1}$ ) state and second excited triplet state ( $E_{T_2}$ ), eliminating the possibility of forming these parasitic states during the TTA process.<sup>39,72,73,76</sup>
4. The annihilator should also have a high fluorescence quantum yield.

These four criteria for the annihilator and the five criteria described in Chapter 3 are the only nine guidelines for designing or choosing annihilator-sensitizer pairs. Finding annihilator-sensitizer pairs fulfilling all or most of the criteria is difficult. As we showed in Paper II, even if all these nine criteria are met, upconversion might still be inefficient. Most of the annihilators presented to date are well known fluorophores such as 9,10-diphenylanthracene (DPA), perylene, 9,10-bis(phenylethynyl)anthracene (BPEA) and other aromatic hydrocarbons and derivatives thereof with high fluorescence quantum

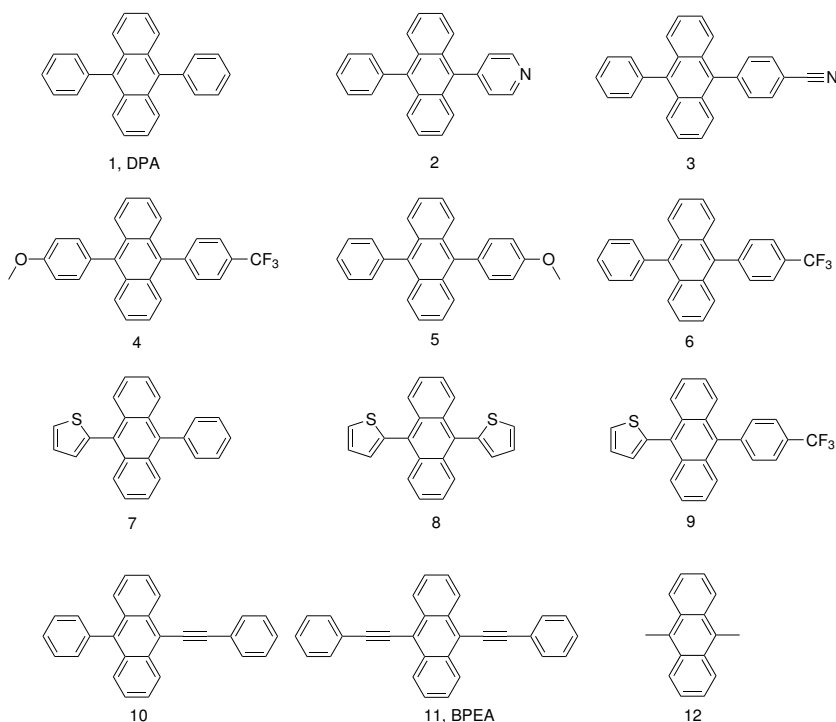


Figure 4.1: Structures of investigated 9,10-disubstituted anthracenes. Adapted from Ref. 129 with permission from The Royal Society of Chemistry.

yields.<sup>27</sup> Of these, DPA is probably the most frequently used annihilator, often combined with palladium or platinum octaethylporphyrin (PdOEP and PtOEP, respectively). DPA fulfils all but criterion 3 above. With  $E_{T_2}$  in the range of  $2 \times E_{T_1}$  the spin-factor  $f$  is predicted to be around 40%<sup>39</sup> and has been determined to  $\sim 50\%$  by Monguzzi *et al*<sup>128</sup> limiting the upconversion quantum yield  $\Phi_{UC}$  to  $\leq 25\%$ .

To understand the effect of the energy levels, two sets of anthracene based chromophores were studied (Paper I and Paper II) and the results are summarized in the following sections.

## 4.2 Substitution Effects on 9,10-Disubstituted Anthracenes

In an attempt to slightly alter the relative  $T_1$ ,  $T_2$  and  $S_1$  energies, nine different anthracene derivatives were synthesized (Structures **2-10**) and compared to DPA, BPEA and 9,10-dimethylanthracene (DMA). The structures are shown in Figure 4.1.

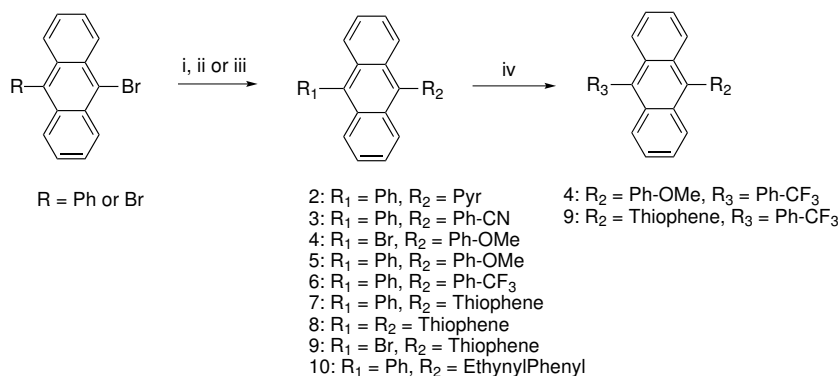


Figure 4.2: Synthesis of 9,10-disubstituted anthracenes. **i**) Suzuki coupling; Arylboronic acid, Pd(PPh<sub>3</sub>)<sub>4</sub>, Na<sub>2</sub>CO<sub>3</sub> or K<sub>2</sub>CO<sub>3</sub> (2 M aq), THF, Toluene, Reflux, **ii**) Stille coupling; 2-Bu<sub>3</sub>Sn-thiophene, Pd<sub>2</sub>(dba)<sub>3</sub>, tri-*o*-tolylphosphine, THF, Reflux. **iii**) Sonogashira coupling; Phenylacetylene, Pd(PPh<sub>3</sub>)<sub>4</sub>, CuI, THF and diisopropylamine. **iv**) CF<sub>3</sub>-Ph-B(OR)<sub>2</sub>, Pd(PPh<sub>3</sub>)<sub>4</sub>, Toluene, THF, Na<sub>2</sub>CO<sub>3</sub> (2 M, aq), Reflux, 18 h. Adapted from Ref. 129 with permission from The Royal Society of Chemistry.

### 4.2.1 Synthesis

The commercially available 9,10-dibromoanthracene and 9-phenylanthracene were used as starting material for Suzuki, Stille and Sonogashira cross-coupling reactions, Figure 4.2. Palladium catalyzed coupling reactions are described in Chapter 7, section 7.2.1. The phenyl-substituents were successfully coupled using Suzuki cross-coupling procedures resulting in good yields (58-84%). A system of THF/Toluene/Na<sub>2</sub>CO<sub>3</sub>(aq) was used, except for nitrogen containing aromatic groups (**2** and **3**) which gave higher yields when carried out in a THF/K<sub>2</sub>CO<sub>3</sub>(aq) mixture. The Stille cross-coupling was performed in dry THF and was preferred for the thiophene-anthracene (**7-9**) coupling as it proceeded smoothly and resulted in high yields (46-80%). The ethynyl spaced phenylanthracene **10** was synthesized through a Sonogashira cross coupling with 9-bromo-10-phenylanthracene and phenylacetylene in dry and degassed THF and diisopropylamine. Full synthetic details and characterization can be found in the supporting information of Paper I and Paper II.

### 4.2.2 Photophysical characterization

Substituents on the phenyl-ring have minor or no effect on the  $S_1$ ,  $T_1$  and  $T_2$  energies as seen in Figure 4.3 for the representative annihilator **2**. Substituting a phenyl with a thiophene slightly redshifts the absorption and most likely this is also paralleled by the  $T_1$  and  $T_2$  states, as observed in our TD-DFT calculations and displayed in Figure 4.3C. The small effect of the phenyl-ring substitution can be explained by the close to perpendicular orientation of the pendant phenyl-group relative the anthracene core, as such the orbital overlap and conjugation is minimized. Introducing one (or more) ethynyl linker, as in **10** and **11**, allows for almost free rotation of the phenyl-group resulting in an extended

Table 4.1: Chemical and photochemical properties determined for 9,10-substituted anthracenes in toluene;  $\Phi_f$  is the fluorescence quantum yield,  $\tau_f$  is the fluorescence lifetime,  $\tau_T$  is the triplet lifetime,  $k_{TET}$  is the bimolecular triplet energy transfer rate constant and  $k_{TTA}$  is the rate constant for triplet-triplet annihilation.

Entry	Solubility (mM)	$\Phi_f^a$ (%)	$\tau_f$ (ns)	$\tau_t$ (ms)	$k_{TET}^b$ ( $\times 10^9 \text{M}^{-1} \text{s}^{-1}$ )	$k_{TTA}$ ( $\times 10^9 \text{M}^{-1} \text{s}^{-1}$ )
<b>1</b>	93	100 <sup>134</sup>	6.97	8.61	2.0 <sup>c</sup>	2.8 <sup>c</sup>
<b>2</b>	39	96 $\pm$ 2	6.93	7.73	1.9	2.3
<b>3</b>	83	99 $\pm$ 0.3	5.54	1.73	1.8	2.0
<b>4</b>	107	77 $\pm$ 2	4.69	8.50	1.9	1.8
<b>5</b>	47	84 $\pm$ 7	5.50	18.95	2.3	-
<b>6</b>	8	100 $\pm$ 1	6.84	9.55	1.9	2.3
<b>7</b>	256	9.0 $\pm$ 0.2	-	0.043	2.1	-
<b>8</b>	61	2.0 $\pm$ 0.0	-	0.005	2.5	-
<b>9</b>	76	2.6 $\pm$ 0.6	-	0.043	2.2	-
<b>10</b>	-	79 $\pm$ 6	3.65	2.41	2.7	4.9
<b>11</b>	-	85 $\pm$ 1	2.80	.50	2.7	4.4
<b>12</b>	115	$\sim$ 70 <sup>135</sup>	-	-	4.0	-

<sup>a</sup> Reported values are the average of two independent measurements. <sup>b</sup> **PtOEP** as the sensitizer. <sup>c</sup> Average of the two reported values in Paper I and Paper II. Adapted with from Ref. 129 with permission from the Royal Society of Chemistry

conjugation observed as a redshifted absorption, Figure 4.3. The extended conjugation in **10** and **11** also leads to a decrease in the  $T_1$  and  $T_2$  energies and our calculations (carried out by Dr. Lundin and Prof. Erhart) suggest that the energy excess required for TTA ( $2 \times E_{T_1} \geq E_{S_1}$ ) is reduced. In fact, for **11**  $2 \times E_{T_1}$  is slightly lower but within error isoenergetic with  $E_{S_1}$ . It should be pointed out at this point that these energies are the calculated  $T_x$ - $S_0$  excitation energies for the relaxed ground state structures and these are not always representative for the whole population of triplet excited annihilators, as will be discussed in section 4.2.4.

Substitutions on the phenyl-ring also affect the emission only to a minor extent. Compounds containing thiophenes, however, are considerably less emissive with fluorescence quantum yields ( $\Phi_{UC}$ )  $< 10\%$ , Table 4.1 and Figure 4.3B, rendering them ineffective as annihilators.

The bimolecular triplet energy transfer (TET) rate constant ( $k_{TET}$ , Table 4.1) determined by Stern-Volmer experiments indicate the same trends of the  $T_1$  energies as our TD-DFT calculations, namely that  $E_{T_1}$  is unaffected by substituents on the phenyl-ring and only decreases slightly ( $k_{TET}$  slightly increases) for the thiophene substituted anthracenes. The difference is, however, small and all rate constants are close to the diffusion limit in toluene. Again, the phenylethynyl substituted anthracenes are more affected, this trend is especially clear when comparing  $k_{TET}$  for **ZnOEP** as the sensitizer;  $k_{TET} = 0.8 \times 10^9 \text{M}^{-1} \text{s}^{-1}$ ,  $1.7 \times 10^9 \text{M}^{-1} \text{s}^{-1}$ , and  $2.6 \times 10^9 \text{M}^{-1} \text{s}^{-1}$  for **1**, **10** and **11**, respectively. As seen in Figure 4.3C,  $E_{T_1}$  of **ZnOEP** is isoenergetic to  $E_{T_1}$  of **1** and as the driving force for TET increases for **10** and **11** so does  $k_{TET}$ .

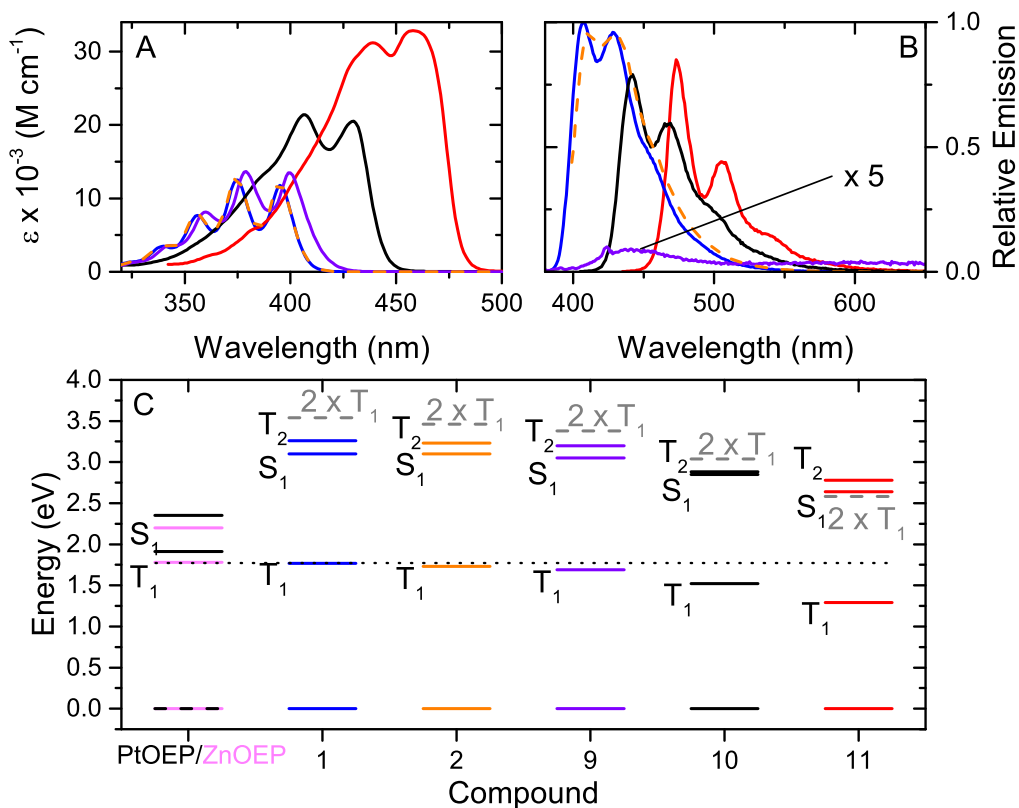


Figure 4.3: A) Molar absorptivity of the representative compounds **1** (—), **2** (- -), **9** (—), **10** (—) and **11** (—) and B) the corresponding relative emission (right). C) Energy level diagram of the annihilators in A and B and the sensitizers PtOEP and ZnOEP.  $E_{S_1}$  are the experimentally determined 0-0 transitions.  $E_{T_1}$  and  $E_{T_2}$  for the annihilators are obtained from TD-DFT calculations<sup>129,130</sup> while  $E_{S_1}$  and  $E_{T_1}$  energies for PtOEP as well as the  $E_{S_1}$  energy of ZnOEP are experimentally obtained. ZnOEP  $E_{T_1}$  is from references<sup>131-133</sup>. The dotted line at 1.78 eV marks the triplet energy of ZnOEP, and dashed lines mark  $2 \times E_{T_1}$  for the annihilators.

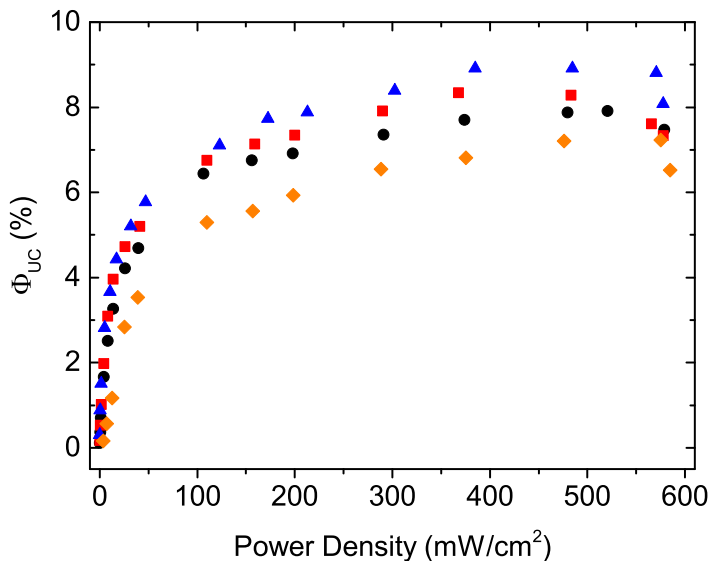


Figure 4.4: Upconversion quantum yield ( $\Phi_{UC}$ ) as a function of excitation power density (532 nm) of solutions containing **PtOEP**, 15  $\mu\text{M}$  and 0.5 mM annihilator. **1** (●), **2** (■), **3** (◆) and **6** (▲). Adapted from Ref. 129 with permission from The Royal Society of Chemistry.

### 4.2.3 Triplet-Triplet Annihilation Photon Upconversion

As expected with unaffected emission properties and excited state energies the upconversion quantum yield ( $\Phi_{UC}$ ) and rate constant of triplet-triplet annihilation ( $k_{TTA}$ ) is similar for the 9,10-diphenyl substituted annihilators **1**, **2**, **3** and **6** as can be seen in Figure 4.5 and Table 4.1.  $\Phi_{UC}$  for these annihilators is about 7-8%. This is lower compared to the highest reported  $\Phi_{UC}$  for **1**, which is closer to 20%.<sup>20,50,128</sup> The most probable reason to this is the freeze-pump-thaw and flame-sealing method, used to protect the samples from oxygen, not being as efficient as samples prepared and sealed in a glove box. For example, later experiments with **1** and PtOEP at similar concentrations prepared in a glove box displayed  $\Phi_{UC}$  around 16%, *vide infra*.

Nanosecond transient absorption was used to determine the rate constant of triplet-triplet annihilation ( $k_{TTA}$ ) and Figure 7.2 shows the recorded transient at 410 nm and 650 nm. The initial positive feature at 410 nm is ascribed to the  $T_1-T_n$  absorption of both the annihilator and the sensitizer. As the triplet energy is transferred from the sensitizer to the annihilator and triplet-triplet annihilation starts to occur the strong emission results in the observed negative feature decaying over a ms. At 650 nm only the phosphorescence of the PtOEP is observed. To fit the recorded transient at 410 nm the contribution from all three factors must be accounted for according to Equation 4.1:

$$\Delta A_{410nm} = \Delta\epsilon_{AT} \times [{}^3A^*] + \Delta\epsilon_{ST} \times [{}^3S^*] - a_{FL} \times [{}^1A^*]. \quad (4.1)$$

where  $\Delta\epsilon_{AT}$  and  $\Delta\epsilon_{ST}$  are the differential absorptivities of the annihilator and sensitizer,

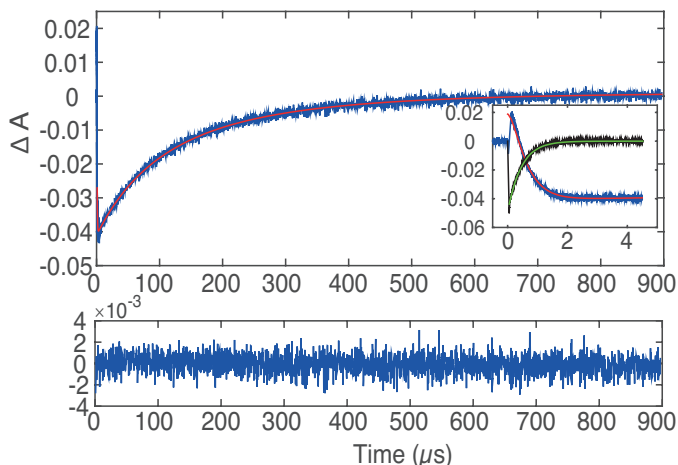


Figure 4.5: Nanosecond transient absorption of **1** (1mM) and **PtOEP** (3.4  $\mu\text{M}$ ) at 410 nm (blue), 650 nm (black) and respective fits to Equations 4.1 (red) and 4.2 (green). The inset shows the first 5  $\mu\text{s}$  and the bottom panel shows the residual of the fit at 410 nm. Adapted from Ref. 129 with permission from The Royal Society of Chemistry.

respectively.  $a_{FL}$  is a scaling factor for the fluorescence intensity of the annihilator and sensitivity of the detector at 410 nm. At 650 nm the observed transient is fit to Equation 4.2:

$$\Delta A_{650\text{nm}} = -a_{Phos} \times [{}^3S^*]. \quad (4.2)$$

where  $a_{Phos}$  is a scaling factor for the sensitizer phosphorescence intensity and detector sensitivity at 650 nm. The sensitizer and annihilator excited state concentrations were obtained by solving the rate equations in Equations 2.22a-2.22e and the fitting procedure was done globally to Equations 4.1 and 4.2, yielding values of  $k_{TTA}$  in good agreement with the few previous reports of  $k_{TTA}$  for anthracene.<sup>74</sup> The, perhaps more interesting, series with no, mono-, and bisethynyl spaced phenyl groups, **1**, **10** and **11**, respectively, is characterized in much the same way as the above discussed phenyl and thiophene substituted anthracenes.  $k_{TTA}$  of **10** and **11** is higher compared to **1**, as can be seen in Table 4.1. Both the triplet lifetime,  $\tau_T$  and fluorescence lifetime  $\tau_f$  are shorter for the ethynyl containing annihilators compared to **1**. Using the rate constants and lifetimes in Table 4.1 and assuming a spin-factor of 52%, as determined for **1** by Monguzzi *et al.*<sup>128</sup>,  $\Phi_{UC}$  is estimated to be around 20% for all three annihilators **1**, **10** and **11** when sensitized by **PtOEP** or **ZnOEP**. As can be seen in Figure 4.6 this is clearly not the case for **11** which reaches a maximum upconversion quantum yield  $\Phi_{UC}$  around 2%.

In fact, in the cases when  $\Phi_{UC}$  has been reported for **11**, with similar porphyrin sensitizers in low viscosity solvents, it is constantly less than 5%.<sup>34,98,136,137</sup> The reason to the low  $\Phi_{UC}$  for **11** can be understood when considering the singlet and triplet surfaces and will be discussed in the next section.

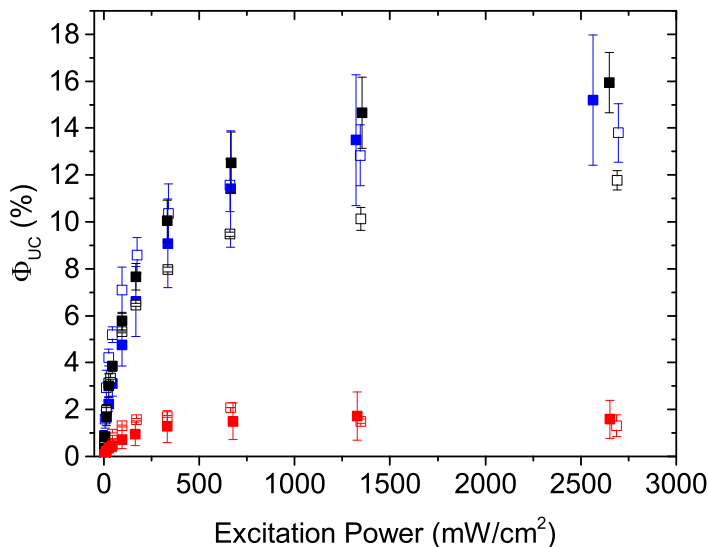


Figure 4.6: Upconversion quantum yield  $\Phi_{UC}$  of solutions containing 0.5 mM annihilator and 15.5  $\mu\text{M}$  sensitizer. **1** (blue), **10** (black) or **11** (red) with either ZnOEP (solid) or PtOEP (open). Average of two measurements, excitation at 532 nm. Adapted from Ref. 130 with permission from The Royal Society of Chemistry.

#### 4.2.4 Loss Channels in Triplet-Triplet Annihilation

At first sight **1** and **11** seem structurally very similar, however, when considering the orientation of the pendant phenyl groups some significant differences are apparent. In **1** the phenyl groups obtain a close to perpendicular angle relative the anthracene core, Figure 4.7B, due to steric interactions. Rotation away from this equilibrium geometry ( $\Delta\theta$ ) in the ground state is restricted to less than  $<30^\circ$  at room temperature, Figure 4.7A. For **11** the situation is quite different, since the phenyl groups are further away from the anthracene core the equilibrium configuration corresponds to a planar structure, Figure 4.7B, and free rotation away from this geometry is possible in the ground state at room temperature, Figure 4.7A.

The effect of phenyl group rotation on the  $S_1$  and  $T_1$  energies were studied closer by TD-DFT calculations (conducted by Prof. Erhart), Figure 4.7C and E. In **1**, rotations away from the equilibrium geometry leads to a more conjugated system, thus both the  $S_1$  and  $T_1$  energies decrease slightly with  $S_1$  showing a larger sensitivity, Figure 4.7C. Consequently, as seen in Figure 4.7D, the triplet-triplet annihilation energy balance  $2 \times E_{T_1} \geq E_{S_1}$  (Equation 2.19) is constantly positive and increases for a majority of the orientations. The opposite is observed for **11**, rotations away from the equilibrium here leads to a broken conjugation, leading to an increase in the  $S_1$  and  $T_1$  energies. Again the  $S_1$  state is more sensitive to the rotation, now leading to a decrease in the energy balance, Figure 4.7F, for a large part of the orientations.

It should be pointed out that the calculations indicate that the energy balance in the

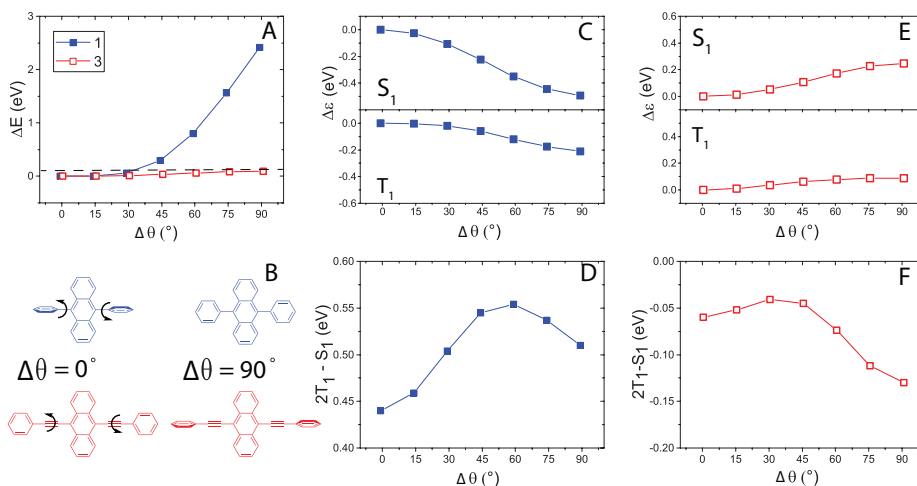


Figure 4.7: A) change in total energy of **1** (blue) and **11** (red) as a function of phenyl group rotation away from the equilibrium geometry ( $\Delta\theta$ ). Dashed line corresponds to  $4 \times k_B T = 0.1$  eV at room temperature. B) Schematic illustration of  $\Delta\theta$  and corresponding phenyl group orientations. C) Relative change in  $E_{S_1}$  excitation energy (top) and  $E_{T_1}$  (lower) for **1**. D) Change in the TTA energy balance (*cf.* Equation 2.19) upon phenyl group rotation for **1**. E) same as C for **11** and F) same as D for **11**. Adapted from Ref. 130 with permission from The Royal Society of Chemistry.

case of **11** is actually negative regardless of the rotation angle, Figure 4.7F, which implies that the conversion is not favorable under any circumstance. The energy difference is, however, small and below the accuracy of the present calculations. Thus, considering the close to isoenergetic energy balance in the equilibrium geometry, the decrease due phenyl group rotation is expected to have a large influence on the triplet-triplet annihilation efficiency, explaining the substantially lower  $\Phi_{UC}$  of **11**.

### 4.3 Evaluation of PPO and other UV annihilators

There are only a few examples of UV emitting annihilators.<sup>106–108</sup> 2,5-diphenyloxazole (PPO) is the annihilator which has demonstrated the highest VIS-to-UV upconversion quantum yield, when sensitized by CdS/ZnS core-shell NCs the upconversion quantum yield  $\Phi_{UC}$  is 2.6% (out of 50%), which is still relatively low. For example, the largest  $\Phi_{UC}$  for VIS-to-VIS upconversion is 38%.<sup>39</sup>

From the study presented in Paper IV we conclude that PPO has a relatively high  $T_1$  energy, so that  $2 \times E_{T_1}$  is not only larger than  $E_{S_1}$ , but also  $E_{T_2}$  and possibly  $E_{Q_1}$ . As such, TTA could be limited to 5.5% due to spin-statistics. Since  $\Phi_{UC}$  is still lower than the spin-statistical limit there must be other factors also leading to a reduced efficiency.

In order to develop new and efficient UV emitting annihilators, fluorophores with  $2 \times E_{T_1}$  only slightly exceeding  $E_{S_1}$  are sought after. Furthermore they must have large fluorescence

quantum yields ( $\Phi_F$ ) and emit below 400 nm, or preferably at even higher energies for many applications. Seeing that fused aromatic systems like DPA are efficient annihilators with large singlet-triplet gaps one might consider naphthalene based annihilators. Although, as for unsubstituted anthracene, naphthalene itself has a low fluorescence quantum yield.<sup>138</sup> Adding phenyl groups increases  $\Phi_F$  somewhat, but also red-shifts the emission. Possibly, sterically crowded phenylnaphthalenes will display smaller red-shifts. However, obtaining a more blue-shifted emission will most likely require other types structures.

Both p-terphenyl and p-quarterphenyl, used as annihilators by Yanai and co-workers, have large  $\Phi_F$  values.<sup>108</sup> However, also here the  $T_1$  energy is high and  $2 \times E_{T_1}$  exceeds  $E_{S_1}$  by more than 1 eV. Other molecular structures with large singlet-triplet gaps are those with conjugated double bonds, for example some carotenoids are capable of singlet fission and triplet-triplet annihilation.<sup>139,140</sup> For efficient UV emission, however, smaller and rigid chromophores are necessary. Recently an interesting patent was filed by Kimizuka and co-workers listing a number of possible UV annihilators based on small conjugated double bonds.<sup>141</sup> Another area that should be explored is the combination of different annihilators, achieving hetero-TTA as such systems have been shown to have higher efficiencies than the separate components.<sup>142</sup>

## 4.4 Summary and Evaluation of Hypotheses

An annihilator should not only have a high fluorescence quantum yield, but also have suitable triplet and singlet energy levels. For example  $2 \times E_{T_1}$  should be larger, but similar to  $E_{S_1}$  in order to avoid parasitic formation of triplet and quintet states upon TTA. This energy requirement must be fulfilled for the whole triplet population to achieve efficient TTA. Paper I and Paper II present our studies of the substitution effect on the singlet and triplet energies of the commonly used annihilator DPA.

The singlet and triplet energies of DPA (**1**) are not affected by substitutions on the phenyl ring, thus having minor effects on the triplet-triplet annihilation (TTA) properties. It can be understood from the close to perpendicular orientation of the phenyl groups relative the anthracene core, resulting in minor coupling between the anthracene and phenyl group substitution. These results disprove the hypothesis that introducing donor/acceptor groups on DPA can alter the energy levels and thus affect the TTA properties. However, with this knowledge it is possible to design other DPA (**1**) based annihilators with substituents (Paper III) or dendrimeric and oligomeric structures<sup>49,143</sup> in order to achieve desired chemical or physical properties without affecting the inherent TTA properties. In Chapter 5 some examples of DPA (**1**) based annihilators capable of coordinating to the sensitizer are discussed.

Introducing a triple bond between the anthracene core and the phenyl groups enables the phenyl to freely rotate resulting in an equilibrium population of **11** in the ground state having a relatively broad distribution of geometries. Since excited triplet states are long-lived it also holds true for the excited triplet population of **11**. The energy balance  $2 \times E_{T_1} \geq E_{S_1}$  decreases upon phenyl group rotation for **11**. Remembering that  $2 \times E_{T_1}$  is close to isoenergetic with  $E_{S_1}$  in the planar equilibrium geometry, only a small part of the triplet excited population fulfills the required energy balance  $2 \times E_{T_1} \geq E_{S_1}$  (Equation

2.19) leading to a reduced driving force for TTA. The difference between the singlet and triplet surfaces can explain the low  $\Phi_{UC}$  observed for **11**, in line with the hypothesis. It also illustrates that solely explaining deviations from the maximum  $\Phi_{UC}$  by introducing the spin factor can be erroneous and should be done with caution.

Two recent reports of BPEA (**11**) in more viscous media reported  $\Phi_{UC}$  of 13-16%.<sup>100,144</sup> There are only a few reports on the effect of viscosity on the TTA efficiency and  $\Phi_{UC}$ .<sup>145,146</sup> and it is not evident why a higher viscosity allows for more efficient upconversion of **11**. One possibility, which is in line with the hypothesis, is: Since diffusion is reduced with a higher viscosity there are fewer collisions per unit of time between triplet excited annihilators. The formed  $T_1 \cdots T_1$  encounter complex, however, would have a longer lifetime as the dissociation rate is also reduced. For molecules like **11**, where we hypothesize that only a fraction of the  $T_1$  population has enough energy to form a singlet, the longer lifetime would allow more time for the encounter complex to adopt a conformation capable of singlet formation. As the long triplet excited lifetime of the annihilators could compensate for the fewer collisions per time in high viscosity solvents the overall effect would be an increase in TTA efficiency and also  $\Phi_{UC}$ , as is observed. Further experiments are required to fully prove this explanation.



# Coordination between Porphyrin Sensitizers and Annihilators

Achieving efficient triplet-triplet annihilation photon upconversion in the solid state is of utmost importance for the development of devices incorporating TTA-UC. Our idea is to develop a supra-molecular structure where TET and TTA both can occur *intra*-molecularly. This chapter focuses on our work with sensitizer-annihilator pairs that can pre-organize with the goal to improve TET. Most of the results presented herein are from Paper III, however, some preliminary, not yet published, results are also included.

The idea to attach the sensitizer and annihilator is not new, however, a major problem is the parasitic quenching of the annihilator singlet state leading to a decrease in  $\Phi_{UC}$ .<sup>19,45,147,148</sup> There has been one recent example of sensitizer-annihilator complexes with an improved  $\Phi_{UC}$  reaching 3.2%, which is still relatively low.<sup>149</sup> By axially coordinating the annihilator to the sensitizer we hope to minimize the singlet quenching while maintaining efficient TET.

## 5.1 Synthesis

Based on the results and molecular structures investigated in Paper I we chose to utilize 9,10-phenylsubstituted anthracene based annihilators containing one pyridine group. The pyridine group, containing a nitrogen atom with two free electrons allows for coordination to metal centers. To systematically study the distance dependence of energy transfer, the pyridine is separated from the anthracene core by 0-4 phenyl groups. The synthetic route to these annihilators is shown in Figure 5.1.

The first step is a metal-halogen exchange of 9-bromo-10-phenylanthracene using *tert*-butyl lithium (*t*-BuLi) at  $-78^{\circ}\text{C}$  followed by the addition of 2-isopropoxy-4,4,5,5-tetramethyl-1,3,2-dioxaborolane yielding the 9-phenylanthracene boronic acid derivative **16**. Compounds **17** and **18** are then obtained from Suzuki cross-coupling reactions of **16** with pyridine derivatives **14a** and **15**, respectively. In the synthesis of **22** compound **16** is first coupled with 4,4'-dibromo-1,1-diphenyl to give **19**. The borylation conditions used in the initial step can not be used for **19** as solubility in THF is limited. Instead, a

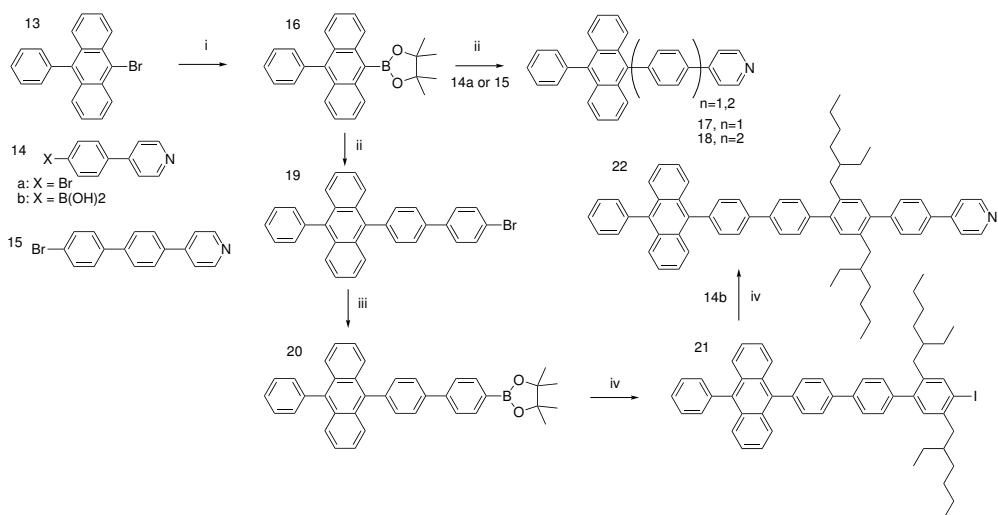


Figure 5.1: Synthetic route for coordinating bridged annihilators **17**, **18** and **22**. i)  $t\text{-BuLi}$ ,  $-78^\circ\text{C}$  1 h, then 2-isopropoxy-4,4,5,5-tetramethyl-1,3,2-dioxaborolane,  $-78^\circ\text{C} \rightarrow \text{RT}$ , 16 h. ii)  $\text{Pd}_2(\text{dba})_3$ , tri-*o*-tolylphosphine, toluene, tetraethylammonium hydroxide (aq, 20%), reflux 72 h. iii) Bis(pinacolato)diboron,  $\text{Pd}(\text{dppf})\text{Cl}_2$ , toluene,  $\text{Et}_3\text{N}$ , reflux 24 h. iv)  $\text{Pd}(\text{PPh}_3)_4$ , CsF, toluene, reflux 72 h.

palladium catalyzed borylation of **19** in refluxing toluene yields **20** in 48% yield. A Suzuki coupling of **20** and 1,4-bis(2-ethylhexyl)-2,5-diiodobenzene introduces a *p*-iodophenyl with solubilizing side-chains. The final product **22** is then obtain from the coupling of **21** with the boronic acid derivative **14b**, with a reasonable yield of 61%.

It is also of interest to study TET to dendrimeric structures, the two dendrimeric arms **22** and **23** in Figure 5.2 are similar to the dendrimers studied in our previous work,<sup>49,143</sup> and are therefore natural candidates for our study. The synthesis of **22** and **23** is based on the previously synthetic route of diphenylanthracene dendrimers,<sup>143</sup> according to the scheme in Figure 5.2. Similar as for the bridged structures, the first step is a borylation using  $t\text{-BuLi}$  and 2-isopropoxy-4,4,5,5-tetramethyl-1,3,2-dioxaborolane at  $-78^\circ\text{C}$  to yield compound **23**. Coupling **23** with excess of 1,3,5-tribromobenzene results in the dibrominated compound **24** in 30% yield, slightly contaminated with anthracene. **24** is reacted in another Suzuki coupling with compound **16** to yield the dendrimeric arm **25** in high yields, 89%. After bromination with molecular bromine (84% yield), **26** is coupled with 4-pyridineboronic acid to yield pyridine containing dendrimer **27**, 78%. Compound **26** can also be transformed into the larger dendrimer **28** by first borylating **26** (60% yield), and then repeating steps **iii** (75%), **iv** (98%) and **v** (37%) in Figure 5.2 with compound **26** rather than compound **16**.

In accordance with the previous study dealing with substituted anthracenes, presented in Chapter 4, the absorption and emission properties are mostly unaffected by the added bridge to the DPA unit. Although, the fluorescence quantum yield,  $\Phi_f$ , decreases from close to unity to about 0.85 for bridge containing anthracenes, Table 5.1.

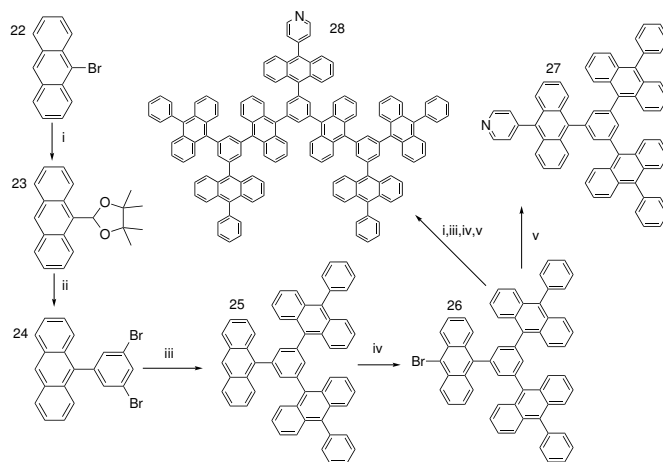


Figure 5.2: Synthetic route for coordinating dendrimeric annihilators **27** and **28**. i)  $t\text{-BuLi}$ ,  $-78^\circ\text{C}$  1 h, then 2-isopropoxy-4,4,5,5-tetramethyl-1,3,2-dioxaborolane,  $-78^\circ\text{C} \rightarrow \text{RT}$ , 16 h. ii) Excess 1,3,5-tribromobenzene,  $\text{Pd}_2(\text{dba})_3$ , tri-*o*-tolylphosphine, toluene, tetraethylammonium hydroxide (aq), reflux 72 h. iii) **16**,  $\text{Pd}_2(\text{dba})_3$ , tri-*o*-tolylphosphine, toluene, tetraethylammonium hydroxide (aq, 20%), reflux 72 h. iv)  $\text{Br}_2$ ,  $\text{CCl}_4$ ,  $0^\circ\text{C}$ , 1 h. v) 4-Pyridineboronic acid,  $\text{Pd}(\text{PPh}_3)_4$ , THF,  $\text{K}_2\text{CO}_3$  (aq. 2M), Aliquat 336.

## 5.2 Annihilator Coordination to ZnOEP

Compound **2** from Chapter 4, containing a pyridine side group, is an excellent annihilator for TTA-UC. With the pyridine substitution it is now also possible to coordinate **3** to the sensitizer, given the metal porphyrin is chosen to have a metal atom capable of forming a complex with pyridine. Figure 5.3 shows the shift in absorption of the porphyrin Q-band upon addition of compound **2**. Similar shifts are also observed for the ligands **17**, **18** and **22**, but not for the annihilator **1**. From the shift in ZnOEP absorption the binding constant  $K_{bind}$  is determined to 2300 - 6000  $\text{M}^{-1}$ , listed in Table 5.1.

Table 5.1: Properties of coordinating annihilators:  $\Phi_f$  is the fluorescence quantum yield,  $K_{bind}$  is the binding constant to ZnOEP,  $\tau_f$  is the fluorescence lifetime of the annihilator alone and  $\tau_q$  is the quenched fluorescence lifetime.

Compound	$\Phi_f$ (%)	$K_{bind}$ ( $\text{M}^{-1}$ )	$\tau_f$ (ns)	$\tau_q$ (ps)	$\eta_{FRET}$
<b>1</b>	100 <sup>134</sup>	0	6.97	-	-
<b>2</b>	96 $\pm$ 2.0	2300	5.29 $\pm$ 0.01	<20	>99.6
<b>17</b>	85 $\pm$ 1.9	5900	3.55 $\pm$ 0.01	<20	>99.4
<b>18</b>	85 $\pm$ 0.3	5800	3.17 $\pm$ 0.01	27 $\pm$ 7	99.2 $\pm$ 0.2
<b>22</b>	86 $\pm$ 5.2	6000	3.33 $\pm$ 0.01	152 $\pm$ 10	95.4 $\pm$ 0.3

Adapted with permission from Gray *et al.*, J. Phys. Chem. C, 2016, 120, 19018-19026.

Copyright (2016) American Chemical Society.

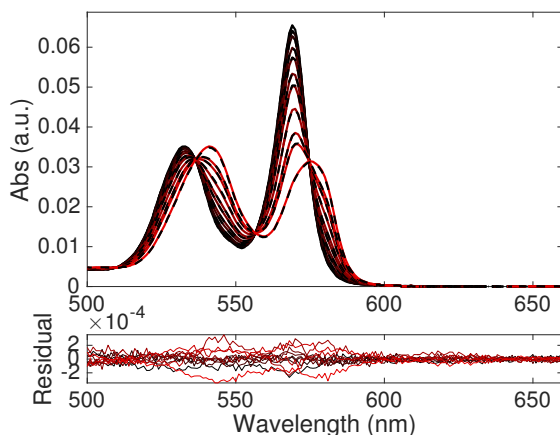


Figure 5.3: Absorption of the ZnOEP Q-band upon coordination by **2**. Measured (dashed) and predicted (solid) spectra with residual below. Titration progression from black to red spectra. 2.5 mM ZnOEP and 0-1.6 mM **2**. Reprinted with permission from Gray *et al.*, J. Phys. Chem. C, 2016, 120, 19018-19026. Copyright (2016) American Chemical Society.

### 5.2.1 Triplet Energy Transfer

For the ZnOEP-annihilator complexes it was not possible to discern TET occurring through the regular *inter*-molecular diffusion controlled manner from that occurring *intra*-molecularly in a coordination complex. The main reason is the low binding constant, requiring a large excess of annihilator to achieve a substantial amount of coordinated ZnOEP. Figure 5.4 illustrates this difficulty: the diffusion controlled TET efficiency,  $\Phi_{TET}$  is calculated, from the Stern-Volmer relationship, for a sensitizer with 200  $\mu$ s triplet lifetime and is compared to the fraction of bound sensitizer at the same concentration. Assuming the optimistic case where TET is quantitative in a coordination complex the fraction of bound sensitizer can be directly compared to  $\Phi_{TET}$  and it is evident that due to the low binding affinity the diffusion controlled TET is always more efficient. For a ten times stronger binding, however, *intra*-molecular TET could be more substantial. In section 5.3 are some preliminary results for a ruthenium porphyrin having a considerably larger binding affinity to pyridine.

### 5.2.2 Singlet Energy Transfer

When the annihilator and sensitizer are in close proximity there is a chance of singlet energy transfer from the annihilator back to the sensitizer. Such quenching of the annihilator singlet is detrimental to the upconversion efficiency. The singlet energy transfer is believed to occur through Förster Resonance Energy Transfer (FRET) which is dependent on the relative orientation between the transition dipole moments in the two chromophores.

The transition dipoles in the anthracene-porphyrin complexes in the solid state are expected to be close to perpendicular<sup>150</sup>. even though, we find FRET to be very effective.

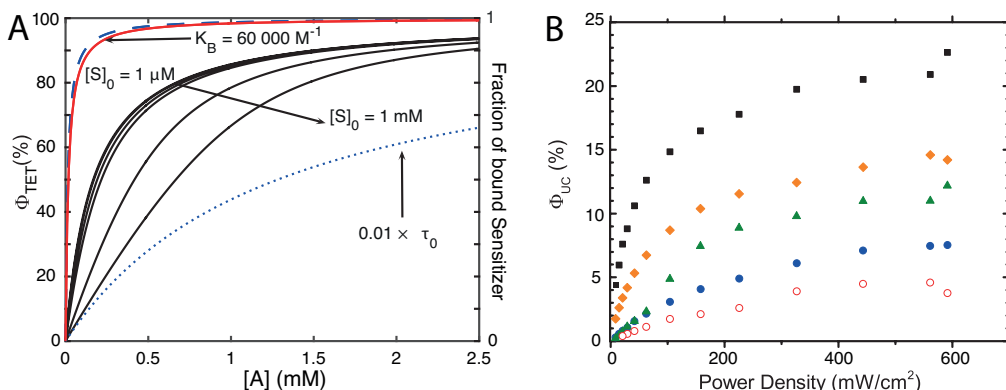


Figure 5.4: A) Calculated triplet energy transfer (TET) efficiency ( $\Phi_{TET}$ ) for diffusion controlled TET with a sensitizer lifetime of 200  $\mu s$  (blue dashed) and 2  $\mu s$  (blue dotted). The fraction of bound sensitizer calculated for  $K_{bind} = 6000 M^{-1}$  and sensitizer concentrations between 1  $\mu M$  and 1 mM (black) as well as the fraction of bound sensitizer calculated for  $K_{bind} = 60000 M^{-1}$  and a sensitizer concentration of 1  $\mu M$  (red). B) Upconversion quantum yield. Samples of 1  $\mu M$  ZnOEP sensitizer and 2.5 mM **1** (black squares), 2.5 mM **2** (orange diamonds), 2.5 mM **17** (blue circles), 0.23 mM **18** (green triangles), and 2.5 mM **22** (red open circles). Reprinted (adapted) with permission from Gray *et al.*, *J. Phys. Chem. C*, 2016, 120, 19018-19026. Copyright (2016) American Chemical Society.

For example, the singlet lifetime of **22** in a complex ( $\tau_q$ ) is only 152 ps, compared to 3.33 ns in its free form, corresponding to a quenching efficiency of >95%, Table 5.1. For the other coordinating annihilators the quenching is even greater. Therefore it seems that the molecular motions in the complexes are large enough to allow FRET to occur.

### 5.2.3 Triplet-Triplet Annihilation Photon Upconversion

Even though the singlet quenching in an annihilator-sensitizer complex is extremely efficient, the low binding affinity of the annihilators to ZnOEP makes it possible to observe efficient TTA-UC,  $\Phi_{UC} \geq 5\%$ , with all coordinating annihilators, Figure 5.4B. Since the binding affinity is low, most annihilators are free in solution when concentrations are chosen to have >90% of ZnOEP sensitizers coordinated with an annihilator, therefore TTA occurs between uncoordinated annihilators and there is no quenching through FRET. The reason for the decrease in  $\Phi_{UC}$  with longer bridges originates from a less efficient TTA step, either the longer bridges reduces the triplet lifetime of the annihilator or they sterically block the annihilators from obtaining an optimal encounter complex geometry, or a combination of both.

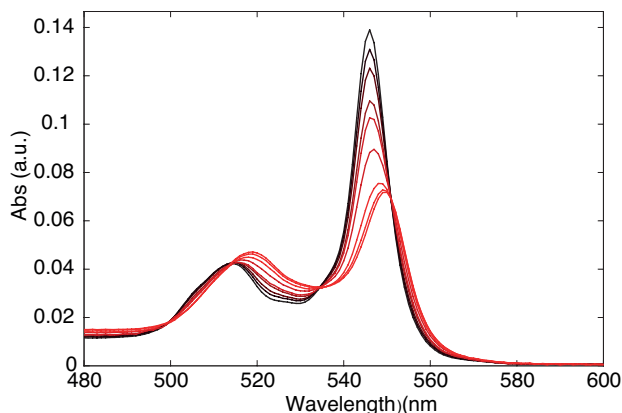


Figure 5.5: Absorption of the RuOEP(CO) Q-band upon coordination by **2**. Titration progression from black to red spectra. 10  $\mu\text{M}$  RuOEP(CO) and 0-10  $\mu\text{M}$  **2**.

### 5.3 Annihilator Coordination to RuOEP(CO)

In this section our yet unpublished data using ruthenium(II) carbonyl octaethylporphyrin (RuOEP(CO)) as sensitizer is discussed. Ruthenium is known to have a much larger binding constant to pyridine compared to zinc.<sup>151,152</sup> Upon titration with the pyridine containing ligands **2**, **17**, **18**, **22**, **27** and **28** a similar shift in RuOEP(CO) Q-band absorption is observed as for ZnOEP, Figure 5.5. The binding is close to quantitative, as a 1:1 mixture of pyridine containing annihilator and RuOEP(CO) results in a shifted absorption that does not change upon further addition of annihilator.

#### 5.3.1 Triplet Energy Transfer

With the larger binding affinity to RuOEP(CO) it is possible to monitor the *intra*-molecular TET to the pyridine containing ligands through transient absorption spectroscopy. Figure 5.6 shows the transient absorption spectra of RuOEP(CO) with only a pyridine ligand (RuOEP(CO)Pyr) and RuOEP(CO) with **2**, **18** and **22** as ligands.

RuOEP(CO)Pyr with no possible TET displays a strong transient absorption in the 400-500 nm region, corresponding to the  $T_1$ - $T_n$  transition of the pyridine. Furthermore, the ground state bleach (GSB) can be observed between 500-550 nm. Both the  $T_1$ - $T_n$  absorption and the GSB decay with the same monoexponential rate, with a lifetime of 20.2  $\mu\text{s}$ . When bound to ligand **2** the GSB of RuOEP(CO)**2** is gone after 27 ns, close to what is possible to resolve on the current setup. Since the  $T_1$ - $T_n$  absorption of DPA (**1**) and other anthracene derivatives is also in the region 400-500 nm the decay at 440 nm for RuOEP(CO)**2** displays a biexponential decay, one fast component with a lifetime of 27 ns and a long lived component with a lifetime of 431  $\mu\text{s}$ . The fast decay is logically explained as the TET component whereas the long component corresponds to the triplet lifetime of **2** when coordinated to RuOEP(CO). The same TET rate is observed for the dendrimeric structures **27** and **28**, which is expected since it is the same distance from RuOEP(CO)

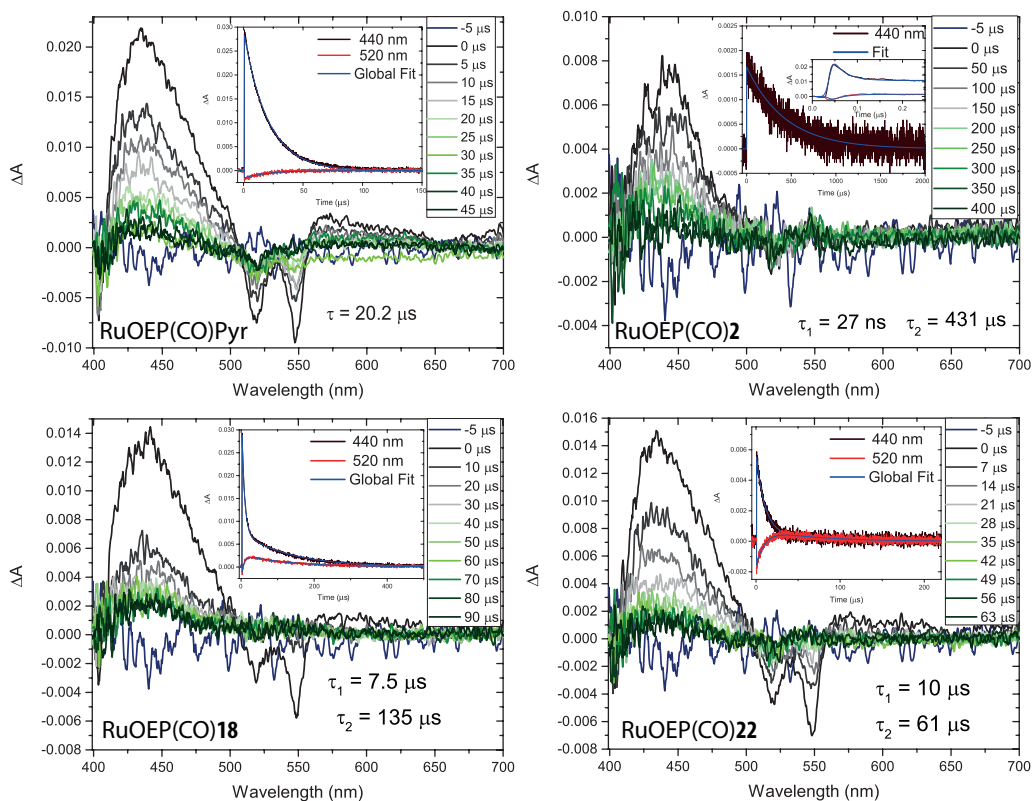


Figure 5.6: Transient absorption spectra of A) RuOEP(CO)Pyr, B) RuOEP(CO)**2**, C) RuOEP(CO)**18** and D) RuOEP(CO)**22**. Inset shows the decay at 440 nm (brown) and 520 nm (red) respectively with the corresponding fit (blue) to mono or biexponential decays.

to the first anthracene unit for all three ligands, **2**, **27** and **28**. The possibility of electron transfer as a competing process can, from a first approximation, be discarded as it would be endergonic ( $\Delta G > 0$ ).

As the bridge is extended from ligand **2** to ligand **22** the TET rate is slowed down from 27 ns to 10  $\mu$ s, as seen for  $\tau_1$  in Figure 5.6. Such a trend is also expected since TET is distance dependent. Even though the driving force for TET is slightly lower in the case of ZnOEP, there is most likely also *intra*-molecular TET in the case of ZnOEP and **2**, since the TET here is much faster than the complex lifetime of ZnOEP**2**. This might, however, not be true for **22** and ZnOEP as the TET rate is much slower. By switching the central atom from Zinc to Ruthenium it possible to achieve *intra*-molecular TET in an annihilator-sensitizer complex. The singlet quenching is, however, still a problem in these axially coordinated annihilator-sensitizer complexes and is currently studied further.

## 5.4 Outlook - Towards all *Intra*-Molecular Triplet-Triplet Annihilation Supra-molecular Structures

In the complexes formed between RuOEP(CO) and the ligands containing only one anthracene unit (**2**, **17**, **18**, and **21**) there is no possibility of *intra*-molecular TTA and annihilation between two complexes would result in efficient quenching of the annihilator singlet state, *vide supra*. If, however, excess annihilator is present the situation is much like the case with NC based sensitizers, as the TET from RuOEP(CO) to the ligand extends the triplet lifetime enabling subsequent TET to free annihilators.

In the dendrimeric sensitizers **27** and **28** it would in principle be possible to have *intra*-molecular TTA. It would, however, require absorption and subsequent TET of another photons to the dendrimer within the lifetime of the triplet excited dendrimer. A larger dendrimer, with multiple sensitizers attached, would possibly be able to achieve both *intra*-molecular TET and TTA. If the dendrimer is large enough the problem with singlet quenching could also be overcome.

## 5.5 Evaluation of Hypothesis

When using ZnOEP as the sensitizer it is not able to enhance the TET since the diffusion limited TET is always more efficient than the formation of ZnOEP-annihilator complexes. Nor did the axial binding minimize the singlet quenching of the annihilator. By switching to RuOEP(CO) which has a much larger binding affinity towards pyridine, it is able to enhance the TET rate for low annihilator concentrations. The singlet quenching is still very efficient in the case with RuOEP(CO). The hypothesis that the "Triplet energy transfer can be enhanced while minimizing the parasitic singlet energy back transfer if the annihilator is coordinated axially to a metalloporphyrin." is therefore disproved. However, design criteria to achieve functioning supra-molecular sensitizer-annihilator complexes with *intra*-molecular TET and TTA, overcoming the singlet quenching problem, are being established.

# Concluding Remarks and Outlook

Triplet-triplet annihilation (TTA) is a process where two triplet excited molecules can combine the triplet energies forming one excited singlet (or triplet, or quintet). If the annihilating molecules are sensitized by an appropriate triplet sensitizer this can result in the upconversion of two low energy photons into one high energy photon, emitted by the annihilator. This thesis focuses on the design criteria of both the sensitizer and annihilator. Moreover, these design criteria are used to develop supra-molecular sensitizer-annihilator complexes with the aim of achieving *intra*-molecular triplet energy transfer (TET) and TTA.

The role of the sensitizer is to absorb photons, generate triplet excited states and transfer the triplet energy to the annihilator. Therefore sensitizers with large molar absorptivities and efficiently intersystem crossing are sought after. Conjugated molecules with heavy atoms or chalcogenide nanocrystals (NCs) are both promising sensitizer candidates. NCs are particularly advantageous as they are photostable and easy to synthesize with desired absorption properties. The facile tunability of NC optical properties has resulted in efficient NC sensitization of both NIR-to-VIS and Green-to-Blue upconversion, in particular the NIR sensitization has proven difficult to achieve with molecular sensitizers, for various reasons. Furthermore, we demonstrate efficient sensitization of the UV emitting annihilator PPO by CdS/ZnS core-shell NCs with a five-fold increase in upconversion quantum yield compared to previous molecular sensitization of PPO. The ZnS shell passivates surface trap states enabling efficient TET.

Upon sensitization by a sensitizer, a triplet excited annihilator must encounter another triplet excited annihilator and fuse the triplet energy through TTA. To facilitate such an encounter the triplet lifetime of the annihilator should be long. Furthermore, to be able to form the emissive singlet state upon TTA the energy relation  $2 \times E_{T_1} \geq E_{S_1}$  must be fulfilled. For long lived triplet excited annihilators in solution, the energy relation above must be satisfied for the whole triplet population to achieve efficient TTA-UC. This is not the case for BPEA (**11**) where the pendant phenyl groups are free to rotate, and rotation away from the equilibrium geometry results in a decrease in the energy balance above. In this way the low efficiency of BPEA (**11**) can be explained, even though it in many ways resembles the efficient annihilator DPA (**1**). It is evident that there is still much to unravel regarding the actual TTA process. For example, spin statistical arguments

on the TTA efficiency are commonly based on the assumption of one encounter of two annihilators followed by dissociation, the effect of the encounter lifetime, geometry and possible re-encounters are often not considered to a full extent. The required encounter geometry for possible TTA is especially interesting to unravel. Geometric factors has been studied and discussed for the reversed process of singlet fission, and has been found to play an important role.<sup>153</sup> Considering TTA as a type of Dexter energy transfer, TTA should be possible as long as there is sufficient coupling through orbital overlap. In future design of supra-molecular annihilator-sensitizer structures it is necessary to know what geometrical orientations pose restriction on the TTA process.

Considering the future for TTA-UC in solar energy applications there are still a number of challenges that must be overcome. For example to achieve PVs with efficiencies exceeding 40%, as predicted theoretically,<sup>154,155</sup> upconversion material must approach upconversion quantum yields close to 50%. So far the only annihilator realizing such high yields is pyrene,<sup>39</sup> and little effort has been put into understanding and rationally designing new, better annihilators. Therefore future research should focus on developing new annihilators with high lying  $T_2$  and  $Q_1$  energies. Some examples of mixed annihilators, achieving hetero-TTA have shown improved efficiencies compared to the individual homo-TTA systems,<sup>142</sup> and fully understanding the reason to the increased hetero-TTA might allow annihilator pairs being designed with yields close to 50%.

Another challenge is the spectral range of upconversion, to benefit solar cells NIR photons must be upconverted. As mentioned previously, the difficulties in synthesizing efficient molecular sensitizers in the NIR spectral region must be addressed. Here NC could play an important role as there are already some examples of efficient NIR absorbing NC sensitizers. It is, however, necessary to fully understand the TET across the inorganic-organic interface in order to design new more efficient NC based sensitizers. For photochemical and photocatalytical reactions a large part of the visible spectrum must be converted to high energy UV photons. Again, more efficient annihilators and sensitizers are necessary. Interesting structures for UV emitting annihilators include various rigidified alkenes.

Alongside the development of new efficient sensitizer-annihilator pairs device incorporation must be considered. There are two distinct ways of integrating an UC material with PVs, either they can be coupled optically, *i.e.* the UC material is located behind the PV device and re-emits the upconverted light for the PV to absorb. In such a case it is important to direct the emission back to the PV device, either by using a back reflector<sup>23,156</sup> and/or through molecular alignment.<sup>157</sup> It is also possible to couple the UC directly with the device, as demonstrated by Hanson and co-workers, showing how DPA (**1**) anchored to a semiconductor surface can directly inject the UC generated excited electron into the semiconductor.<sup>158,159</sup> What device structure will be the better is difficult to predict, and likely depends on both the UC material and the PV type. The device structure for photocatalytical reactions relying on upconverted UV photons is reasonably different from that of UC-PVs. One possibility is to fabricate a core structure of UC-materials and cover it with the photocatalyst, in that way any re-emitted UC photon will be able to be reabsorbed. It would also be possible to incorporate such a core-shell structure into a solar concentrator, such as a parabolic-trough.

An important factor to consider when incorporating UC materials into devices is the

inherent oxygen sensitivity of the triplet states. Therefore, even with new annihilator-sensitizer pairs with quantum yield approaching 50%, efficient oxygen scavenging or sealing must be applied. Some recent examples of oxygen scavengers for TTA-UC applications have been demonstrated.<sup>100,160-162</sup> It is also possible that self-assembled or supra-molecular structures capable of *intra*-molecular TET and TTA would be less sensitive to oxygen, if the processes are fast enough.

Finally, the design parameters established for DPA based annihilators within this work will be essential for developing novel anthracene based annihilators, for proof-of-concept devices. The work presented herein also highlights many of the energetic aspects necessary to address in future studies of annihilators. Furthermore, the studies of supra-molecular sensitizer-annihilator structures presented in Chapter 5 has significantly advanced our understanding of what is needed to achieve efficient *intra*-molecular TTA-UC and this goal is closer than ever before.



# 7

## Methods

In this chapter the synthetic and spectroscopic methods used are presented. Both steady state and time-resolved spectroscopic techniques are described. The synthetic methods focuses on Suzuki and Stille cross-coupling reactions as they are the two main types of reactions used in the organic synthesis of the anthracene derivatives.

### 7.1 Absorption and Emission

#### 7.1.1 Steady State Measurements

The absorption of light by a molecule is studied using a spectrophotometer. In a spectrophotometer the intensity of the incident light on a sample ( $I_0$ ) is compared to the light intensity transmitted by the sample ( $I_T$ ) and the absorbance (A) is then calculated by equation 7.1:

$$A = \log\left(\frac{I_0}{I_T}\right) \quad (7.1)$$

The absorbance is related to the ability of the molecule to absorb light (molar absorptivity,  $\epsilon$ ), the concentration of the molecule (c) in the sample and the path length (l) of the light, this is described by the Lambert-Beer law, equation 7.2.

$$A(\lambda) = \epsilon(\lambda)cl \quad (7.2)$$

The molar absorptivity,  $\epsilon$  is commonly presented in  $\text{M}^{-1}\text{cm}^{-1}$ , the concentration in M and the path length in cm. As the molar absorptivity varies with the wavelength a spectrum is obtained when the absorption is measured over a wavelength interval, bands in the spectra correspond to wavelength regions where the molecule absorbs light.

To study the emission of a molecule a spectrofluorometer is used. The spectrofluorometer can be run in two modes; emission and excitation mode and the resulting spectra are called emission and excitation spectrum, respectively. Emission spectra are obtained by irradiating the sample at one wavelength ( $\lambda_{Ex}$ ) and collecting the emission over a wavelength interval. The emission can be collected either at a right angle or at a small angle (front face) to the excitation beam. To record an excitation spectrum the emission intensity is recorded at a fixed wavelength while scanning the excitation wavelength. Since, emission only occurs after absorption of a photon the excitation spectrum resembles the absorption spectrum.

## Quantum Yield Determination

The photoluminescence quantum yield, or fluorescence quantum yield,  $\Phi_f$  if the emission originates from the singlet state, is the number of photons emitted per number of photons absorbed. Most often  $\Phi_f$  is determined relative a reference with known quantum yield according to Equation 7.3

$$\Phi_x = \Phi_r \frac{F_x}{F_r} \frac{A_r}{A_x} \frac{n_x^2}{n_r^2} \frac{I_r}{I_x} \quad (7.3)$$

where  $\Phi_i$  is the quantum yield,  $F_i$  is the integrated emission intensity,  $A_i$  is the absorption at the excitation wavelength,  $n_i$  is the refractive index of the solvent and  $I_i$  is the excitation intensity. Subscripts  $x$  and  $r$  denote the unknown sampled and reference, respectively. The upconversion quantum yield  $\Phi_{UC}$  can also be determined according to Equation 7.3, however, since at least two low energy photons are consumed for each emitted high energy photon the maximum quantum yield of upconversion is 50%.

### 7.1.2 Time-resolved Measurements

#### Time Resolved Emission

A population of molecules in the excited state that have been excited simultaneously will not all relax to the ground state at the same time. For a fluorescent molecule the average time for a population to decay is called the fluorescence lifetime  $\tau_f$ . Considering the fluorescence intensity ( $I$ ) of the population it will decay with time as the excited state is depopulated. The intensity decay will follow equation 7.4

$$I(t) = I_0 \exp\left(-\frac{t}{\tau_f}\right) \quad (7.4)$$

where  $I_0$  is the initial intensity and  $t$  is the time since excitation.

To determine the fluorescence lifetime a technique called Time-Correlated Single Photon Counting (TCSPC) is often used. In TCSPC the time between excitation and the first photon reaching the detector is measured. This is done by exciting the sample with a short laser pulse and at the same time using a fraction of the laser pulse to start a timer. When an emitted photon from the sample hits the detector the timer is stopped. The recorded time is stored and the sample is excited again. All the stored times are plotted in a histogram where the x-axis represents the time difference from pulse to detection and the y-axis is the number of photons detected. A typical decay is shown in figure 7.1.

In reality the samples is excited by a pulsed laser with a repetition rate of 1 - 80 MHz, if the detection rate is much less, meaning that *e.g.* only 1 photon is detected every 100 pulses the histogram will resemble the decay in equation 7.4. The repetition rate has to be chosen so that the sample has returned to its ground state before the next excitation pulse, *e.g.* with a repetition rate of 10 MHz there is one shot every 100 ns and only samples with lifetimes <10 ns will have decayed completely.

As the laser pulse is not a perfect dirac pulse it will still excite the sample a short time after the timer is started. Therefore the laser pulse and instrument response is recorded from a scattering sample. This instrument response function (IRF) is then deconvoluted from the fluorescence decay to obtain the lifetime in equation 7.4.<sup>60</sup>

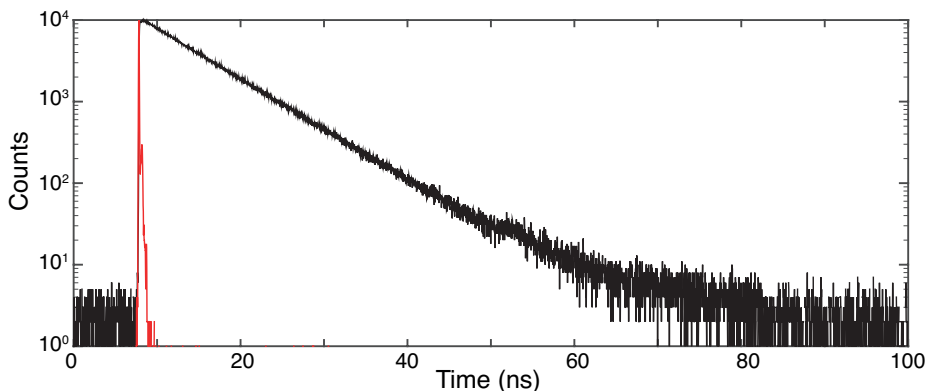


Figure 7.1: Fluorescence decay curve of 9,10-diphenylanthracene (black) in toluene and the corresponding instrument response function (red).

If there are two species that are emissive the fluorescence decay will not follow equation 7.4. Instead it will follow a biexponential decay, with a lifetime corresponding to each species as in equation 7.5:

$$I(t) = A \exp\left(-\frac{t}{\tau_{fA}}\right) + B \exp\left(-\frac{t}{\tau_{fB}}\right) \quad (7.5)$$

where  $A$  and  $B$  are the magnitude of the decay pathway for species A and B respectively,  $\tau_{fA}$  and  $\tau_{fB}$  are the lifetimes of the species A and B respectively.

Time-resolved emission can also be measured by exciting the sample with a pulsed laser and detecting the emission with a photomultiplier tube (PMT) detector. The resolution is limited by the laser pulse-width and detector electronics. It is a common way of measuring the emission decay of long lived excited states such as phosphorescence or delayed fluorescence.

### Transient Absorption Measurements

There are excited states that do not decay radiatively and can thus not be studied using TCSPC. Another technique that does not rely on the emission of a photon is transient absorption spectroscopy (TAS). In TAS the absorption of excited states is followed over time. Depending on the detector used one can either look at one wavelength at a time, or over a wavelength interval.

A TAS setup consists of three main components; pump, probe and detector. A simplified illustration of a TAS setup is shown in figure 7.2. The pump sources generates a laser pulse used to excite the sample. Perpendicular to the pump beam is the probe beam, which can be of a single wavelength or white light. The probe beam passes through the sample and into the detector. The probe beam is detected both with and without the pump beam exciting the sample and the difference between these is the signal obtained from the measurement. The difference can both be positive and negative. A positive

signal corresponds to the absorption of an excited state and a negative peak can either be the depopulation of the ground state absorption, called ground state bleach, or emission from the sample.

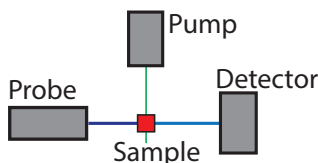


Figure 7.2: A simplified illustration of the main components of a transient absorption spectroscopy setup.

## 7.2 Synthesis

### 7.2.1 Stille and Suzuki Cross-coupling Reactions

Both the Stille and Suzuki reactions are cross-coupling reactions forming new carbon-carbon bonds. They are quite similar and the main difference is the type of metallated coupling species used, as well as the requirement for a base in the Suzuki reaction. The Stille reaction use a stannyl-compound as one coupling partner where as the Suzuki reaction uses a boronic acid derivative. Both reactions use a palladium catalyst. The other coupling partner is generally an aromatic or vinyl halogen or triflate.<sup>163,164</sup>

The general catalytic cycle is described in figure 7.3. The first step is the oxidative addition of the halide to the palladium(0) catalyst. Secondly the transmetalation of the stanyl or boronic acid compound occurs. This step requires a base to activate the boronic acid for the transmetalation step in the case of the Suzuki reaction.<sup>164</sup> The desired cross-coupling product is formed in the final step, the reductive elimination, also returning the catalyst to its initial oxidation state, palladium(0).<sup>164</sup>

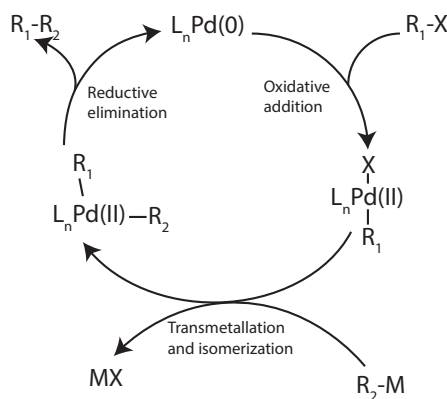


Figure 7.3: Catalytic cycle of the palladium catalyzed Stille and Suzuki reactions.

# Acknowledgements

There are many people that I would like to thank and acknowledge for their contribution in various way to the work presented in this Thesis. First I would like to thank my supervisor Kasper for taking me on to this project. Your encouragement, creative solutions, steady support and always letting me try my own ideas has helped me develop a lot during these 4.5 years. The group atmosphere that you have achieved is also worth mentioning as it is and has been a pleasure to work together with all present and former group members, Thank you all! I would like to continue with acknowledging the support from my co-supervisor Maria and examiner Bosse who not only have helped me with all the spectroscopic challenges within the project but also been great mentors.

All present and former colleagues on the 8th and 5th floor which I have had the pleasure to interact with. I think there are few work places that have such a joyful and supportive atmosphere and I am happy to have had the chance to be part of it. There are some colleagues that I want to name in particular. Karl Börjesson, for introducing me to the project and photochemistry in general. Anders Lennartsson for teaching me about organic synthesis and for your company in and outside the lab. Damir, it has been inspiring to work with you and without your help and hard work on developing our methodologies to characterize upconversion systems this thesis would be a lot shorter! I would like to thank Ambra, for great discussions and collaborations, also for thoroughly reading my thesis. Christian Rohner, I appreciate your helpful suggestions and for reading my thesis. Mattias and Anders, who I shared my office with for most of my time at Chalmers, it was a pleasure being your office mate. I also wish to mention Lotta and Frida for always helping out and making everything run smoothly at Applied Chemistry. Also Roger Forsberg for always finding what we need!

I also want to thank professor Ming Lee Tang at UC Riverside and her group for the hospitality, helping me out and sharing their experience with me during my stay at UCR.

Thanks to my family and friends for being there for me even though I have been very caught up in work a lot of the time, especially David for being a fantastic friend and helping me realize there's a life outside of University! I really appreciate your visit to California, I enjoyed it a lot! A special thanks to my Wife, for your unconditional support, encouragement and love! You can always make me laugh and enjoy life when it is most needed! I look forward to a great and long future together, I Love you! Sarah, thanks for being the best possible sister! Finally, I would like to thank my parents. You have always encouraged me to pursue my own dreams and supported me unconditionally, I know I don't say it enough, but I do Love you and I appreciate everything you have done for me!

# Bibliography

- [1] Arrhenius, S. *Philosophical Mag. J. Sci.* **1896**, *41*, 237–276.
- [2] International Energy Agency, In *Solar Energy Perspectives*; International Energy Agency,, Ed.; 2011.
- [3] Lewis, N. S.; Nocera, D. G. *Proc. Natl. Acad. Sci. U. S. A.* **2006**, *103*, 15729–15735.
- [4] International Energy Agency, In *Key World Energy Statistics*; International Energy Agency,, Ed.; 2011.
- [5] Ginley, S. D., Cahen, D., Eds. *Fundamentals of Materials for Energy end Environmental Sustainability*; Cambridge University Press, New York: New York, 2012.
- [6] Fujishima, A.; Honda, K. *Nature* **1972**, *238*, 37–38.
- [7] Shockley, W.; Queisser, H. J. *J. Appl. Phys.* **1961**, *32*, 510–519.
- [8] Rühle, S. *Sol. Energy* **2016**, *130*, 139–147.
- [9] Baglione, M. L. Development of System Analysis Methodologies and Tools For Modeling and Optimizing vehicle System Efficiency. Thesis for the degree of Doctor of Philosophy in Mechanical Engineering, University of Michigan, 2007.
- [10] Bandivadekar, A.; Bodek, K.; Cheah, L.; Evans, C.; Groode, T.; Heywood, J.; Kasseris, E.; Kromer, M.; Weiss, M. *On the Road in 2035*; 2008; p 23.
- [11] Balushev, S.; Miteva, T.; Yakutkin, V.; Nelles, G.; Yasuda, a.; Wegner, G. *Phys. Rev. Lett.* **2006**, *97*, 7–9.
- [12] Balushev, S.; Yakutkin, V.; Wegner, G.; Miteva, T.; Nelles, G.; Yasuda, A.; Chernov, S.; Aleshchenkov, S.; Cheprakov, A. *Appl. Phys. Lett.* **2007**, *90*, 1–4.
- [13] Singh-Rachford, T. N.; Castellano, F. N. *Coord. Chem. Rev.* **2010**, *254*, 2560–2573.
- [14] Parker, C. A.; Hatchard, C. G. *Proc. R. Soc. A Math. Phys. Eng. Sci.* **1962**, *269*, 147.
- [15] Parker, C. A.; Hatchard, C. G. *Proc. Chem. Soc.* **1962**, 386–387.

- [16] Parker, C. A. *Proc. R. Soc. A Math. Phys. Eng. Sci.* **1963**, *276*, 125–135.
- [17] Parker, C. a.; Joyce, T. a. *Chem. Commun.* **1967**, *6*, 744.
- [18] Keivanidis, P. E.; Balushev, S.; Miteva, T.; Nelles, G.; Scherf, U.; Yasuda, A.; Wegner, G. *Adv. Mater.* **2003**, *15*, 2095–2098.
- [19] Kozlov, D. V.; Castellano, F. N. *Chem. Commun.* **2004**, *1*, 2860–2861.
- [20] Khnayzer, R. S.; Blumhoff, J.; Harrington, J. a.; Haeefe, A.; Deng, F.; Castellano, F. N. *Chem. Commun.* **2012**, *48*, 209–2011.
- [21] Cao, X.; Hu, B.; Zhang, P. *J. Phys. Chem. Lett.* **2013**, 2334–2338.
- [22] Cheng, Y. Y.; Fückel, B.; MacQueen, R. W.; Khoury, T.; Clady, R. G. C. R.; Schulze, T. F.; Ekins-Daukes, N. J.; Crossley, M. J.; Stannowski, B.; Lips, K.; Schmidt, T. W. *Energy Environ. Sci.* **2012**, *5*, 6953–6959.
- [23] Schulze, T. F.; Cheng, Y. Y.; Fckel, B.; MacQueen, R. W.; Danos, A.; Davis, N. J. L. K.; Tayebjee, M. J. Y.; Khoury, T.; Clady, R. G. C. R.; Ekins-Daukes, N. J.; Crossley, M. J.; Stannowski, B.; Lips, K.; Schmidt, T. W. *Aust. J. Chem.* **2012**, *65*, 480–485.
- [24] Schulze, T. F.; Czolk, J.; Cheng, Y.-Y.; Fückel, B.; MacQueen, R. W.; Khoury, T.; Crossley, M. J.; Stannowski, B.; Lips, K.; Lemmer, U.; Colsmann, A.; Schmidt, T. W. *J. Phys. Chem. C* **2012**, *116*, 22794–22801.
- [25] Kim, J.-h.; Kim, J.-h. *J. Am. Chem. Soc.* **2012**, *134*, 17478–17481.
- [26] Nattestad, A.; Cheng, Y.; Macqueen, R.; Schulze, T.; Thompson, F.; Mozer, A.; Fu, B.; Khoury, T.; Crossley, M.; Lips, K.; Wallace, G.; Schmidt, T. W. *J. Phys. Chem. Lett.* **2013**, *4*, 2073–2078.
- [27] Gray, V.; Dzebo, D.; Abrahamsson, M.; Albinsson, B.; Moth-Poulsen, K. *Phys. Chem. Chem. Phys.* **2014**, *16*, 10345–10352.
- [28] Monguzzi, A.; Bianchi, F.; Bianchi, A.; Mauri, M.; Ruffo, R.; Tubino, R.; Meinardi, F. *Adv. Energy Mater.* **2013**, *3*, 680–686.
- [29] Börjesson, K.; Dzebo, D.; Albinsson, B.; Moth-Poulsen, K. *J. Mater. Chem. A* **2013**, *1*, 8521–8524.
- [30] Wohnhaas, C.; Turshatov, A.; Mailänder, V.; Lorenz, S.; Balushev, S.; Miteva, T.; Landfester, K. *Macromol. Biosci.* **2011**, *11*, 772–778.
- [31] Liu, Q.; Yang, T.; Feng, W.; Li, F. *J. Am. Chem. Soc.* **2012**, *134*, 5390–5397.
- [32] Liu, Q.; Yin, B.; Yang, T.; Yang, Y.; Shen, Z.; Yao, P.; Li, F. *J. Am. Chem. Soc.* **2013**, *135*, 5029–5038.

- [33] Wohnhaas, C.; Mailänder, V.; Dröge, M.; Filatov, M. A.; Busko, D.; Avlasevich, Y.; Balushev, S.; Miteva, T.; Landfester, K.; Turshatov, A. *Macromol. Biosci.* **2013**, *13*, 1422–1430.
- [34] Kwon, O. S.; Song, H. S.; Conde, J.; Kim, H.-i.; Artzi, N.; Kim, J.-H. *ACS Nano* **2016**, *10*, 1512–1521.
- [35] Askes, S. H. C.; Bahreman, A.; Bonnet, S. *Angew. Chemie - Int. Ed.* **2014**, *53*, 1029–1033.
- [36] Askes, S. H.; Kloz, M.; Bruylants, G.; Kennis, J. T.; Bonnet, S. *Phys. Chem. Chem. Phys.* **2015**, *17*, 27380–27390.
- [37] Kondakov, D. Y. *Philos. Trans. R. Soc. A Math. Phys. Eng. Sci.* **2015**, *373*, 20140321.
- [38] Di, D.; Yang, L.; Richter, J. M.; Meraldi, L.; Altamimi, R. M.; Alyamani, A. Y.; Credgington, D.; Musselman, K. P.; MacManus-Driscoll, J. L.; Friend, R. H. *Adv. Mater.* **2017**, *29*, 1605987.
- [39] Hoseinkhani, S.; Tubino, R.; Meinardi, F.; Monguzzi, a. *Phys. Chem. Chem. Phys.* **2015**, *17*, 4020–4024.
- [40] Goudarzi, H.; Keivanidis, P. E. *J. Phys. Chem.* **2014**, *118*, 14256–14265.
- [41] Kim, J. H.; Deng, F.; Castellano, F. N.; Kim, J. H. *Chem. Mater.* **2012**, *24*, 2250–2252.
- [42] Duan, P.; Yanai, N.; Nagatomi, H.; Kimizuka, N. *J. Am. Chem. Soc.* **2015**, *137*, 1887–1894.
- [43] Sripathy, K.; MacQueen, R. W.; Peterson, J. R.; Cheng, Y. Y.; Dvorák, M.; McCamey, D. R.; Treat, N. D.; Stingelin, N.; Schmidt, T. W. *J. Mater. Chem. C* **2015**, *3*, 616–622.
- [44] Vadrucci, R.; Weder, C.; Simon, Y. C. *Mater. Horiz.* **2015**, *2*, 120–124.
- [45] Tilley, A. J.; Kim, M. J.; Chen, M.; Ghiggino, K. P. *Polymer (Guildf)*. **2013**, *54*, 2865–2872.
- [46] Tilley, A. J.; Robotham, B. E.; Steer, R. P.; Ghiggino, K. P. *Chem. Phys. Lett.* **2015**, *618*, 198–202.
- [47] Ogawa, T.; Yanai, N.; Monguzzi, A.; Kimizuka, N. *Sci. Rep.* **2015**, *5*, 10882.
- [48] Yanai, N.; Kimizuka, N. *Chem. Commun.* **2016**, *52*, 5354–5370.
- [49] Dzebo, D.; Börjesson, K.; Gray, V.; Moth-Poulsen, K.; Albinsson, B. *J. Phys. Chem. C* **2016**, *120*, 23397–23406.
- [50] Gray, V.; Börjesson, K.; Dzebo, D.; Abrahamsson, M.; Albinsson, B.; Moth-Poulsen, K. *J. Phys. Chem. C* **2016**, *120*, 19018–19026.

- [51] Zhao, J.; Wu, W.; Sun, J.; Guo, S. *Chem. Soc. Rev.* **2013**, *43*, 5323–5351.
- [52] Huang, Z.; Li, X.; Mahboub, M.; Hanson, K.; Nichols, V.; Le, H.; Tang, M. L.; Bardeen, C. J. *Nano Lett.* **2015**, *15*, 5552–5557.
- [53] Wu, M.; Congreve, D. N.; Wilson, M. W. B.; Jean, J.; Geva, N.; Welborn, M.; Voorhis, T. V.; Bulovi, V.; Bawendi, M. G.; Baldo, M. A. *Nat. Photonics* **2015**, *10*, 31–34.
- [54] Mongin, C.; Garakyaraghi, S.; Razgoniaeva, N.; Zamkov, M.; Castellano, F. N. *Science* **2016**, *351*, 369–371.
- [55] Glusac, K. *Nat. Chem.* **2016**, *8*, 734–735.
- [56] Schrödinger, E. *Phys. Rev.* **1926**, *28*, 1049–1070.
- [57] Anslyn, E. V.; Dougherty, D. A. *Modern Physical Organic Chemistry*; University Science Books: USA, 2006.
- [58] Atkins, P.; de Paula, J.; Friedman, R. *Quanta, Matter and Change, a molecular approach to physical chemistry*; Oxford university press: Oxford, 2009.
- [59] Turro, N. J.; Ramamurthy, V.; Scaiano, J. *Modern Molecular Photochemistry of Organic Molecules*; University Science Books, 2010.
- [60] Lakowicz, J. R. *Principles of Fluorescence Spectroscopy*, 3rd ed.; Springer Science: New York, 2006.
- [61] Marcus, R. A. *J. Chem. Phys.* **1956**, *24*, 966–978.
- [62] Marcus, R. A. *J. Chem. Phys.* **1957**, *26*, 872–877.
- [63] Marcus, R. A. *J. Chem. Phys.* **1957**, *26*, 867–871.
- [64] Marcus, R. A. *Anu. Rev. Phys. Chem.* **1964**, *15*, 155–196.
- [65] Marcus, R. A.; Energy, E. F. *J. Chem. Phys.* **1965**, *43*, 679–701.
- [66] Miller, J. R.; Calcaterra, L. T.; Closs, G. L. *J. Am. Chem. Soc.* **1984**, *106*, 3047–3049.
- [67] Albinsson, B.; Eng, M. P.; Pettersson, K.; Winters, M. U. *Phys. Chem. Chem. Phys.* **2007**, *9*, 5847–5864.
- [68] Albinsson, B.; Mårtensson, J. *J. Photochem. Photobiol. C Photochem. Rev.* **2008**, *9*, 138–155.
- [69] Gilbert, M.; Albinsson, B. *Chem. Soc. Rev.* **2015**, *44*, 845–862.
- [70] Balzani, V.; Bolletta, F.; Scandola, F. *J. Am. Chem. Soc.* **1980**, *102*, 2152–2163.
- [71] Scandola, F.; Balzani, V. *J. Chem. Educ.* **1983**, *69*, 814–823.

- [72] Cheng, Y. Y.; Fückel, B.; Khoury, T.; Clady, R. G. C. R.; Tayebjee, M. J. Y.; Ekins-Daukes, N. J.; Crossley, M. J.; Schmidt, T. W. *J. Phys. Chem. Lett.* **2010**, *1*, 1795–1799.
- [73] Schmidt, T. W.; Castellano, F. N. *J. Phys. Chem. Lett.* **2014**, *5*, 4062–4072.
- [74] Saltiel, J.; Atwater, B. W. In *Adv. Photochemistry, Vol. 14*; Volman, D. H., Hammond, G. S., Gollnick, K., Eds.; John Wiley & Sons, Inc, 1988; Chapter 1, pp 1–90.
- [75] Dick, B.; Nickel, B. *Chem. Phys.* **1983**, *78*, 1–16.
- [76] Cheng, Y. Y.; Khoury, T.; Clady, R. G. C. R.; Tayebjee, M. J. Y.; Ekins-Daukes, N. J.; Crossley, M. J.; Schmidt, T. W. *Phys. Chem. Chem. Phys.* **2010**, *12*, 66–71.
- [77] Haefele, A.; Blumhoff, J.; Khnayzer, R. S.; Castellano, F. N. *J. Phys. Chem. Lett.* **2012**, *3*, 299–303.
- [78] Tabachnyk, M.; Ehrler, B.; Gélinas, S.; Böhm, M. L.; Walker, B. J.; Musselman, K. P.; Greenham, N. C.; Friend, R. H.; Rao, A. *Nat. Mater.* **2014**, *13*, 1033–1038.
- [79] Thompson, N. J.; Wilson, M. W. B.; Congreve, D. N.; Brown, P. R.; Scherer, J. M.; Bischof, T. S.; Wu, M.; Geva, N.; Welborn, M.; Voorhis, T. V.; Bulović, V.; Bawendi, M. G.; Baldo, M. A. *Nat. Mater.* **2014**, *13*, 1039–1043.
- [80] Willard, D. M.; van Orden, A. *Nat. Mater.* **2003**, *2*, 575–576.
- [81] Jares-Erijman, E. A.; Jovin, T. M. *Nat. Biotechnol.* **2003**, *21*, 1387–1395.
- [82] Li, X.; Nichols, V. M.; Zhou, D.; Lim, C.; Shu, G.; Pau, H.; Bardeen, C. J.; Tang, M. L. *Nano Lett.* **2014**, *14*, 3382–3387.
- [83] Li, X.; Slyker, L. W.; Nichols, V. M.; Shu, G.; Pau, H.; Bardeen, C. J.; Tang, M. L. *J. Phys. Chem. Lett.* **2015**, *6*, 1709–1713.
- [84] Hildebrandt, N.; Spillmann, C. M.; Algar, W. R.; Pons, T.; Stewart, M. H.; Oh, E.; Susumu, K.; Sebastian, A. D.; Delehanty, J. B.; Medintz, I. L. *Chem. Rev.* **2017**, *117*, 536–711.
- [85] Ding, T. X.; Olshansky, J. H.; Leone, S. R.; Alivisatos, A. P. *J. Am. Chem. Soc.* **2015**, *137*, 2021–2029.
- [86] de Mello Donegá, C. *Chem. Soc. Rev.* **2011**, *40*, 1512–1546.
- [87] Brus, L. E. *J. Chem. Phys.* **1983**, *79*, 5566–5571.
- [88] Brus, L. *J. Phys. Chem.* **1986**, *90*, 2555–2560.
- [89] Kippeny, T.; Swafford, L. A.; Rosenthal, S. J. *J. Chem. Educ.* **2002**, *79*, 1094–1100.
- [90] Alivisatos, A. P. *J. Phys. Chem.* **1996**, *100*, 13226–13239.

- [91] Scholes, G. D. *Adv. Funct. Mater.* **2008**, *18*, 1157–1172.
- [92] Efros, A. L.; Rosen, M.; Kuno, M.; Nirmal, M.; Norris, D. J.; Bawendi, M. *Phys. Rev. B* **1996**, *54*, 4843–4856.
- [93] Zhu, H.; Lian, T. *Energy Environ. Sci.* **2012**, *5*, 9406–9418.
- [94] Kubista, M.; Sjoback, R.; Albinsson, B. *Anal. Chem.* **1993**, *65*, 994–998.
- [95] Zhao, J.; Ji, S.; Guo, H. *RSC Adv.* **2011**, *1*, 937–950.
- [96] Schulze, T. F.; Schmidt, T. W. *Energy Environ. Sci.* **2015**, *8*, 103–125.
- [97] Yakutkin, V.; Aleshchenkov, S.; Chernov, S.; Miteva, T.; Nelles, G.; Cheprakov, A.; Balushev, S. *Chem. - A Eur. J.* **2008**, *14*, 9846–9850.
- [98] Balushev, S.; Yakutkin, V.; Miteva, T.; Wegner, G.; Roberts, T.; Nelles, G.; Yasuda, A.; Chernov, S.; Aleshchenkov, S.; Cheprakov, A. *New J. Phys.* **2008**, *10*, 013007.
- [99] Singh-Rachford, T. N.; Castellano, F. N. *J. Phys. Chem. Lett.* **2010**, *1*, 195–200.
- [100] Mongin, C.; Golden, J. H.; Castellano, F. N. *ACS Appl. Mater. Interfaces* **2016**, *8*, 24038–24048.
- [101] Sommer, J. R.; Shelton, A. H.; Parthasarathy, A.; Ghiviriga, I.; Reynolds, J. R.; Schanze, K. S. *Chem. Mater.* **2011**, *23*, 5296–5304.
- [102] Balushev, S.; Yakutkin, V.; Miteva, T.; Avlasevich, Y.; Chernov, S.; Aleshchenkov, S.; Nelles, G.; Cheprakov, A.; Yasuda, A.; Müllen, K.; Wegner, G. *Angew. Chemie - Int. Ed.* **2007**, *46*, 7693–7696.
- [103] Singh-Rachford, T. N.; Nayak, A.; Muro-Small, M. L.; Goeb, S.; Therien, M. J.; Castellano, F. N. *J. Am. Chem. Soc.* **2010**, *132*, 14203–14211.
- [104] Deng, F.; Sommer, J. R.; Myahkostupov, M.; Schanze, K. S.; Castellano, F. N. *Chem. Commun.* **2013**, *49*, 7406–7408.
- [105] Deng, F.; Sun, W.; Castellano, F. N. *Photochem. Photobiol. Sci.* **2014**, 813–819.
- [106] Singh-Rachford, T. N.; Castellano, F. N. *J. Phys. Chem. A* **2009**, *113*, 5912–5917.
- [107] Merkel, P. B.; Dinnocenzo, J. P. *J. Lumin.* **2009**, *129*, 303–306.
- [108] Yanai, N.; Kozue, M.; Amemori, S.; Kabe, R.; Adachi, C.; Kimizuka, N. *J. Mater. Chem. C* **2016**, *4*, 6447–6451.
- [109] Piland, G. B.; Huang, Z.; Tang, M. L.; Bardeen, C. J. *J. Phys. Chem. C* **2016**, *120*, 5883–5889.
- [110] Huang, Z.; Simpson, D. E.; Mahboub, M.; Li, X.; Tang, M. L. *Chem. Sci.* **2016**, *7*, 4101–4104.

- [111] Li, X.; Huang, Z.; Zavala, R.; Tang, M. L. *J. Phys. Chem. Lett.* **2016**, *7*, 1955–1959.
- [112] Xia, P.; Huang, Z.; Li, X.; Romero, J. J.; Vullev, V. I.; Pau, G. S. H.; Tang, M. L. *Chem. Commun.* **2017**, *53*, 1241–1244.
- [113] Okumura, K.; Mase, K.; Yanai, N.; Kimizuka, N. *Chem. - A Eur. J.* **2016**, *22*, 7721–7726.
- [114] Li, X.; Fast, A.; Huang, Z.; Fishman, D. A.; Tang, M. L. *Angew. Chemie Int. Ed.* **2017**, *56*, 5598–5602.
- [115] Mahboub, M.; Huang, Z.; Tang, M. L. *Nano Lett.* **2016**, *16*, 7169–7175.
- [116] Wu, M.; Jean, J.; Bulović, V.; Baldo, M. A. *Appl. Phys. Lett.* **2017**, *110*, 211101.
- [117] Garakyaraghi, S.; Mongin, C.; Granger, D. B.; Anthony, J. E.; Castellano, F. N. *J. Phys. Chem. Lett.* **2017**, *8*, 1458–1463.
- [118] Lecoq, J. C.; Mechin, R.; Tanielian, C.; Bazin, M.; Santus, R. *Chem. Phys. Lett.* **1978**, *54*, 616–618.
- [119] Peng, X.; Schlamp, M. C.; Kadavanich, A. V.; Alivisatos, A. P. *J. Am. Chem. Soc.* **1997**, *119*, 7019–7029.
- [120] Chen, D.; Zhao, F.; Qi, H.; Rutherford, M.; Peng, X. *Chem. Mater.* **2010**, *22*, 1437–1444.
- [121] Zhu, H.; Song, N.; Lian, T. *J. Am. Chem. Soc.* **2010**, *132*, 15038–15045.
- [122] Hilinski, E. F.; Lucas, P. A.; Wang, Y. *J. Chem. Phys.* **1988**, *89*, 3435–3441.
- [123] Park, S. H.; Morgan, R. A.; Hu, Y. Z.; Lindberg, M.; Koch, S. W.; Peyghambarian, N. *J. Opt. Soc. Am. B* **1990**, *7*, 2097–2105.
- [124] Klimov, V.; Hunsche, S.; Kurz, H. *Phys. Rev. B* **1994**, *50*, 8110–8113.
- [125] Norris, D. J.; Sacra, A.; Murray, C. B.; Bawendi, M. G. *Phys. Rev. Lett.* **1994**, *72*, 2612–2615.
- [126] Klimov, V. I. *J. Phys. Chem. B* **2000**, *104*, 6112–6123.
- [127] Gray, V.; Xia, P.; Huang, Z.; Moses, E.; Fast, A.; Fishman, D. A.; Vullev, V. I.; Abrahamsson, M.; Moth-poulsen, K.; Tang, M. L. *Chem. Sci.* **2017**, *8*, 5488–5496.
- [128] Monguzzi, A.; Tubino, R.; Hoseinkhani, S.; Campione, M.; Meinardi, F. *Phys. Chem. Chem. Phys.* **2012**, *14*, 4322–4332.
- [129] Gray, V.; Dzebo, D.; Lundin, A.; Alborzpour, J.; Abrahamsson, M.; Albinsson, B.; Moth-Poulsen, K. *J. Mater. Chem. C* **2015**, *3*, 11111–11121.
- [130] Gray, V.; Dreos, A.; Erhart, P.; Albinsson, B.; Moth-poulsen, K.; Abrahamsson, M. *Phys. Chem. Chem. Phys.* **2017**, *19*, 10931–10939.

- [131] Ohno, O.; Kaizu, Y.; Kobayashi, H. *J. Chem. Phys.* **1985**, *82*, 1779.
- [132] Wu, G.-Z.; Gan, W.-X.; Leung, H.-K. *J. Chem. Soc. Faraday Trans.* **1991**, *87*, 2933–2937.
- [133] Liu, X.; Yeow, E. K. L.; Velate, S.; Steer, R. P. *Phys. Chem. Chem. Phys.* **2006**, *8*, 1298–1309.
- [134] Heinrich, G.; Schoof, S.; Gusten, H. *J. Photochem.* **1974**, *3*, 315–320.
- [135] Barnes, R. L.; Birks, J. B. *Proc. R. Soc. A Math. Phys. Eng. Sci.* **1966**, *291*, 570–582.
- [136] Kang, J. H.; Reichmanis, E. *Angew. Chemie - Int. Ed.* **2012**, *51*, 11841–11844.
- [137] Moor, K.; Kim, J.-H.; Snow, S.; Kim, J.-H. *Chem. Commun.* **2013**, *49*, 10829–10831.
- [138] Berlman, I. *Handbook of Fluorescence Spectra of Aromatic Molecules*, 2nd ed.; Academic Press: New York and London, 1971.
- [139] Wang, C.; Schlamadinger, D. E.; Desai, V.; Tauber, M. J. *ChemPhysChem* **2011**, *12*, 2891–2894.
- [140] Musser, A. J.; Maiuri, M.; Brida, D.; Cerullo, G.; Friend, R. H.; Clark, J. *J. Am. Chem. Soc.* **2015**, *137*, 5130–5139.
- [141] Kimizuka, N.; Arimizu, K.; Duan, P.; Kozue, M.; Amemori, S. Photon Up Conversion Composition, JP 2016-056368. 2016; <https://www4.j-platpat.inpit.go.jp/eng/tokujitsu/tkbs{ }en/TKBS{ }EN{ }GM401{ }Detailed.action>.
- [142] Turshatov, A.; Busko, D.; Avlasevich, Y.; Miteva, T.; Landfester, K.; Balushev, S. *ChemPhysChem* **2012**, *13*, 3112–3115.
- [143] Börjesson, K.; Gilbert, M.; Dzebo, D.; Albinsson, B.; Moth-Poulsen, K. *RSC Adv.* **2014**, *4*, 19846.
- [144] Kang, J. H.; Lee, S. S.; Guerrero, J.; Fernandez-Nieves, A.; Kim, S. H.; Reichmanis, E. *Adv. Mater.* **2017**, 1606830.
- [145] Yokoyama, K.; Wakikawa, Y.; Miura, T.; Fujimori, J.-i.; Ito, F.; Ikoma, T.; Yokoyama, K.; Wakikawa, Y.; Miura, T.; Fujimori, J.-i.; Ito, F. *J. Phys. Chem. B* **2015**, *119*, 15901–15908.
- [146] Zhou, Q.; Zhou, M.; Wei, Y.; Zhou, X.; Liu, S.; Zhang, S.; Zhang, B. *Phys. Chem. Chem. Phys.* **2017**, *19*, 1516–1525.
- [147] Bergamini, G.; Ceroni, P.; Fabbri, P.; Cicchi, S. *Chem. Commun.* **2011**, *47*, 12780.
- [148] Yu, X.; Cao, X.; Chen, X.; Ayres, N.; Zhang, P. *Chem. Commun.* **2015**, *51*, 588–591.
- [149] Fan, C.; Wu, W.; Chruma, J. J.; Zhao, J.; Yang, C. *J. Am. Chem. Soc.* **2016**, *138*, 15405–15412.

- [150] Cullen, D. L.; Meyer Jr, E. F. *Acta Cryst.* **1976**, *B32*, 2259–2269.
- [151] Kadish, K. M.; Leggett, D. J.; Chang, D. *Inorg. Chem.* **1982**, *21*, 3618–3622.
- [152] Kadish, K. M.; Chang, D. *Inorg. Chem.* **1982**, *21*, 3614–3618.
- [153] Smith, M. B.; Michl, J. *Chem. Rev.* **2010**, *110*, 6891–6936.
- [154] Trupke, T.; Green, M. A.; Würfel, P. *J. Appl. Phys.* **2002**, *92*, 4117–4122.
- [155] Tayebjee, M. J. Y.; McCamey, D. R.; Schmidt, T. W. *J. Phys. Chem. Lett.* **2015**, *6*, 2367–2378.
- [156] Schulze, T. F.; Cheng, Y. Y.; Khoury, T.; Crossley, M. J.; Stannowski, B.; Lips, K.; Schmidt, T. W. *J. Photonics Energy* **2013**, *3*, 034598.
- [157] Börjesson, K.; Rudquist, P.; Gray, V.; Moth-Poulsen, K. *Nat. Commun.* **2016**, *7*, 12689.
- [158] Hill, S. P.; Dilbeck, T.; Baduelli, E.; Hanson, K. *ACS Energy Lett.* **2016**, *1*, 3–8.
- [159] Dilbeck, T.; Hill, S. P.; Hanson, K. *J. Mater. Chem. A* **2017**, *5*, 11652–11660.
- [160] Marsico, F.; Turshatov, A.; Peköz, R.; Avlasevich, Y.; Wagner, M.; Weber, K.; Donadio, D.; Landfester, K.; Balushev, S.; Wurm, F. R. *J. Am. Chem. Soc.* **2014**, *136*, 11057–11064.
- [161] Filatov, M. a.; Heinrich, E.; Busko, D.; Ilieva, I. Z.; Landfester, K.; Balushev, S. *Phys. Chem. Chem. Phys.* **2015**, *17*, 6501–6510.
- [162] Dzebo, D.; Moth-Poulsen, K.; Albinsson, B. *Photochem. Photobiol. Sci.* **2017**, DOI:10.1039/C7PP00201G.
- [163] Nicolaou, K. C.; Bulger, P. G.; Sarlah, D. *Angew. Chemie Int. Ed.* **2005**, *44*, 4442–4489.
- [164] Li, J. J. *Name reactions : a collection of detailed reaction mechanisms*, 3rd ed.; Springer: New York, 2006.